STOCHASTIC ANALYSIS OF EFFECTS OF SPATIAL VARIABILITY ON UNSATURATED FLOW

By

Tian-Chyi Jim Yeh

Submitted in Partial Fulfillment of
the Requirements for the Degree of
Doctor of Philosophy

NEW MEXICO INSTITUTE OF MINING AND TECHNOLOGY

Socorro, New Mexico

July, 1982

This dissertation is accepted on behalf of the faculty of the Institute by the following committee:

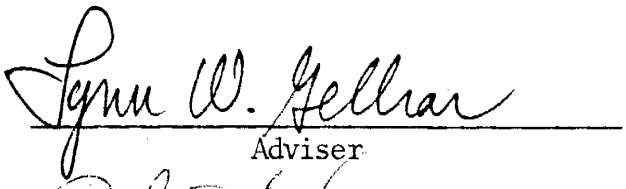

Adviser

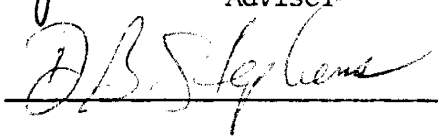

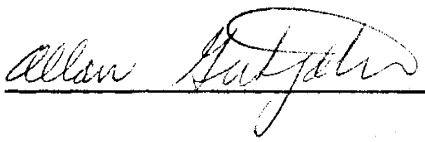

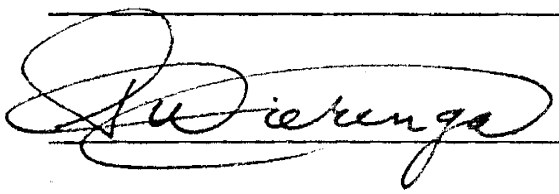

Date

ACKNOWLEDGMENTS

Thanks are extended to Professor L. W. Gelhar for his guidance and encouragement during my stay at New Mexico Institute of Mining and Technology. The author is particularly indebted to Professor L. W. Gelhar and Professor A. Gutjahr for directing his attention to stochastic analysis of flow in a heterogeneous medium.

Helpful comments and suggestions from Drs. P. J. Wierenga and D. B. Stephens are gratefully acknowledged. The author would also like to thank Dr. D. R. Nielsen for providing some useful field data for this study. Many thanks go to Mr. M. Y. Seood for his hard work in helping with the field work associated with this study. The editing of the manuscript by K. M. O'Brien is also acknowledged.

Finally, I would like to express my deepest appreciation to my wife, Mei- Lin, for her patience during the years while I was a graduate student.

ABSTRACT

Effects of spatial variability of soil properties on unsaturated flows are analyzed by solving stochastic steady state infiltration partial differential equations. The unsaturated hydraulic conductivity is assumed to be of the form $K(\psi)=K_s e^{-\alpha\psi}$ where ψ is the capillary pressure head. The variability of saturated hydraulic conductivity K_s and soil-water characteristic variable α are treated as homogeneous stochastic processes. Head variance and covariance functions for one-and three-dimensional flows are determined by using isotropic and anisotropic $\ln K_s$ and α covariance functions as inputs.

The results show that head variance derived from three dimensional flow analysis is less than that of one-dimensional flow. For large values of the correlation length scale and the pore-size distribution parameter, the one and three dimensional results become equivalent, indicating that the flow is predominantly one-dimensional under this condition. The variance of soil moisture content obtained from the theoretical analysis is found to be in close agreement with that observed in the field. In addition,the results of the study demonstrate the importance of the variance of $\ln K_s$ and α, mean capillary pressure head, and mean pore-size distribution parameter in determining the effective unsaturated hydraulic conductivity.

Steady-state infiltration in a heterogeneous medium with arbitrarily oriented stratifications was also analyzed. The results of the analysis demonstrate that effective unsaturated hydraulic conductivity of the medium is a symmetric tensor of rank two, and the analysis derives the complete tensor components of the unsaturated hydraulic conductivity. In general, the principal unsaturated hydraulic conductivities are bounded by the harmonic and arithmetic means of the conductivity. The effective hydraulic conductivity tensor is affected by the magnitude and direction of the gradient, the orientation of stratification, degree of saturation, and some statistical properties of the medium. As a result of the stratification and the pore-size distribution variation, the anisotropy of the unsaturated hydraulic conductivity depends on the degree of saturation. At low saturations horizontal hydraulic conductivity can be several orders of magnitude greater than the vertical. A lateral flow effect in the unsaturated zone is suggested.

Possible applications of such anisotropy in liquid waste isolation problems, and design of shallow underground waste storage facilities are discussed.

TABLE OF CONTENTS

LIST OF FIGURES

LIST OF TABLES

CHAPTER 1
INTRODUCTION

1.1 General Literature Review

Recently, there has been increasing interest in problems involving the movement of groundwater in unsaturated porous media. Flow in the unsaturated zone plays an important role in many practical problems. Examples of such problems include: estimation of groundwater recharge, determination of moisture distribution and groundwater quality, selection of waste depository sites, prediction of streamflow, and evaluation of slope stability.

Traditional analyses of water movement in the unsaturated zone assume that individual soil series are generally homogeneous and isotropic. In general, hydrologists and soil scientists accept and use this simplistic assumption. Field heterogeneity has been considered only in the problems associated with large scale areas where several distinct soil types or geologic formations exist. However several field studies (Nielsen et al., 1973; Coelho, 1974; Carvallo et al., 1976) do not support this simplistic assumption for natural soil formations, even for a single soil type or geologic unit. These studies reveal a large degree of spatial variability of soil hydrologic properties. Stockton and Warrick (1971) found that a 20 to 30 percent variation in the unsaturated hydraulic conductivity value could result from one standard deviation to either side of the average soil water characteristic curve in estimating

the unsaturated hydraulic conductivity in an area of 40 hectares of Pima clay loam. Furthermore, it has been found that the variation of the hydraulic conductivity possesses correlation structures in space (Bakr, 1976; Smith, 1980; Russo and Bresler, 1981; and Vieira et al, 1982). Thus, the effect of such variability on the predictive capabilities of unsaturated flow models needs to be evaluated. More specifically, the effective or mean properties of a spatially variable system and some measure of the variation of the property about the mean has to be determined.

A number of studies that attempted to account for aquifer heterogeneity in saturated flow or soil heterogeneity in unsaturated flow were carried out during the past few years. Freeze (1975), using Monte Carlo simulation, treated the hydraulic conductivity as an uncorrelated random variable, and indicated that variation of saturated hydraulic conductivity has significant effects on the magnitude of the variation of predicted hydraulic head. In addition, he found that the standard deviation of predicted head increases with the block size used to discretize the flow domain. These findings led him to raise doubts about the accuracy of traditional deterministic groundwater flow models.

Recent studies for saturated flow (Bakr et al., 1978; Gelhar, 1976; and Smith and Freeze, 1979) have demonstrated that the spatial variability of the hydrologic properties of aquifer material can be most appropriately represented by

the concept of a statistically homogeneous random field. A Monte Carlo simulation, which takes the spatially correlated structure of the random field into account by a nearest-neighbor model, was carried out by Smith and Freeze (1979). The results of their study show that the predicted head variance is directly proportional to the length scale of the correlation structure, but they do not provide any clear relationship between these parameters. The numerical experiments are based on both finite difference and finite element analog of the flow system which most likely involves some discretization errors and pre-filtering of the randomness of the hydraulic conductivity field.

A similar type of analysis based on conditional simulation was conducted by Delhomme (1979). Conditional simulation is a technique of the Monte Carlo type. It assures that the simulated random field agrees with measurements at any points of observation.

Gelhar (1976), and Bakr, et al., (1978) used spectral analysis, which takes into account the stochastic structure of porous media, and allows flow analysis without parameter discretization. With this approach they found that a more realistic and complicated model (three-dimensional model) would produce less head variance than a one-dimensional flow model. Equaions relating the output head variance and the input variance of hydraulic conductivity were derived.

The effective hydraulic conductivity of saturated heterogeneous porous media was evaluated by Gutjahr et al.,

(1978), using the spectral method. For one-dimensional flow, they found the effective hydraulic conductivity to be equivalent to the harmonic mean used to describe the behavior of flow normal to the layers in deterministic stratified media. The effective hydraulic conductivity in the two-dimensional case is equal to the geometric mean. However, it is slightly greater than the geometric mean in the three-dimensional case.

Dagan (1979) developed a self-consistent model to analyze the effect of field heterogeneity on saturated flow. The results obtained by the model are in agreement with those obtained by spectral analysis.

Gelhar and Axness (1981) used the spectral method to determine the effective hydraulic conductivity of saturated flow in three-dimensional statistically anisotropic media; in that case the effective conductivity was found to be a second rank tensor.

Several investigations on the uncertainties involved in modeling unsaturated flow due to the spatially variable soil properties have been undertaken in the past few years. The studies by Warrick et al., (1977a) treated the effects of variability, but considered hydraulic conductivity as a spatially uncorrelated random variable. Moreover, a simplified drainage equation was used to conduct a Monte Carlo simulation to obtain soil water flux, water content distribution, and to estimate an optimal number of samples required to obtain the mean flux. The simplified drainage equation is

derived from a one-dimensional flow equation, which already averages the variability over the other two dimensions. The one-dimensional flow equation is further integrated over a certain depth to obtain the flux. Thus, the simplified equation is merely a lumped parameter model. This implies that the results of the analysis may not provide the effects of spatial variability, but may provide the sensitivity of the equation to changes of parameters.

In the field of watershed hydrology, Smith and Hebbert (1979) conducted Monte Carlo analyses of the effects of spatially varied hydraulic conductivity on infiltration rate. Similar to their work, Freeze's study (1980) includes consideration of spatial correlation structure of hydraulic conductivity and stochastic rainfall patterns. It also places emphasis on the statistical distribution of runoff resulting from such a heterogeneous watershed. Both studies consider that the infiltration process can be adequately described by a simple, spatially averaged algebraic equation instead of a more realistic spatially dependent partial differential equation.

Due to the significant variation in hydrologic properties of unsaturated porous media, Warrick et al (1977b) developed a method based on the concept of similar media to scale field data for soil water characteristic relationships and unsaturated hydraulic conductivity. Although this may provide a means to obtain the average soil water characteristic relationship and unsaturated hydraulic conduc-

tivity, this approach does not consider the possible anisotropy in the hydraulic conductivity due to layering of soil formations.

Dagan and Bresler (1979) apply the scale concept to derive equations for solute concentration distribution in an unsaturated heterogeneous field under randomly distributed recharge. In addition to the similar media concept, one of the basic assumption employed in their analysis is to regard an actual field as a collection of homogeneous vertical soil columns. The influence between columns is neglected. This implies statistical independence of soil hydrologic properties in the horizontal plane. In fact, this assumption may not necessarily hold for natural soil formations where soil tends to exhibit horizontal stratification. The variation of soil properties in the vertical plane is evidently closer to statistical independence than that in the horizontal.

Philip (1980) uses a random walk to analyze the variation of sorptivity, and points out some of the difficulty in the investigation of unsaturated flow through heterogeneous media. He also discusses the inaccuracy of representing the unsaturated heterogeneous system by the similar media concept. The importance of recognizing the three-dimensionality of field heterogeneity is emphasized as well.

To be more realistic, the hydraulic conductivity should be regarded as a spatially correlated variable random field. The usual continuum flow equations should be employed in the analysis. Then the resulting flow is described by a stochas-

tic differential equation. By solving the stochastic equation, one can therefore obtain realistic statistical properties of the flow in heterogeneous field.

1.2 Objective and Scope of This Study

The general goal of this study is to use spectral analysis to analyze the effect of the spatial variability of soil properties on unsaturated flow. The logarithm of the saturated hydraulic conductivity, $\ln K_s$, and the pore-size distribution parameter, α, which are generally used to characterize unsaturated porous media, are represented by statistically homogeneous stochastic processes. In order to describe the flow system in such a random field, the stochastic properties of the processes are input into the general steady state unsaturated flow equation. A stochastic partial differential equation is formed and is solved by utilizing the Fourier-Stieltjes representation theorem to obtain statistical properties of the output processes.

The specific objectives of this analysis are outlined as follows:

(1) To obtain one-dimensional head variances and covariances, which result from different input covariance functions to evaluate the sensitivity of the model to the input covariance functions.

(2) To derive three-dimensional head variances and covariance functions for comparison with one-dimensional results.

(3) To determine the effective unsaturated hydraulic conductivities and their variances in one- and three-dimensional flow systems.

(4) To determine the anisotropy of the effective hydraulic conductivity in large scale unsaturated media.

The results of the analysis are applied to some practical situations, and compared with observation of variability in the field. Overall, it is expected that this stochastic analysis will provide more information pertaining to the influence imposed by the spatial variability on unsaturated flow. Furthermore, the theory may allow us to assess to some degree the confidence with which predictions can be made.

CHAPTER 2

STOCHASTIC REPRESENTATION OF LARGE SCALE HETEROGENEOUS UNSATURATED POROUS MEDIA

2.1 Introduction

The primary purpose of this chapter is to unravel the motivation behind the stochastic analysis of field heterogeneity of unsaturated flow, or more specifically, the necessity of representing the soil hydrologic properties as stochastic processes. Since flows in unsaturated porous media are far more complex than in saturated media, this chapter will start with a review of the properties of hydraulic conductivity of unsaturated media. Then statistical distributions of some hydrological properties of unsaturated soils observed in the field will be examined. Finally, the representation of the large scale heterogeneous unsaturated field employed in the sequel analyses is discussed.

2.2 Hydraulic Conductivity of Unsaturated Porous Medium

To understand unsaturated hydraulic conductivity, one must start with saturated hydraulic conductivity. Hydraulic conductivity is the ability of the porous material to conduct water through it under hydraulic gradients and is a combined property of porous media and the fluid flowing through it (Bear, 1972). A more concise definition can be given as the volume of water at the existing kinematic

viscosity that will move in a unit time under a unit hydraulic gradient through a unit area measured at right angles to the direction of flow (U. S. Geological Survey, 1972, p. 4).

In general, the saturated hydraulic conductivity depends on pore size, porosity, and structure of the media, as well as fluid properties. The main difference between saturated and unsaturated hydraulic conductivity is the dependence of unsaturated conductivity on capillary pressure or moisture content. Since all of the pores of the porous media are filled with water when it is saturated, the conductivity of the porous material is maximal. Once the material is desaturated, a portion of the pore space of the media is airfilled. As a result, there is a corresponding reduction of the hydraulic conductivity. Under drainage conditions, the large pores that have lower capillary force and higher conductance are emptied first. Thus, water must flow in the smaller pores which are less effective conductors. In addition, airfilled pores become an obstacle. Water has to deflect around them and the the flow paths become more tortuous and longer. Furthermore, a reduction of moisture content causes the water in some pores to be no longer connected with the rest of the continuous flow network, the water phase is no longer continuous and hence there is no flow under such a circumstance. This combined effect causes a rather drastic reduction in the hydraulic conductivity as the soil moisture content decreases. The

amount of water drained is also related to the capillary pressure present in the pores. Hence, the unsaturated hydraulic conductivity can be regarded as a function of capillary pressure. This pressure is the pressure difference at interfaces of water and air at each individual pore. In unsaturated soils, the air phase is usually assumed to be continuous and at atmospheric pressure; the amount that pressure in the water phase is below atmospheric pressure is then the capillary pressure (a positive quantity). When expressed in terms of the height of a water column, the terms capillary pressure head (ψ) or tension head are used.

The general trend of reduction in conductivity of a particular soil is associated with its pore-size distribution. Soils with different pore-size distributions behave differently in the reduction of their hydraulic conductivity as the capillary pressure increases. For instance, a coarse-textured soil such as sandy soil generally has a large percent of large pores. Once the soil is desaturated, the large pores empty first and become nonconductive. Thus, the hydraulic conductivity decreases steeply, as capillary pressure increases. On the other hand, in a clayey soil, the pore-size distribution is more uniform. The reduction in hydraulic conductivity is more gradual as soil capillary pressure increases. Therefore, the behavior of the unsaturated hydraulic conductivity of any soil can usually be characterized by its pore size distribution and saturated hydraulic conductivity.

There have been a number of investigations during the past few decades attempting to derive a physically based equation to describe the relation of hydraulic conductivity to capillary pressure or moisture content. None of those equations allow the reliable prediction of unsaturated conductivity from basic soil properties (Hillel, 1971). However, a variety of empirical equations are available. One of these empirical formulas,

$$K = K_s \, e^{-\alpha \psi} \qquad (2.2.1)$$

relates unsaturated conductivity, K, to capillary pressure head, ψ, saturated hydraulic conductivity, K_s, and the pore-size distribution parameter, α (Gardner, 1958). This equation will serve as the fundamental relationship between unsaturated hydraulic conductivity and capillary pressure in this study, because of its convenience for analytical purposes.

One of the most important features of unsaturated flow in heterogenous media, which should be recognized, arises from the form of the dependence of K on ψ and α, and their interdependence of these parameters. One typical situation is that of a soil formation consisting of two materials of different textures, for instance, sandy and clayey soils. The saturated hydraulic conductivity of sandy soil usually is several orders of magnitude higher than that of clayey soil. As a result of the capillary pressure dependence of

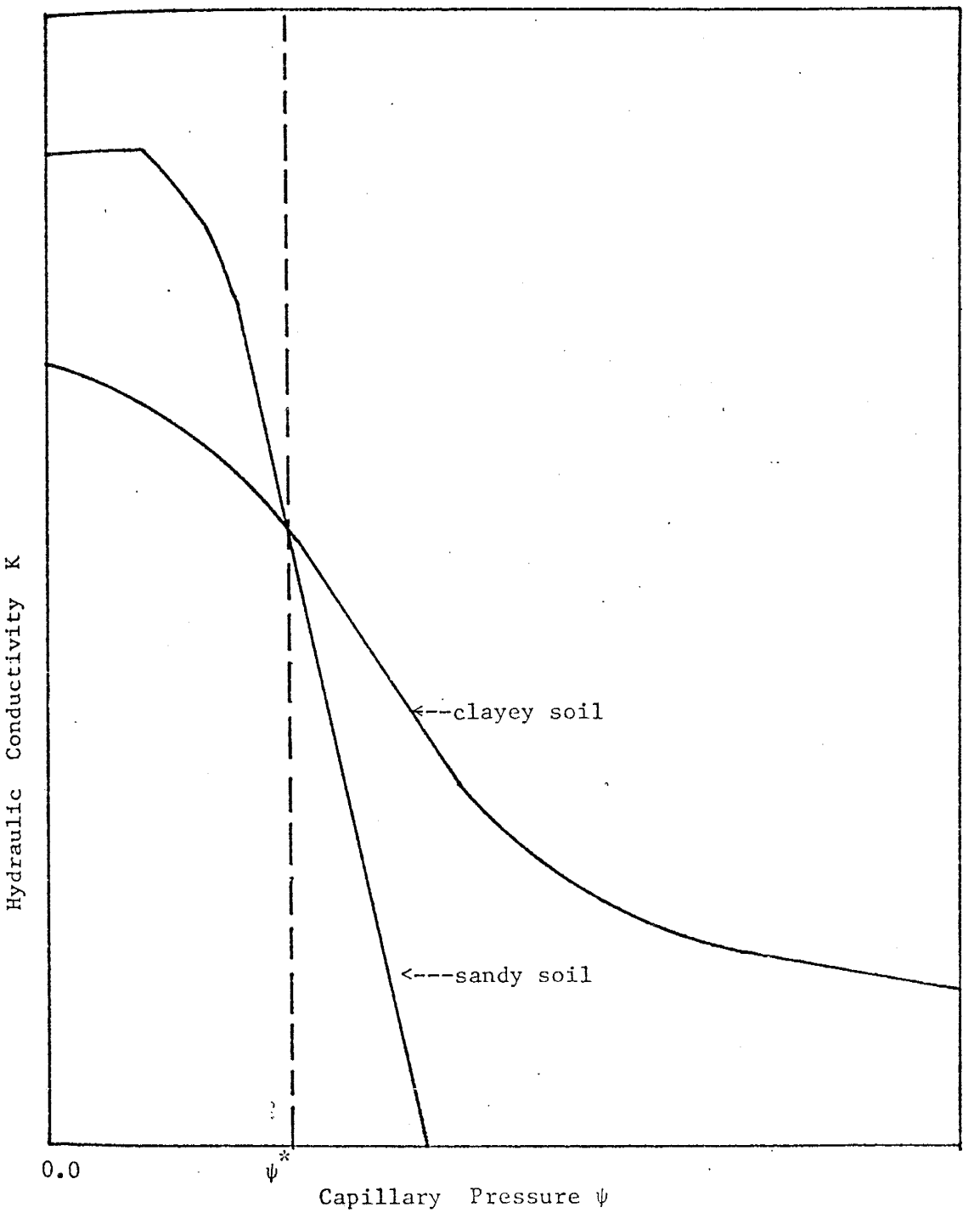

Figure 2.2.1: Dependence of hydraulic conductivity on capillary pressure in soils of different textures.

hydraulic conductivity in unsaturated porous media, sandy soil is not necessarily more permeable than clayey soil at certain ranges of capillary pressure. Such a situation is illustrated in Figure (2.2.1). Note that for $\psi > \psi^*$ the coarser-textured medium is the less permeable.

2.3 Statistical Distribution of Hydrological Properties of Unsaturated Soils

Hydrologists and soil scientists have long recognized the natural variability of soil properties. In the past few decades, numerous field data of physical and chemical soil properties, such as conductivity, particle size, bulk density, moisture content, porosity index, pH, and EC, were collected to characterize their spatial variabilities in large areas. Summaries of these works is given by Coelho (1974), Bakr (1976), Gajem (1980), and Warrick and Nielsen (1980). In general, it has been reported that saturated hydraulic conductivity is log-normally distributed with a large degree of variability. Magnitudes of variation in saturated hydraulic conductivity found by various authors are summarized in Table (2.3.1). The bulk density showed a frequency distribution close to the normal. Frequency distribution for sand and clay particle-size distribution is considered normal. The variations of water content increase with increasing capillary pressures. The coefficient of variation of unsaturated hydraulic conductivity increases as

Table 2.3.1: Variation of saturated hydraulic conductivity of some soils.

Soil type	$\ln K_s$ Variance	Source
Panoche Soil	2.0	Nielsen et al, 1973 Instantaneous profile method.
Adelanto Soil	2.2	Rogowski, 1972
Adams Soil	0.9	-
Houston Black Soil	1.0	-
Cecil Soil	2.4	-
Dwellingup	2.9	Peck et al., 1980
Bakers Hill	1.6	slug test
Collie West	4.1	
Collie East	1.7	
Upper Helena	2.5	
Hamra Red Mediterranean Soil	0.2	Russo and Bresler, 1980
Pima clay loam	1.6	Coelho, 1974

moisture content decreases (Nielsen et al., 1973). Warrick et al. (1977a) used the exponential function,

$$K = K_0 \, e^{[\beta (\theta - \theta_0)]} \qquad (2.3.1)$$

to fit in situ hydraulic conductivity and moisture content of Panoche clay loam and concluded that the parameter, β, of the empirical equation has a log-normal frequency distribution.

Most earlier studies on the variability of soil hydrologic properties treat the observations of a given soil property as being statistically independent, regardless of their spatial location. A recent study by Bakr (1976), however, shows that variation of the permeability of core samples of the Mt. Simon Sandstone aquifer, Illinois, are not spatially independent. He reports that variations in the vertical direction are correlated for a distance of about 1 meter. Smith (1978) analyzes saturated hydraulic conductivity data for samples from the Quadra Sand unit, a late Wisconsin stratified glacial outwash deposit in Vancouver, B.C.. He reports that the estimated correlation length of the conductivity is about 38 cm and 400 cm in the vertical and horizontal directions, respectively. However, a relative small value of the variance of log hydraulic conductivity, 0.71, is calculated from his data. Russo and Bresler (1980) investigate the measurements of saturated

hydraulic conductivity, K_s, the water entry value, h_w, saturated water content, θ_s, residual water content, θ_r, sorptivity, S, and a pore-size distribution parameter, β, from samples collected in a 0.8 hectare plot of Hamra Red Mediterranean soil at Beta Dagon, Israel. They conclude that the spatial variability of each of the six parameters has a structure characterized by an integral scale, indicating the variability of the parameters are not disordered in space. The integral scales for the six parameters, K_s, h_w, θ_s, θ_r, S, and β are 15, 31, 39, 18, 25, and 11 meters, respectively. Gajem (1980) examines the spatial structure of soil properties at the University of Arizona Experiment Station at Marana, Arizona. He also finds the spatial variation of soil properties is correlated in space. In addition, the anisotropy in the correlation scale is evident in some of the data as well (see his table 9). Sisson and Wierenga (1981) report data showing spatial correlation of steady-state infiltration rates. Vieira et al (1981) determine the correlation scale of steady infiltration rate at 1280 sites by using a semi-variogram. It is shown that the length scale is approximately 40 meters. Fritton (1981) investigates the spatial variability of soil capillary pressure in a corn field. A large degree of variation of the capillary pressure head is observed. The variation of the head is found to increase with the dryness of the soil. A variogram (Figure 2.3.1) calculated from the Fritton's (1981) data reveals a correlation structure of the random

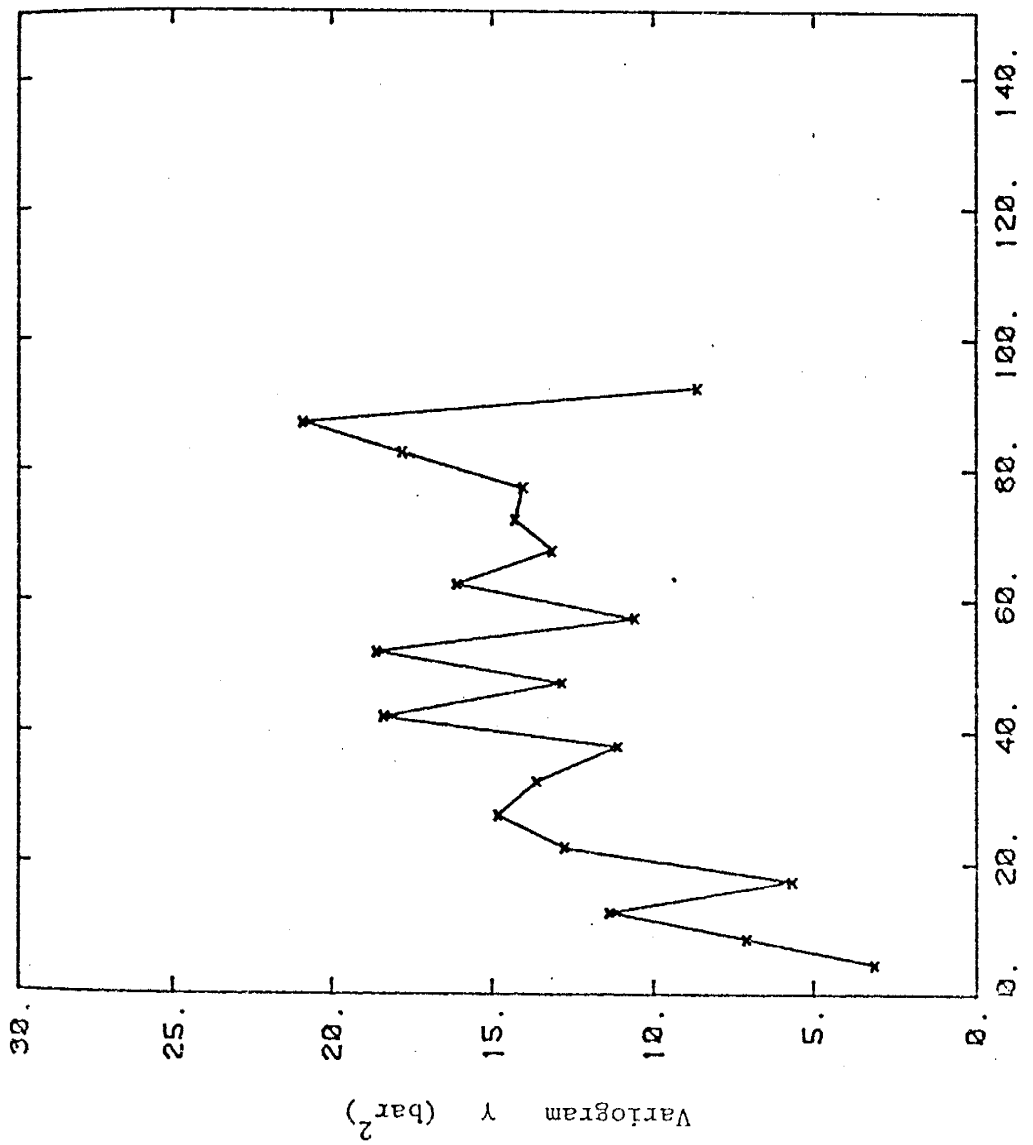

Figure 2.3.1: Variogram of soil capillary pressures in a corn field showing a spatial correlation structure.

capillary pressure field of which the correlation scale is approximately 50 feet. A similar field observation carried out by the writer in an alfalfa field near San Acacia, New Mexico, also demonstrates the correlated spatial variations of soil capillary pressures (see appendix A).

2.4 Stochastic Representation of Heterogeneous Unsaturated Porous Media

As has been discussed in the previous sections of this chapter, parameters such as saturated hydraulic conductivity, K_s, and pore-size distribution parameter, α, controlling the flow process in unsaturated media could vary significantly. Their variations are not totally disordered in space but characterized by spatial correlation length scales. How can such a heterogeneous natural system be represented in a quantitative fashion? One of the approaches is to conduct a large number of measurements of these soil hydraulic parameters so that their variabilities can be depicted in a deterministic sense. However, the effort and expense involved in performing such a formidable task make it practically impossible. The only alternative is to treat the spatially varied soil property as a stochastic process in space. One can, therefore, use its statistical properties derived from a reasonable number of data points to characterize the spatial variability of soil properties.

A stochastic process, by definition, is an ordered set of random variables with its associated probability distribution (Jenkins and Watts, 1968). More precisely, v(x) is a stochastic process if for each fixed x, for instance, x_0, v(x_0) is a random variable with a probability distribution. A space series of hydraulic conductivity measurements, then, is merely one of the many realizations that might have arisen from an ensemble . Thus, a complete description of the heterogenous porous media, in contrast to a single random variable, would require the probability distribution functions for all the random variables and joint probability density functions between the random variables at all points in space. However, such a complete specification generally requires evaluation of all statistical moments. Sufficient data for this calculation rarely exist. A more practical approach is to resort to a description of the process by using the mean and the covariance function.

In order to apply the mean and the covariance function to describe a stochastic process, an assumption of the statistical stationarity of the process is required. A statistically stationary (or homogeneous) process is defined as a process that has a constant mean and a covariance function depending only upon the separation distance in space or time. It is not a function of location in space or time. Physically, this implies that the process has some form of steady state or equilibrium in the sense that the statisti-

cal properties of the process are independent of absolute position in space or time domain. (Jenkins and Watts, 1968).

The covariance function often can be characterized by a correlation length scale and a variance. This length scale is generally defined as the distance beyond which the autocorrelation of the process no longer exists. Occasionally, it is referred to as the integral scale (Lumley and Panosky, 1968), which is precisely defined as the area under the autocorrelation function.

However, one has to recognize that the mean and covariance function mentioned above are the statistical properties of an ensemble consisting of an infinite number of realizations. A series of hydraulic conductivity measurements in space merely is one possible realization in an ensemble. In fact, we can only collect data of one realization. Now a question arises: how can we make use of the space average of data from one realization of finite length to obtain the ensemble mean? The hypothesis most commonly used is ergodicity. The ergodic hypothesis states: if we form an average of a realization of a process over a finite length, then this average must approach the mean value of the process as the averaging record length grows. In other words, the average must approach a stable value, and this value must be the ensemble mean (Lumley and Panofsky, 1964). The same argument can be applied to the covariance if the integral

scale exists. Thus, the stationarity assumption about the variability of soil properties and the ergodic hypothesis allows us to apply stochastic Fourier-Stieltjes representation (Lumley and Panosky, 1968) to the fluctuation of the soil properties in the flow equations used in this analysis.

Since vertical infiltration is of most interest in all the practical fields of hydrology and soil physics, the theoretical analysis in the following chapters will concentrate on the effects of field heterogeneity on steady-state infiltration process. The analyses assume that the relationship between unsaturated hydraulic conductivity and capillary pressure of all the soils can be portrayed by a simple exponential function (equation 2.2.1). Thus, a saturated hydraulic conductivity and a pore-size distribution parameter define the characteristics of an unsaturated medium. In chapters 3 and 4, heterogeneous media are assumed to be characterized by a statistically homogeneous, isotropic saturated hydraulic conductivity and a constant pore-size distribution parameter. To illustrate the physical meaning behind this assumption, the log of the unsaturated hydraulic conductivity of this hypothetical porous medium is shown in Figure (2.4.1a) as a function of the capillary pressure head. Since the pore-size distribution parameter is a constant, variation of unsaturated hydraulic conductivity is affected only by the variation of saturated hydraulic conductivity. The variance of lnK will remain the

same for the whole range of the capillary pressure head. Statistical anisotropy in the saturated hydraulic conductivity will be introduced in chapter 4 to analyze its effects on head variance. In chapter 5, the analysis deals with flow in a more realistic medium where both K_s and α are treated as statistically homogeneous and anisotropic stochastic processes. Schematic representation of such a random field is demonstrated in Figure 2.4.2b by the $\ln K - \psi$ relation curves. As shown in the figure, the variation of the conductivity is influenced not only by the spatial variability of K_s but also by the capillary pressure head due to the additional consideration of the variability of the pore-size distribution parameter.

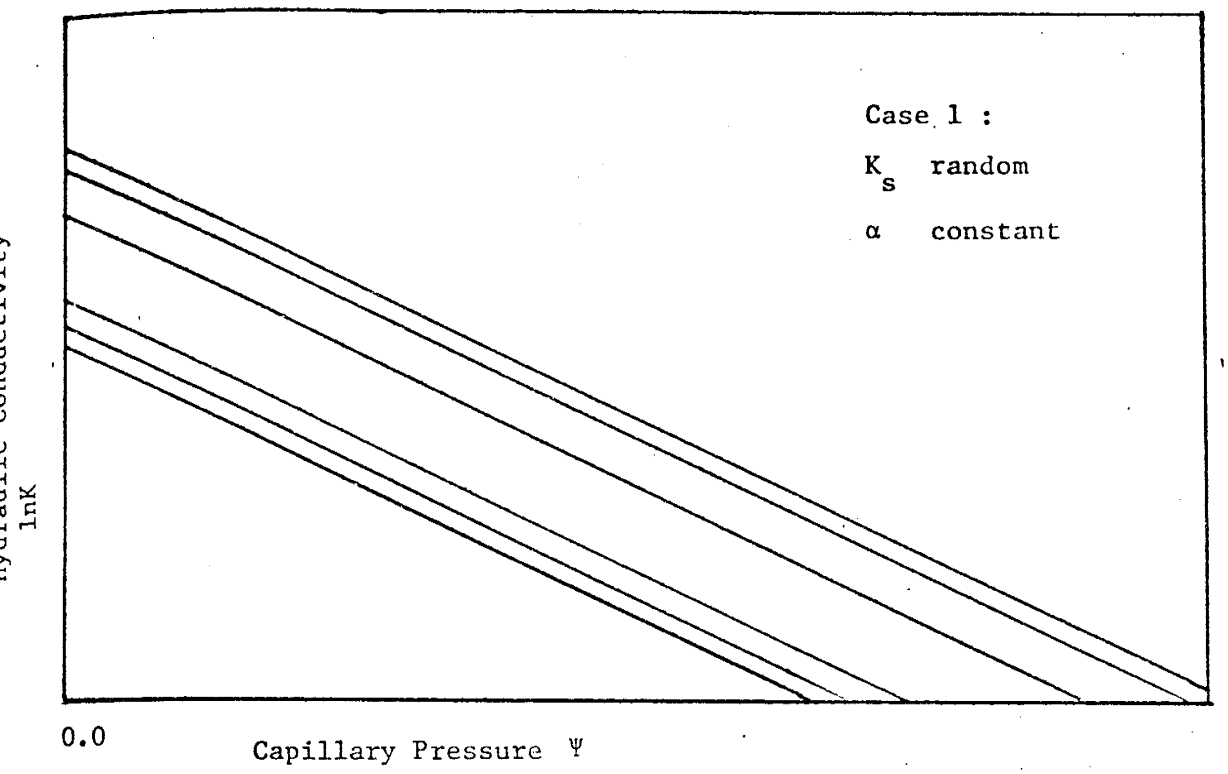

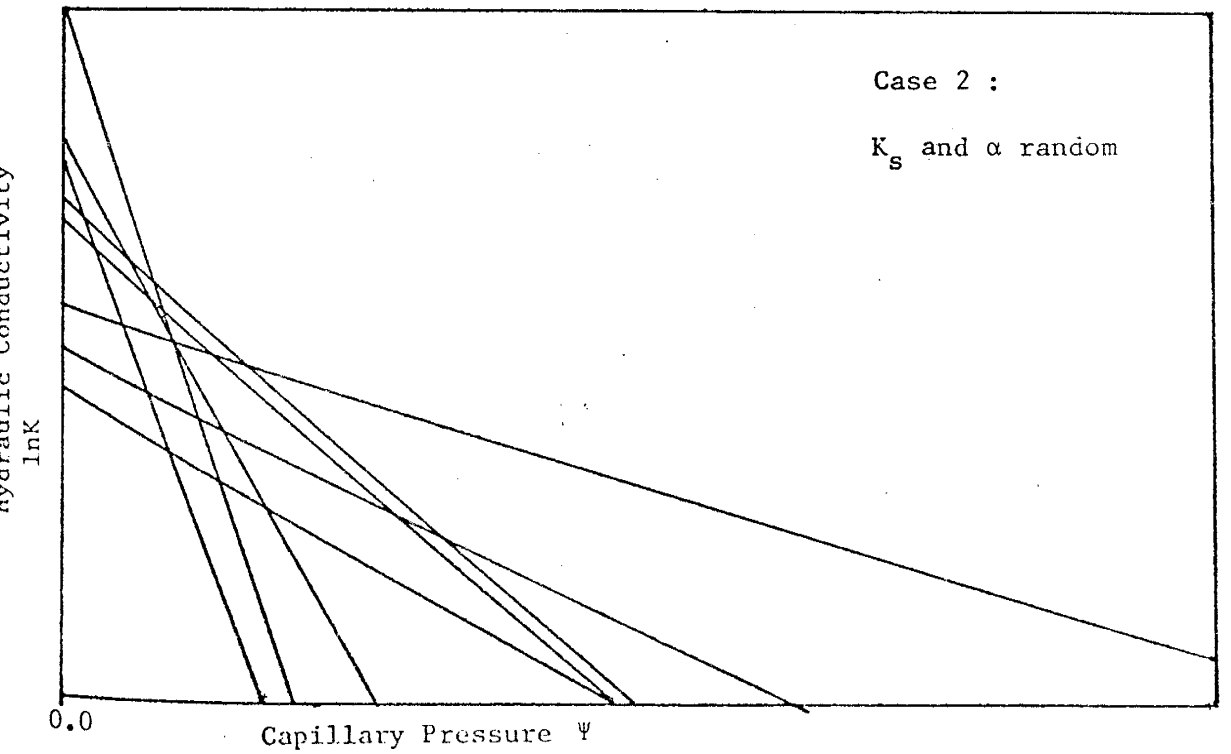

Figure 2.4.1: Schematic representation of heterogeneous porous media of Case I and Case II.

CHAPTER 3

FLOW THROUGH STATISTICALLY ISOTROPIC MEDIA

3.1 Introduction

Saturated hydraulic conductivity of soil may vary drastically from point to point throughout the natural flow system. Variations in this soil property are complex and are not practically depictable by any deterministic mathematical function in detail. Additionally, these properties generally exhibit spatially correlated structures. Hence, the saturated hydraulic conductivity is most appropriately thought of as a stochastic process. Complexity in unsaturated hydraulic conductivity is further intensified by its dependence on the pore-size distribution of porous media. A recent field study (Warrick,1977a) has shown that an unsaturated flow property (the slope of $\ln K - \theta$ curve), also varies from place to place in porous media, and generally is log-normally distributed. To obtain a more realistic and complete description of effects of field heterogeneity on the flow, it is necessary to take the variability of pore-size distribution into account. However, for convenience, it is assumed to be a deterministic constant in the analyses in this chapter.

In the following analyses, we will regard the logarithmic saturated hydraulic conductivity as a stochastic process instead of saturated hydraulic conductivity itself, that is,

$$\ln[\ K_s(\vec{x})\ ] = \log_e K_s(\vec{x}),$$

where $K_s(\vec{x})$ is a saturated hydraulic conductivity stochastic process. The use of logarithmic saturated hydraulic conductivity is simply a convenience in the analysis. $\ln[K(\vec{x})]$ is assumed to be statistically homogeneous and isotropic. Statistical isotropic implies that the covariance function is independent of direction. Based on these assumptions, the effects of spatial variability on unsaturated flow are investigated by evaluating the statistics of flow properties resulting from such a heterogeneous medium. More precisely, head variance and covariance, effective hydraulic conductivity, variance of hydraulic conductivity, and variance of specific discharge of one- and three-dimensional flows are examined in this chapter.

3.2 Head Variances and Covariances of One-dimensional Flow

Consider one-dimensional, steady-state, infiltration through a heterogeneous medium. The governing equation is expressed as follows:

$$\frac{d}{dz}\left\{ K(z,\psi) \frac{d\Phi}{dz} \right\} = 0 \qquad (3.2.1)$$

where $\Phi = - z - \psi$ is the piezometric head, z is the vertical position measured downward from the ground surface, and ψ is the capillary pressure head; $\psi \geq 0$. $K(z,\psi)$ in (3.2.1) is the unsaturated hydraulic conductivity that varies with location and capillary pressure head. For convenience, $K(z,\psi)$ may be expressed as follows (Gardner, 1958):

$$K(z,\psi) = K_s(z)\, e^{-\alpha\psi} \qquad (3.2.2)$$

in which $K_s(z)$ is the saturated hydraulic conductivity at any point z. The saturated hydraulic conductivity is considered as a statistically homogeneous and isotropic stochastic process. α is the pore-size distribution parameter, a deterministic constant.

Applying a logarithmic linearization on $K(z,\psi)$, equation (3.2.1) can be written in the form of

$$\frac{d^2\psi}{dz^2} + \frac{d\ln K}{dz}\left[\frac{d\psi}{dz} + 1\right] = 0 \qquad (3.2.3)$$

If we express the variables in terms of mean and perturbation,

$$\psi = H + h \qquad E[\psi] = H \qquad E[h] = 0 \qquad (3.2.4a)$$

$$\ln K_s = F + f \qquad E[\ln K_s] = F \qquad E[f] = 0 \qquad (3.2.4nb)$$

then (3.2.2) can be written as

$$\ln K = F + f - \alpha(H + h) \quad ; \quad (\ln = \log_e) \qquad (3.2.5a)$$

$$\ln K_m = E[\ln K] = F - \alpha H \qquad (3.2.5b)$$

After substituting (3.2.5) into (3.2.3), and assuming $\frac{dF}{dz} = 0$, we obtain

$$\begin{aligned} &- \frac{df}{dz} + \alpha \frac{dH}{dz} + \alpha \frac{dh}{dz} - \frac{df}{dz}\frac{dH}{dz} + \alpha\left[\frac{dH}{dz}\right]^2 + \\ &2\alpha \frac{dH}{dz}\frac{dh}{dz} - \frac{d^2H}{dz^2} - \frac{d^2h}{dz^2} - \frac{dhdf}{dzdz} + \alpha\left(\frac{dh}{dz}\right)^2 = 0 \end{aligned} \qquad (3.2.6)$$

Taking the expected value of (3.2.6) results in the mean flow equation which takes the form

$$\alpha \frac{dH}{dz} + \alpha\left[\frac{dH}{dz}\right]^2 - \frac{d^2H}{dz^2} - \frac{\overline{dhdf}}{dzdz} + \alpha\overline{\left(\frac{dh}{dz}\right)^2} = 0$$

where the overbar indicates the expected value. Subtracting the mean flow equation from (3.2.5) and neglecting terms involving the product of perturbations produces a definition of the governing flow equation in terms of the perturbations which have a mean zero. This equation takes the form

$$\frac{df}{dz}\left[1 + \frac{dH}{dz}\right] - \alpha\left[1 + 2\frac{dH}{dz}\right]\frac{dh}{dz} + \frac{d^2h}{dz^2} = 0 \qquad (3.2.7)$$

The mean hydraulic gradient, J , is

$$J = -E\left[\frac{d\Phi}{dz}\right] = 1 + \frac{dH}{dz} \qquad (3.2.8)$$

so that the flow equation describing the perturbations in capillary pressure head, (3.2.7), can be written

$$J\frac{df}{dz} - \alpha(2J - 1)\frac{dh}{dz} + \frac{d^2h}{dz^2} = 0 \qquad (3.2.9)$$

Note that during a downward flow J is always positive.

We assume that the mean zero perturbed terms are statistically homogeneous. By using the stochastic Fourier-Stieltjes integral representation (Lumley and Panofsky,

1964) for the perturbed terms

$$f = \int_{-\infty}^{\infty} e^{ikz} dZ_f(k), \qquad h = \int_{-\infty}^{\infty} e^{ikz} dZ_h(k) \qquad (3.2.10)$$

where $dZ_f(k)$ and $dZ_h(k)$ represent the complex Fourier amplitudes of the fluctuations of f and h over wave number space k, respectively. Using these representations in (3.2.9) leads to the following relationship between the Fourier amplitudes

$$dZ_h = \frac{iJdZ_f}{(k + i\alpha(2J-1))} \qquad (3.2.11)$$

The spectral density function S_{hh} of h is then related to the generalized Fourier amplitude by

$$E\{ dZ_h(k) dZ_h^*(k') \} = 0 \qquad k \neq k'$$

$$E\{ dZ_h(k) dZ_h^*(k') \} = S_{hh}(k)dk \qquad k = k'$$

where the asterisk denotes the complex conjugate (Lumley and Panofsky, 1964). The spectrum of capillary pressure head can thus be expressed in terms of the spectrum S_{ff} of $\ln K_s$ as

$$S_{hh} = \frac{J^2 S_{ff}}{k^2 + \alpha^2 (2J - 1)^2} \qquad (3.2.12)$$

A simple exponential form for the autocovariance function of $\ln K_s$ is assumed in order to evaluate (3.3.12)

$$R_{ff}(\xi) = \sigma_f^2 \exp[-|\xi|/\lambda] \qquad (3.2.13)$$

where σ_f^2 is the variance of f , ξ is the separation distance or lag, and λ is the correlation length. This function implies that correlations between neighboring values of the saturated hydraulic conductivity in a given medium drop off rapidly with increased spacing. By taking the inverse Fourier transform of R_{ff}, one obtains the spectrum of $\ln K_s$:

$$S_{ff}(k) = \frac{\sigma_f^2 \lambda}{\pi(1+\lambda^2 k^2)} \qquad (3.2.14)$$

The spectrum S_{hh} of fluctuations in capillary pressure head is found by using (3.2.12) and (3.2.14). The Fourier transform of S_{hh} leads to the autocovariance, R_{hh}, of head fluctuations:

$$R_{hh}(\xi) = \int_{-\infty}^{\infty} e^{ik\xi} S_{hh}(k)dk =$$

$$\frac{J^2\sigma_f^2}{\lambda}\left\{\frac{\lambda^2}{(1-\lambda^2\beta^2)}\left[\frac{e^{-\beta|\xi|}}{\beta} - \lambda e^{-|\xi|/\lambda}\right]\right\} \qquad (3.2.15)$$

where $\beta = \alpha(2J-1)$. When ξ is equal to zero, the variance σ_h^2 of capillary pressure head fluctuation is obtained as

$$\sigma_h^2 = R_{hh}(0) = \frac{J^2\sigma_f^2\lambda}{\beta(1+\lambda\beta)} \qquad (3.2.16)$$

Another form of the autocovariance function of $\ln K_s$, which has been used to produce a statistically homogeneous solution with finite head variance in the stochastic analysis of one-dimensional, saturated groundwater flow (Bakr et al., 1978), takes the form:

$$R_{ff}(\xi) = \sigma_f^2\left[1 - \frac{|\xi|}{\eta}\right] \exp[-|\xi|/\eta] \qquad (3.2.17)$$

where η is the correlation length. The spectrum of fluctuations in $\ln K_s$ associated with this autocovariance function (the so-called "hole function") is:

$$S_{ff}(k) = \frac{2\sigma_f^2\eta^3k^2}{\pi(1+\eta^2k^2)^2} \qquad (3.2.18)$$

This spectrum S_{ff} of the fluctuations in $\ln K_s$ results in the autocovariance of head fluctuations:

$$R_{hh}(\xi) = \frac{J^2\sigma_f^2\eta^2}{(1-\beta^2\eta^2)^2}\left\{\left[1-\beta^2\eta^2\right]\left[1+\frac{|\xi|}{\eta}\right]e^{\frac{-|\xi|}{\eta}}\right. \quad (3.2.19)$$

$$\left. - 2\beta\eta e^{-\beta|\xi|} + 2\beta^2\eta^2\, e^{\frac{-|\xi|}{\eta}}\right\}$$

where $\beta = \alpha(2J-1)$. This head covariance function and the hydraulic conductivity covariance functions are graphed in Figure (3.2.1). Note that the autocorrelation function of the soil capillary pressure head depends not only on the ratio of the separation distance to the correlation scale of $\ln K_s$ as in saturated flow case (Bakr et al., 1978) but also on the gradient, J, and $\alpha\lambda$. Thus, the correlation scale of the head process could vary with the gradient and $\alpha\lambda$. The corresponding variance of the head fluctuation is then

$$\sigma_h^2 = R_{hh}(0) = \frac{J^2\sigma_f^2\eta^2}{(1+\beta\eta)^2} \quad (3.2.20)$$

The head variances resulting from the exponential and hole covariance functions are shown in Figure (3.2.2) as a function of $\lambda\beta$.

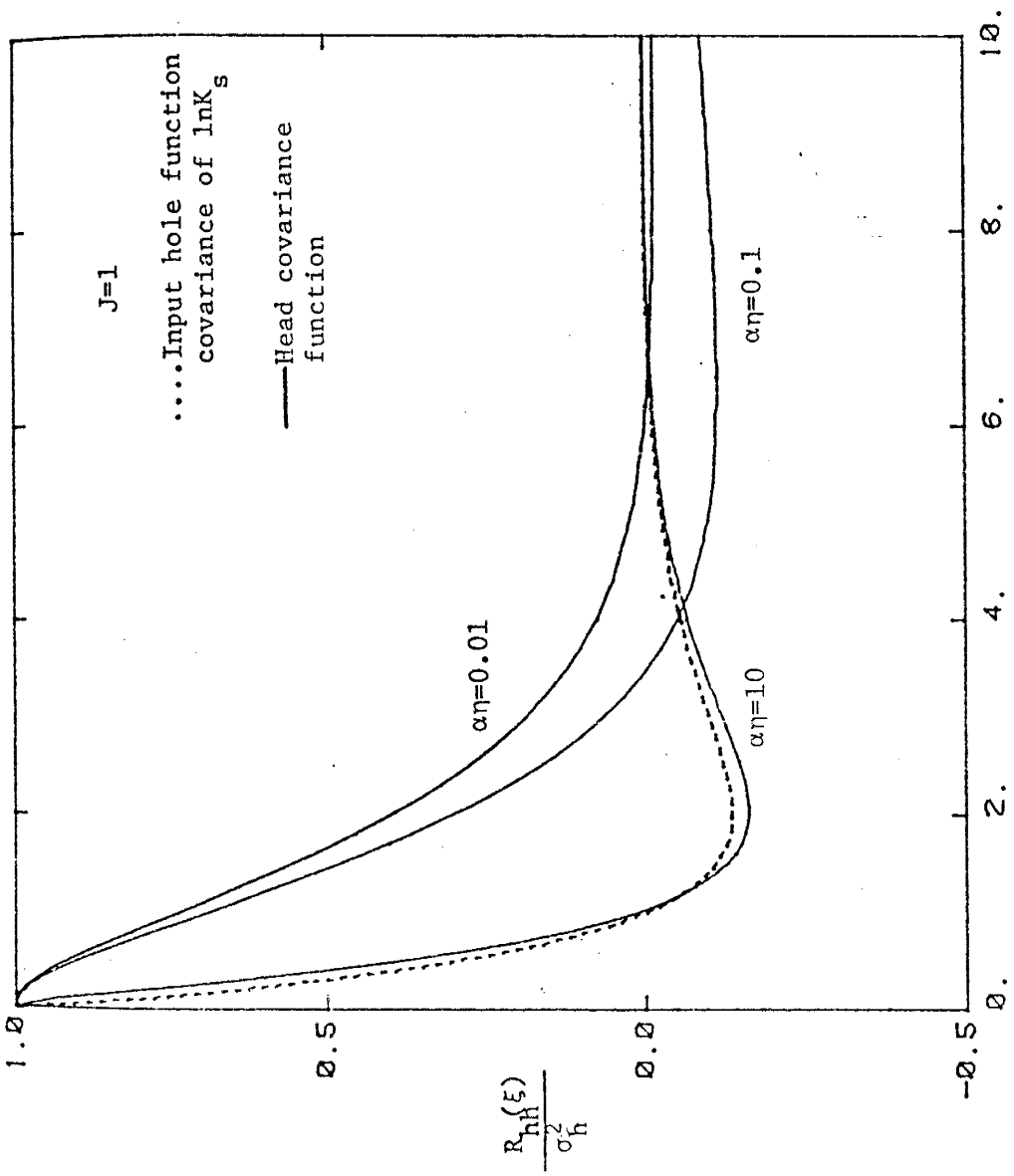

Figure 3.2.1: Dimensionless plots of head covariances function (3.2.19) of different αη values and input lnKs covariance function (3.2.17) versus the dimensionless lag ξ/η.

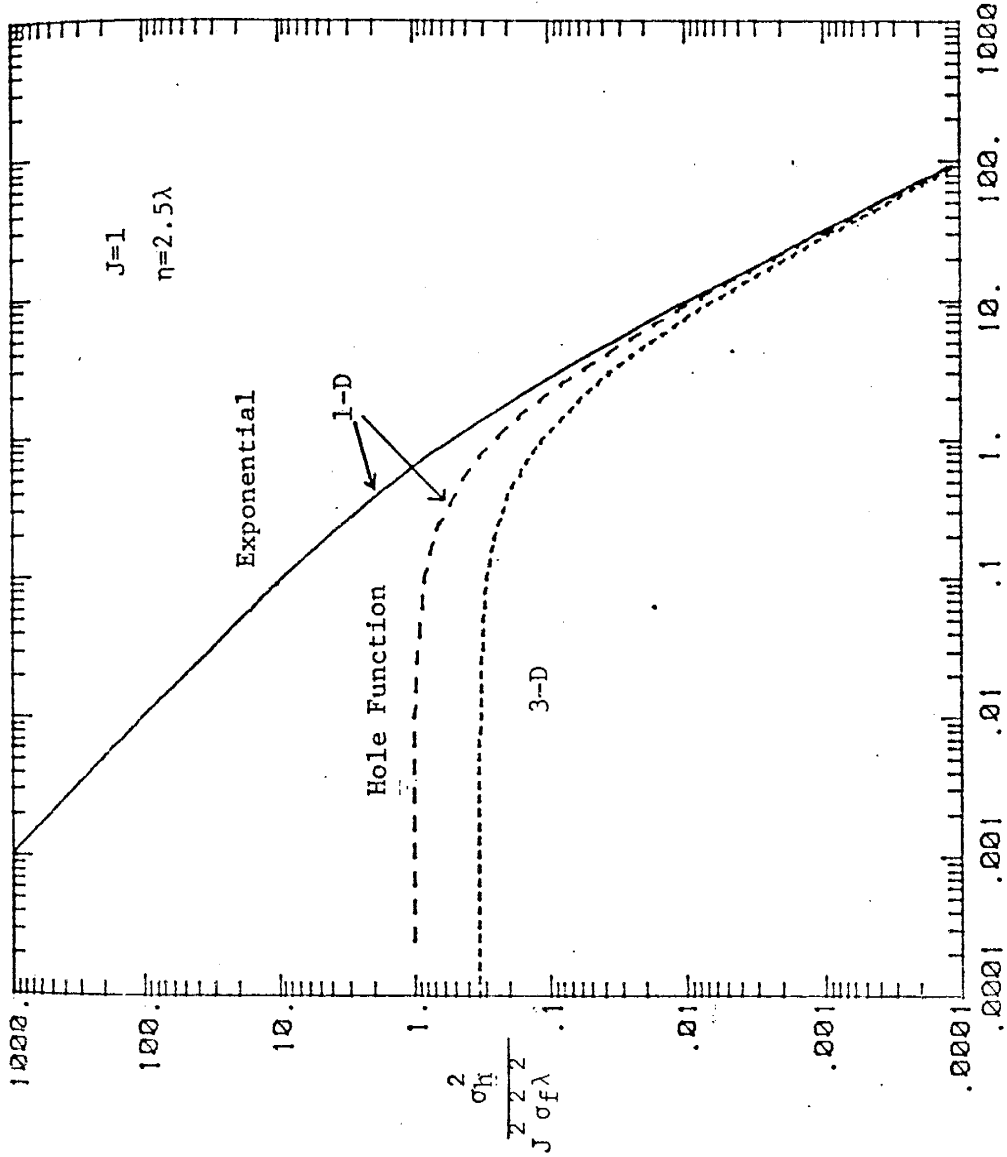

Figure 3.2.2: Comparison of two one-dimensional head variances resulting from the exponential and hole functions (3.2.16) and (3.2.20), respectively, in which $\eta=2.5\lambda$, and a three-dimensional head variance (3.3.13).

3.3 Head Variance and Covariance of Three-Dimensional Flow

The previous one-dimensional flow analysis is somewhat unrealistic because it oversimplifies the variability of hydraulic conductivity of natural soil formations, which is inherently multidimensional. In addition, a one-dimensional flow model tends to force water flow through the low permeability layers. In reality, flow may move in the lateral direction to the place where higher conductivity exists so that it allows the flow to pass around the less permeable zones. It is therefore of importance to investigate the effects of multi-dimensional soil property variations on a multi-dimensional flow system. This is carried out as discussed below.

The governing equation of steady-state, three-dimensional flow through an isotropic porous medium is generally expressed as:

$$\nabla\cdot(K\nabla\Phi) = 0 \qquad (3.3.1)$$

where $\Phi = -z-\psi$.

After carrying out a log transformation for K, we obtain

$$\nabla^2\psi + \nabla\ln K\cdot\nabla(z + \psi) = 0 \qquad (3.3.2)$$

If we consider an unbounded unsaturated porous medium

that has a mean hydraulic gradient J in the z direction but perturbations to both the flow and the hydraulic conductivity K in three dimensions, then one can express the capillary pressure head in terms of mean and perturbations as follows:

$$\Psi = H + h = (J-1)z + h(x,y,z) \; ; \quad J-1 = \frac{\partial H}{\partial z} \qquad (3.3.3)$$

Also following (3.2.5), LnK is represented by

$$LnK = F + f \; -\alpha(H + h) \qquad (3.3.4)$$

Substituting (3.3.4) and (3.3.3) into (3.3.2) and carrying out the same operations employed in one-dimensional analysis, one obtains

$$\nabla^2 h + J\frac{\partial f}{\partial z} - \alpha(2J - 1)\frac{\partial h}{\partial z} = 0 \qquad (3.3.5)$$

This is the governing equation for the output fluctuations in capillary pressure head in terms of variations in input lnK_s where both the fluctuations in head and in lnK_s are treated as spatial stochastic processes. If f and h are again taken to be statistically homogeneous processes, stochastic Fourier-Stieltjes integrals can be used to represent the fluctuations in three dimensions as follows:

$$h(x_1,x_2,x_3) = \int_{-\infty}^{\infty} e^{i\vec{k}\cdot\vec{x}}\, dZ_h(\vec{k})$$

$$f(x_1,x_2,x_3) = \int_{-\infty}^{\infty} e^{i\vec{k}\cdot\vec{x}}\, dZ_f(\vec{k}) \qquad (3.3.6)$$

where $\vec{x}= (x_1,x_2,x_3)$ is the position vector ($x_1 \equiv z$) and $\vec{k} = (k_1,k_2,k_3)$ is the wave number vector. After substitution and manipulation, an expression relating the complex Fourier amplitudes of head and f fluctuations results in the following form

$$dZ_h = \frac{ik_1 J dZ_f}{k^2 + i\alpha(2J-1)k_1} \qquad (3.3.7)$$

The spectral relationship associated with the above equation is given by

$$S_{hh} = \frac{J^2 k_1^2 S_{f\,f}}{(k^4 + \alpha^2(2J-1)^2 k_1^2)} \qquad (3.3.8)$$

If we consider a simple exponential form for the auto-covariance function of f (see Bakr et al., 1978) ,namely,

$$R_{ff}(\vec{\xi}) = \sigma_f^2 \exp[-|\vec{\xi}|/\lambda] \qquad (3.3.9)$$

where σ_f^2 is the variance of $\ln K_s$, $\xi = [\xi_1^2 + \xi_2^2 + \xi_3^3]^{1/2}$ is

the length of the separation vector, and λ is the integral scale

$$\lambda = \int_0^\infty \left[\frac{R_{ff}(\xi)}{\sigma_f^2} \right] d\xi \qquad (3.3.10)$$

The corresponding spectrum of lnK (Bakr et al., 1978), then, is given by

$$S_{ff} = \frac{\sigma_f^2 \lambda^3}{\pi^2 (1+k^2\lambda^2)^2} \qquad (3.3.11)$$

and the spectrum of the head fluctuations is expressed as

$$S_{hh} = \frac{J^2 \sigma_f^2 \lambda^3 k_1^2}{\pi^2 (1+k^2\lambda^2)^2 (k^4+\beta^2 k_1^2)} \qquad (3.3.12)$$

where $\beta = \alpha(2J-1)$.

The head variance is found by integrating the spectrum in (3.3.12) over wave number space and is given by (see Appendix C)

$$\sigma_h^2 = \frac{J^2 \sigma_f^2 \lambda^2}{(\beta\lambda)^2} \left[1 - \frac{2\ln(1+\lambda\beta)}{\lambda\beta} + \frac{1}{1+\lambda\beta} \right] \qquad (3.3.13)$$

In order to examine the behavior of the unsaturated flow system in the three-dimensional random field, one would have to evaluate the head covariance function. The three-dimensional head covariance function obtained by taking the Fourier transform of S_{hh} given by (3.3.12), can be expressed as:

$$R_{hh}(\xi,\chi) = \iiint_{-\infty}^{\infty} e^{i\vec{k}\cdot\vec{\xi}} S_{hh}(\vec{k})d\vec{k} \qquad (3.3.14)$$

where χ is the angle between the separation vector $\vec{\xi}$ and the direction of mean flow (see Figure 3.3.1) and $\xi=|\vec{\xi}|$. Transforming $\vec{k}$ into spherical coordinates and using the following relationships (Bakr et al, 1978)

$$\begin{aligned} k_1 &= |\vec{k}|\cos\beta \\ q &= \frac{k_1}{k} = \cos\Phi\cos\chi + \sin\Phi\sin\chi\cos\theta \\ d\vec{k} &= \sin\Phi dk d\Phi d\theta \end{aligned} \qquad (3.3.15)$$

The integral after integrating over k (see Appendix D) becomes:

$$R_{hh}(\xi,\chi)=C\int_{\gamma=0}^{2\pi}\int_{\theta=0}^{\pi}\frac{q^2\sin\Phi}{(\beta^2q^2-1)}\left[\frac{-\beta q e^{-\beta q|\tau|}}{(\beta^2q^2-1)} + \frac{\beta^2q^2e^{-|\tau|}}{(\beta^2q^2-1)} - \frac{(|\tau|+1)e^{-|\tau|}}{2}\right]d\theta d\Phi \qquad (3.3.16)$$

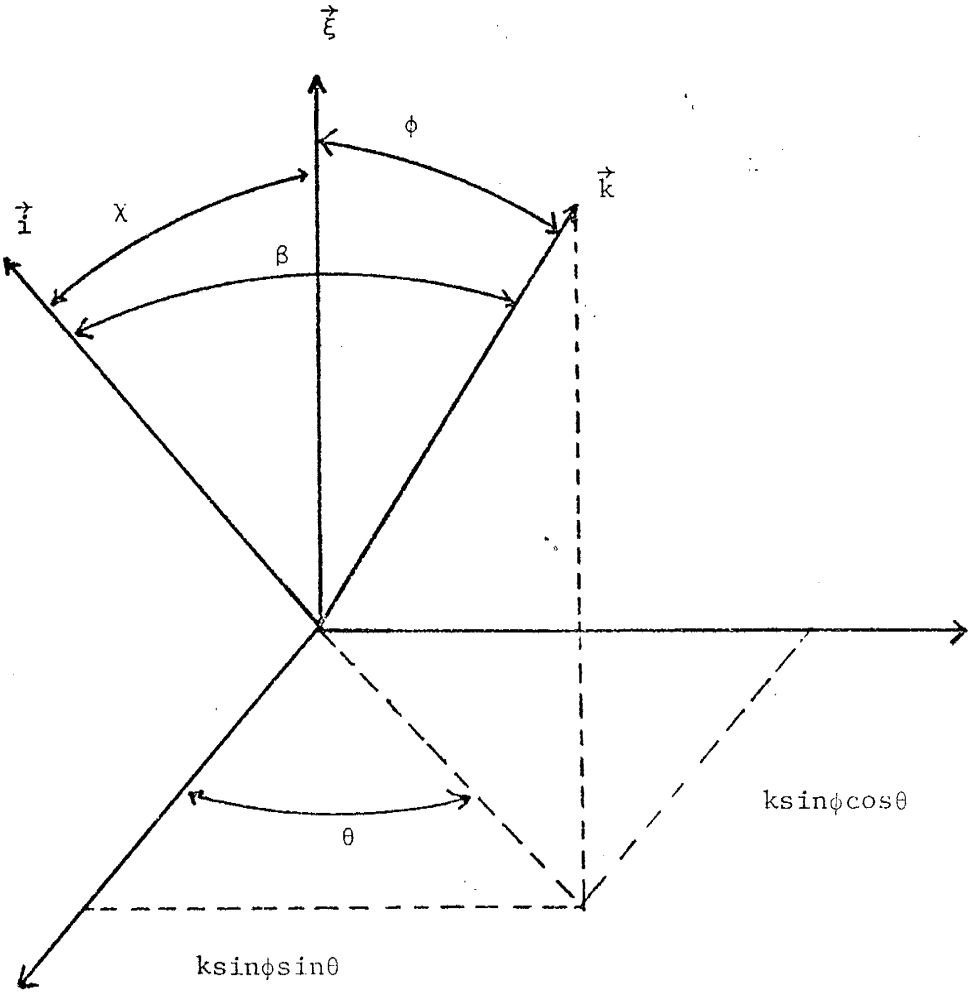

Figure 3.3.1: Geometry of the wave number vector $\vec{k}$ and separation vector, $\vec{\xi}$, relative to the mean flow $\vec{i}$.

where $q = \frac{k_1}{k}$, $\beta = \alpha\lambda$, $\tau = \frac{\xi}{\lambda}\cos\Phi$, and $C = \frac{J^2\sigma_f^2\lambda^2}{2\pi^2}$. The remaining integral is evaluated numerically. The result of the head covariance function is shown in Figure (3.3.2).

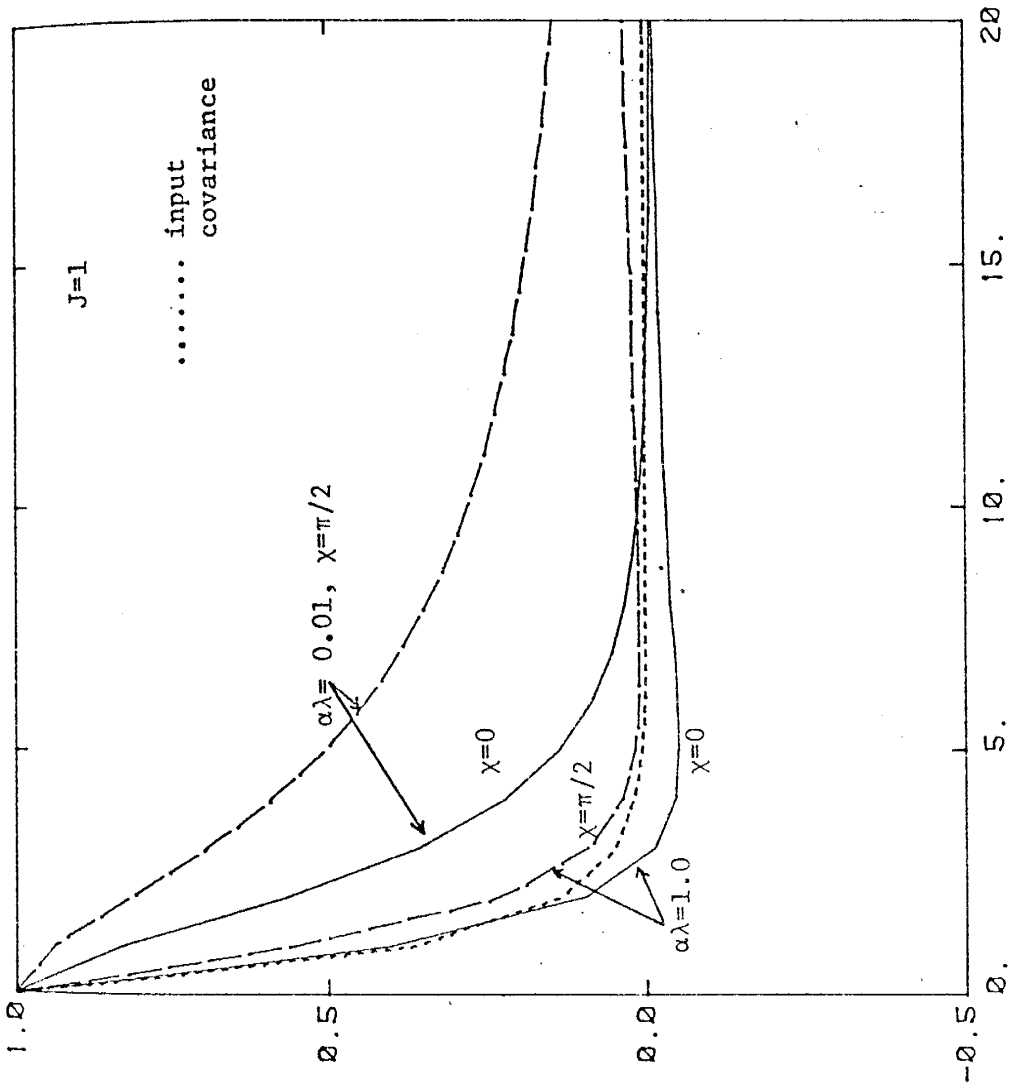

Figure 3.3.2: The covariance function (3.3.16) of three-dimensional head perturbations at different angles from the mean flow compared with that of $\ln K_s$.

3.4. Variance of Log Unsaturated Hydraulic Conductivity

Since the hydraulic conductivity is one of the important parameters in the flow equation, it is of interest to know the variation of the parameter in the random field under an unsaturated condition.

If the log of the unsaturated hydraulic conductivity is taken as a stochastic process, it can be expressed in terms of mean and perturbation as in (3.3.4):

$$\ln K = F + f - \alpha(H + h) \tag{3.4.1}$$

The corresponding equation describing the fluctuation of lnK is given by:

$$\ln K - E[\ln K] = f - \alpha h \tag{3.4.2}$$

The variance of lnK, then, can be directly obtained by

$$\sigma^2_{\ln K} = E[f^2] + \alpha^2 E[h^2] - 2\alpha E[fh] \tag{3.4.3}$$

$$= \sigma^2_f + [\alpha^2 - 2(\alpha\beta/J)]\sigma^2_h$$

since, for the one-dimensional case using (3.2.11), (3.2.13), and (3.2.16),

$$E[f\ h] = \int_{-\infty}^{\infty} E\left[dZ_f dZ_h^*\right] dk$$
$$= \int_{-\infty}^{\infty} \frac{J\beta S_{ff}}{k^2+\beta^2}\, dk = \frac{\sigma_f^2 \lambda J}{1+\lambda\beta} = \frac{\beta}{J}\sigma_h^2 \qquad (3.4.4)$$

This result is also valid for the one-dimensional case with the hole covariance function as well as the three-dimensional case as is easily shown by using (3.3.7). Substituting (3.2.16) and (3.2.20) for the one-dimensional head variance in (3.4.4), one can write the variances of one-dimensional unsaturated flow hydraulic conductivity resulting from a simple exponential autocovariance function (3.2.13) and a hole function (3.2.17) as,

$$\sigma_{lnK}^2 = \sigma_f^2\left[1+(\alpha^2-2\frac{\alpha\beta}{J})\frac{J^2\lambda}{\beta(1+\lambda\beta)}\right] \qquad (3.4.5a)$$

$$\sigma_{lnK}^2 = \sigma_f^2\left[1+(\alpha^2-2\frac{\alpha\beta}{J})\frac{J^2\eta^2}{(1+\beta\eta)^2}\right] \qquad (3.4.5b)$$

respectively. In the case of J = 1, (3.4.5) can be reduced to

$$\sigma_{lnK}^2 = \frac{\sigma_f^2}{(\alpha\lambda+1)}, \text{ and } \quad \sigma_{lnK}^2 = \sigma_f^2\left[\frac{(1+2\alpha\eta)}{(1+\alpha\eta)^2}\right] \qquad (3.4.6)$$

for the simple exponential covariance function and the hole

function inputs, respectively. To evaluate the variance of unsaturated hydraulic conductivity of the three- dimensional model, one has only to substitute the head variance of a three-dimensional model (3.3.13) into (3.4.4) for the σ_h^2. This gives:

$$\sigma_{\ln K}^2=\sigma_f^2\left[1+(\alpha^2-\frac{2\alpha\beta}{J})\frac{J^2\lambda^2}{(\beta\lambda)^2}\left[1-\frac{2\ln(1+\lambda\beta)}{\lambda\beta}+\frac{1}{1+\lambda\beta}\right]\right] \quad (3.4.7)$$

If J is equal to unity, the variance of the log of the unsaturated hydraulic conductivity can be expressed as

$$\sigma_{\ln K}^2 = \sigma_f^2\left[\frac{2\ln(1+\alpha\lambda)}{\alpha\lambda}-\frac{1}{1+\alpha\lambda}\right] \quad (3.4.8)$$

3.5 Effective Unsaturated Hydraulic Conductivity

Hydrologists or soil scientists often encounter the dilemma of space averaging of hydraulic conductivities in unsaturated heterogeneous porous media. Little investigation has been carried out on this subject. In this section, we will derive the effective hydraulic conductivity in both one- and three-dimensional flow systems based on the stochastic analysis.

To determine the effective hydraulic conductivity, the stochastic solutions obtained in the previous sections will be used. For one-dimensional flow the Darcy equation states that:

$$q = K\left[\frac{d\psi}{dz} + 1\right] \tag{3.5.1}$$

where q is the specific discharge. Using (3.2.5a) and (3.2.5b) this can be written as:

$$q = K_m e^{(f-\alpha h)}\left[\frac{d\psi}{dz} + 1\right] =$$

$$K_m(1+f-\alpha h+(f-\alpha h)^2/2+\cdots)\left[\frac{dH}{dz} + \frac{dh}{dz} + 1\right] \tag{3.5.2}$$

where $K_m = K_G\exp(-\alpha H)$, $\ln K_G = E[\ln K_s]$. Taking the expected value and neglect the third and higher order terms,

$$E[\,q\,] \simeq K_m\left[\,1+\tfrac{1}{2}E\left[(f-\alpha h)^2\right]\right]J$$

$$+\,K_m\,E\left[(f-\alpha h)\frac{dh}{dz}\right] \qquad (3.5.3)$$

where $J = 1 + \frac{dH}{dz}$ is the mean hydraulic gradient. The first expected value term on the right hand side of (3.5.3) is simply the variance of the logarithem of the unsaturated hydraulic conductivity, σ^2_{lnk}, as evaluated in section 3.4. If the exponential covariance function is used, the second expected value term can be determined as:

$$E\left[(f-\alpha h)\frac{dh}{dz}\right] = E\left[f\frac{dh}{dz}\right] = \int_{-\infty}^{\infty} E\left[dZ_f(-ik)dZ_h^*\right]dk$$

$$= \int_{-\infty}^{\infty} \frac{-Jk^2}{k^2+\beta^2}\,S_{ff}dk = -\,\frac{\sigma_f^2 J}{1+\lambda\beta}$$

since:

$$E\left[h\frac{dh}{dz}\right] = \int_{-\infty}^{\infty} E\left[dZ_h(-ik)dZ_h^*\right]dk = \int_{-\infty}^{\infty} \frac{-ikJ^2}{k^2+\beta^2}\,S_{ff}dk = 0,$$

Similarly, the hole covariance function produces:

$$E\left[(f-\alpha h)\frac{dh}{dz}\right] = -\,\frac{\sigma_f^2 J(1+2\beta\eta)}{(1+\beta\eta)^2}$$

Using these results, (3.5.3) can be written as:

$$E[q]/J = K_m\left[1+\frac{\sigma_f^2}{2}\left[1+(\alpha^2-\frac{2\alpha\beta}{J})\frac{J^2\lambda}{\beta(1+\lambda\beta)} - \frac{2}{1+\lambda\beta}\right]\right] \equiv K_e,$$

(3.5.4)

$$\text{and} \quad E[q]/J = K_m\left[1+\frac{\sigma_f^2}{2}\left[1+(\alpha^2-\frac{2\alpha\beta}{J})\frac{J^2\eta^2}{(1+\beta\eta)^2} - \frac{2(1+2\beta\eta)}{(1+\beta\eta)^2}\right]\right] \equiv K_e$$

for the effective hydraulic conductivities resulting from the exponential and the hole function covariances, respectively.

The right hand side of (3.5.4) is the effective hydraulic conductivity for one-dimensional flow, K_e, which when multiplied by the mean hydraulic gradient produces the mean moisture flux or specific discharge. Note, K_e is generally dependent on the mean hydraulic gradient; i.e., the mean Darcy equation is nonlinear. When $J = 1$, ($\beta = \alpha(2J-1) = \alpha$), (3.5.4) implies a relationship between the mean infiltration rate and the mean capillary pressure. Since $K_m = K_G\exp(-\alpha H)$ and $K_G=\exp E[\ln K_s]$ is the geometric mean of the saturated hydraulic conductivity. In this case, the effective conductivity of the unsaturated flow reduces to

$$K_e = K_G e^{-\alpha H}\left[1 - \frac{\sigma_f^2}{2(1+\alpha\lambda)}\right] \qquad (3.5.5a)$$

Using the relationships in (3.4.6), (3.5.5a) can be related to $\sigma^2_{\ln K}$ by

$$K_e = K_G e^{-\alpha H}\left[1 - \frac{\sigma^2_{lnk}}{2}\right] \qquad (3.5.5b)$$

Equation (3.5.5b) represents the mean or effective conductivity-capillary pressure relationship for steady vertical infiltration through a perfectly stratified heterogeneous soil of unbounded vertical extent.

Note that as $\sigma_f^2/[2(1+\alpha\lambda)]>1$, K_e becomes negative. This impossible result can be ascribed to the neglect of higher order terms in (3.5.2). For the saturated flow case, Gutjahr et al. (1978) found an 18 percent error in this type of first order approximation for one-dimensional flow perpendicular to layering with a log-normally distributed K and $\sigma_f^2=1$. For the unsaturated flow case, the error due to the approximation depends on σ_f^2, α, and λ for J=1. Although we can not quantify the magnitude of $\sigma_f^2/[2(1+\alpha\lambda)]$ in natural soil formations, it is expected that its value for many hydrologic media is likely greater than 1. One possible way to circumvent this difficulty is to consider the quantities in brackets in (3.5.4) and (3.5.5) as the first two terms of the Taylor series expansion for e^x (Gelhar and Axness, 1981). Therefore, for $\sigma_f^2/[2(1+\alpha\lambda)] >1$, equation (3.5.5) becomes

$$K_e = K_G \exp\{-\alpha H-[\sigma_f^2/2(1+\alpha\lambda)]\} \qquad (3.5.6)$$

The more general formula (equation (3.5.4)) in which J is not restricted to be 1, then, can be expressed as:

$$K_e = K_G \exp\left\{-\alpha H + \frac{\sigma_f^2}{2}\left[1+(\alpha^2 - \frac{2\alpha\beta}{J})\frac{J^2\lambda}{\beta(1+\lambda\beta)} - \frac{2}{1+\lambda\beta}\right]\right\} \qquad (3.5.7a)$$

The same exponential generalization can also apply to the effective hydraulic conductivity obtained from the hole covariance function which is given by:

$$K_e = K_G \exp\left\{-\alpha H + \frac{\sigma_f^2}{2}\left[1+(\alpha^2 - \frac{2\alpha\beta}{J})\frac{J^2\eta^2}{(1+\beta\eta)^2} - \frac{2(1+2\beta\eta)}{(1+\beta\eta)^2}\right]\right\} \qquad (3.5.7b)$$

A similar analysis is carried out for the case of three-dimensional isotropic variation in saturated hydraulic conductivity represented by the covariance in (3.3.10). The procedure is identical to that of the one-dimensional case although the integrations are more involved. If we assume the mean gradient only exists in the x_1 direction, Darcy's flux in this direction takes the form

$$\begin{aligned} q_1 &= K_m e^{(f-\alpha h)}(J_1 + \frac{\partial h}{\partial x_1}) \\ &= K_m[1 + (f-\alpha h) + (f-\alpha h)^2/2 + \cdots](J + \frac{\partial h}{\partial x_1}) \end{aligned} \qquad (3.5.8)$$

Taking the expected value of (3.5.8) and neglecting the higher order terms, the mean flux in this direction is given

by:

$$E[q_1] = K_m\left[1 + \frac{E[(f-\alpha h)]^2}{2}\right]J_1 + E\left[(f-\alpha h)\frac{\partial h}{\partial x_1}\right] \quad (3.5.9)$$

where $E[(f - \alpha h)^2] = \sigma^2_{lnK}$ (see (3.4.3)). Since the covariance of h and $\partial h/\partial x_1$ is zero, the last term of the right hand side of (3.5.9) can be determined as follows:

$$E[fj] = E\left[f\frac{\partial h}{\partial x_1}\right] = \iiint_{-\infty}^{\infty} S_{f\,j}(\vec{k})d\vec{k}$$
$$= \frac{-J_1\sigma_f^2\lambda^3}{\pi^2}\iiint_{-\infty}^{\infty}\frac{(k_1^2k^2+ik_1^3\beta)dk_1dk_2dk_3}{(k^4+k_1^2\beta^2)(k^2\lambda^2+1)^2} \quad (3.5.10a)$$

This results in the cross-covariance of f and $\partial h/\partial x_1$=J, and it is given as:

$$E[fj] = J_1\sigma_f^2\left\{\frac{2}{y^2}\left[1 - \frac{2\ln|1+y|}{y} + \frac{1}{1+y}\right] - \frac{1}{1+y}\right\} \quad (3.5.10b)$$

where y is $\lambda\beta$. The detailed derivation of (3.5.10) can be found in Appendix E. Thus, the effective hydraulic conductivity for the three-dimensional flow case:

$$E[q_1]/J_1 = K_e = K_G e^{-\alpha H}\left[1 + \frac{\sigma^2_{\ln k}}{2} + \frac{E[f_j]}{J_1}\right] \quad (3.5.11)$$

when $J_1 = 1$, (3.5.11) can be simplified into the form:

$$K_e = K_G e^{-\alpha H}\left\{1 + \sigma_f^2\left[\frac{\ln(1+\alpha\lambda)}{\alpha\lambda} - \frac{1}{2(1+\alpha\lambda)} + \frac{3}{(\alpha\lambda)^2}\right.\right. \quad (3.5.12)$$

$$\left.\left. - \frac{1}{\alpha\lambda} - \frac{4\ln(1+\alpha\lambda)}{(\lambda\alpha)^3} + \frac{1}{(\alpha\lambda)^2(1+\alpha\lambda)}\right]\right\}$$

Using the exponential approach given in (3.5.6) and (3.5.7) to generalize (3.5.12), this results in

$$K_e = K_G \exp\left\{-\alpha H + \sigma_f^2\left[\frac{\ln(1+\lambda\alpha)}{\alpha\lambda} - \frac{1}{2(1+\alpha\lambda)} + \frac{3}{(\alpha\lambda)^2}\right.\right. \quad (3.5.13)$$

$$\left.\left. - \frac{1}{\alpha\lambda} - \frac{4\ln(1+\alpha\lambda)}{(\lambda\alpha)^3} + \frac{1}{(\alpha\lambda)^2(1+\alpha\lambda)}\right]\right\}$$

Figure (3.5.1) shows the effective hydraulic conductivities (3.5.6) and (3.5.13) of one- and three-dimensional models as a function of the magnitude of the σ_f^2. The dependence of effective hydraulic conductivity on the mean gradient is demonstrated in Figure (3.5.2)

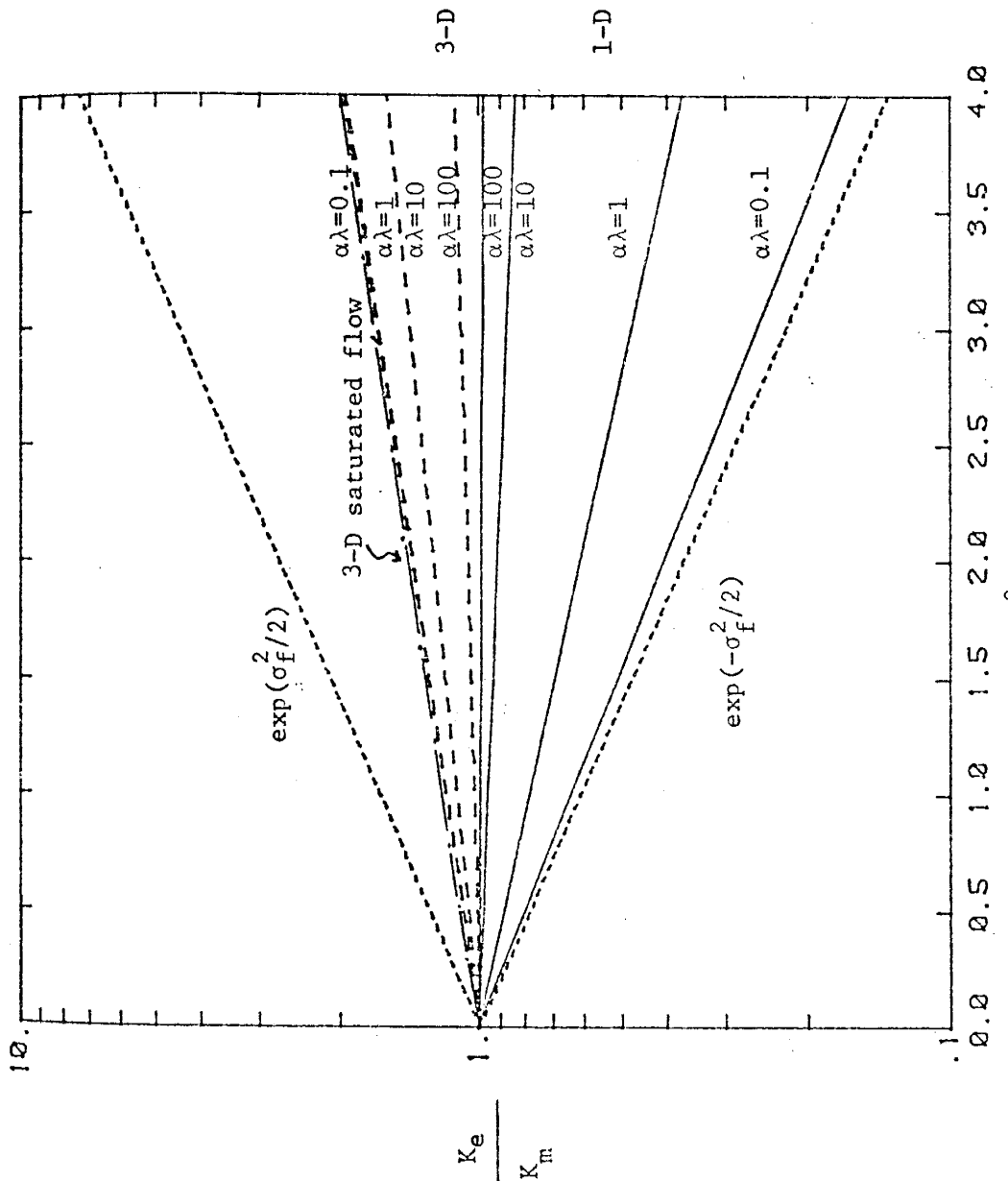

Figure 3.5.1: Ratio between effective hydraulic conductivities (3.5.7a) and (3.5.13) and geometric mean of saturated hydraulic conductivity, K_m.

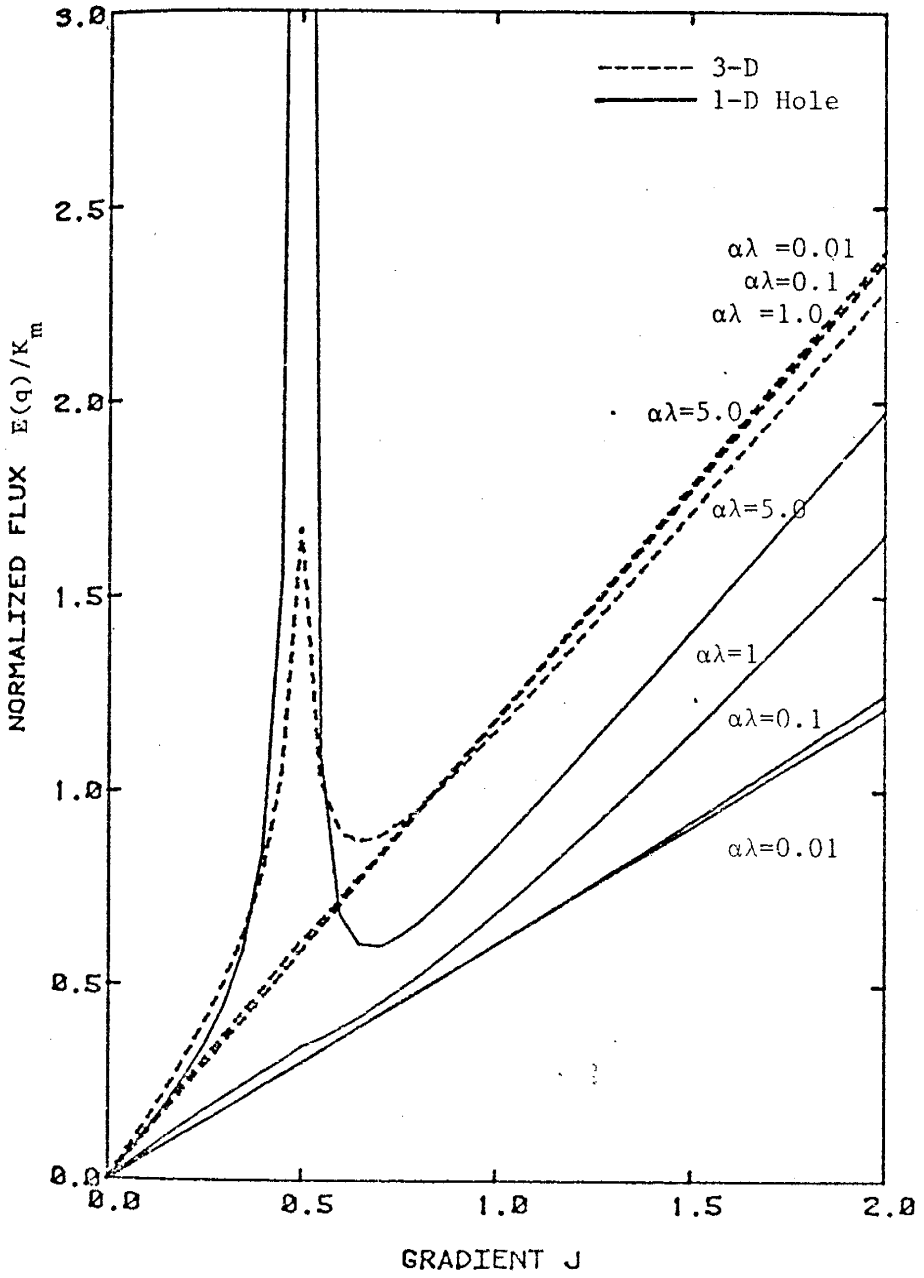

Figure 3.5.2: Comparison of the non-linearity of one- and three-dimensional Darcy's fluxes, (3.5.7b) and (3.5.13), respectively.

3.6 Flux Variance

Subtracting (3.5.9) from (3.5.8), and neglecting the higher order terms, the equation describing the fluctuation of the flux is in the form:

$$q_1' \simeq K_m\left[J(f - \alpha h) + \frac{\partial h}{\partial x_1}\right] \qquad (3.6.1)$$

If (3.6.1) is represented by the stochastic Fourier-Stieltjes integral, the relationship among the Fourier amplitudes of the perturbations q_1', f, and h is derived as:

$$dZ_{q_1'} = K_m\left[J dZ_f - (\alpha J - ik_1) dZ_h\right] \qquad (3.6.2)$$

Then the corresponding spectral relationship is

$$S_{q_1'} = K_m^2\left[J^2 S_{ff} - 2\alpha J^2\ \mathrm{Re}[S_{fh}] + 2J\ \mathrm{Re}[S_{fj}] + (\alpha^2 J^2 + k_1^2) S_{hh}\right] \qquad (3.6.3)$$

where Re denotes the real part of the spectrum. The variance of q_i' can be obtained by taking a Fourier transform of (3.6.3) with the specified covariance function for f process, (in this case (3.3.9) is used). The resulting variance of q_1' is

$$\sigma^2_{q_1'} = K_m^2 \sigma_f^2 J^2 \left[1 - \frac{3}{2\lambda\beta} + \frac{5}{(\lambda\beta)^2} + \frac{2}{(\lambda\beta)^3} - \frac{5}{(\lambda\beta)^4} + \right.$$

$$\frac{\ln(1+\lambda\beta)}{(\lambda\beta)^3}\left[-8 + \frac{6}{(\lambda\beta)^2}\right] + \frac{2}{(\lambda\beta)^2(1+\lambda\beta)} - \frac{1}{(\lambda\beta)^4(1+\lambda\beta)} \quad (3.6.4)$$

$$\left. - \frac{\alpha^2\lambda^2 J(3J-2)}{(\lambda\beta)^2}\left[1 - \frac{2\ln(1+\lambda\beta)}{\lambda\beta} + \frac{1}{1+\lambda\beta}\right]\right]$$

The details of the derivation of (3.6.4) are given in Appendix F. The variance of flux perpendicular to the mean gradient, J, is evaluated as follows:

$$q_2' = K_m \, e^{(f-\alpha h)} \frac{\partial h}{\partial x_2}$$

$$\simeq K_m (1 + (f - \alpha h) + \cdots) \frac{\partial h}{\partial x_2} \quad (3.6.5)$$

The corresponding spectral relationship of perturbations of q_2' and h is of the form

$$S_{q_2'} = K_m^2 \, (k_2^2 S_{hh}) \quad (3.6.6)$$

The variance of q_2' is obtained by integrating (3.6.6) over the wave number $\vec{k}$ (see Appendix G).

$$\sigma^2_{q_2'} = K_m^2 \frac{J^2 \sigma_f^2 \lambda^3}{\pi^2} \iiint_{-\infty}^{\infty} \frac{k_1^2 k_2^2}{(1+k^2\lambda^2)^2 (k^4+\beta^2 k_1^2)} dk_1 dk_2 dk_3$$

This results in

$$\sigma^2_{q_2'} = \frac{K_m^2 J^2 \sigma_f^2}{2} \left\{ \frac{6}{(\lambda\beta)^4} - \frac{3}{(\lambda\beta)^3} - \frac{2}{(\lambda\beta)^2} + \frac{1}{2\lambda\beta} + \right. \tag{3.6.7}$$

$$\left. \frac{\ln(1+\lambda\beta)}{(\lambda\beta)^3} \left[4 - \frac{6}{(\lambda\beta)^2} \right] \right\}$$

To demonstrate the effects of $\alpha\lambda$ on the results, the ratio of $\sigma^2_{q_1'}$ and $\sigma^2_{q_2'}$ as well as $\sigma^2_{q_1'}$ and $\sigma^2_{q_2'}$ are evaluated for the case of $J = 1$ as a function of $\alpha\lambda$ and are displayed in Figure (3.6.1). Note that for small $\alpha\lambda$ the ratio $\sigma^2_{q_2'} / \sigma^2_{q_1'}$ is 1/8, the saturated flow value. For large $\alpha\lambda$, reflecting unsaturated flow effects, the ratio $\sigma^2_{q_2'} / \sigma^2_{q_1'}$ decreases; this trend of decreasing transverse flow variation further shows the tendency toward one-dimensional flow.

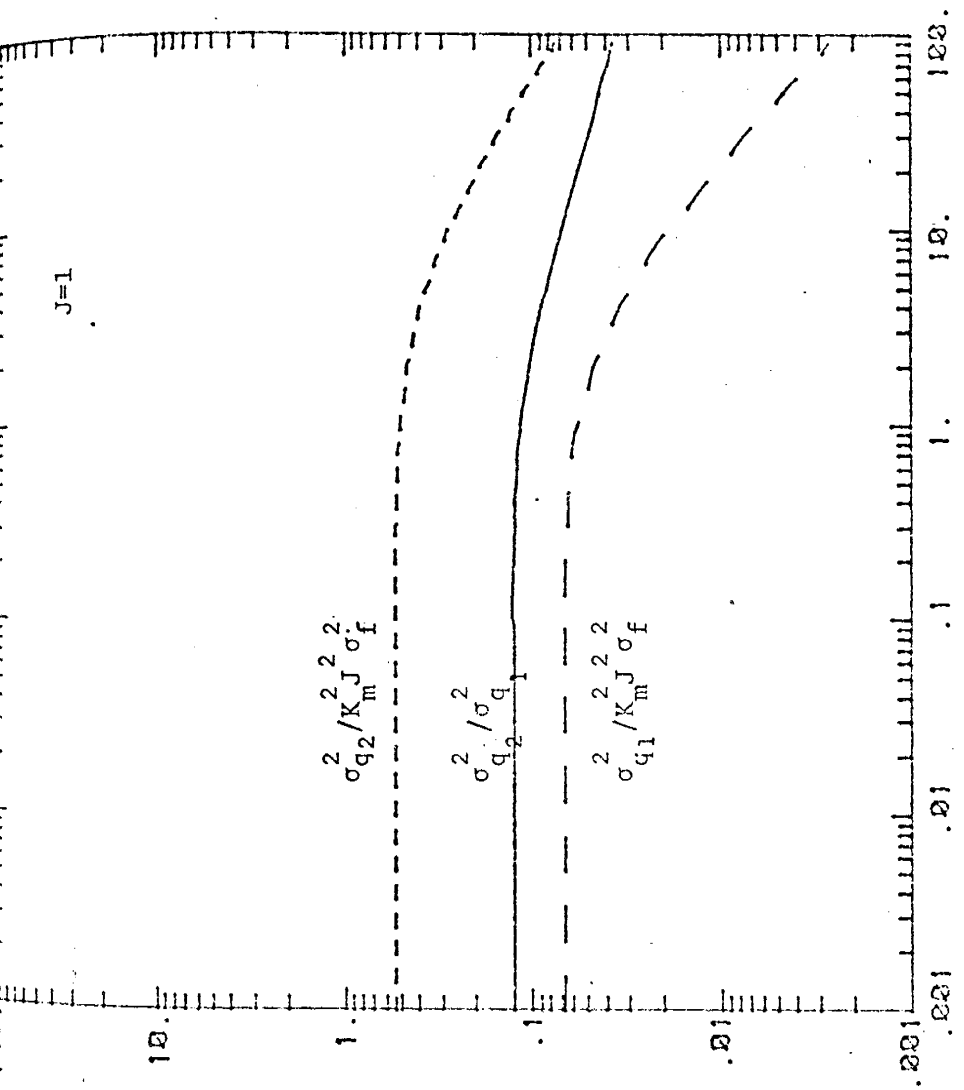

Figure 3.6.1: Comparison of longitudinal and transverse flux variances of the three-dimensional flows.

3.7 Variance of Pressure Gradient

In practice, hydrologists or soil scientists often assume that capillary pressure gradient is negligible (unit hydraulic gradient), One may question the validity of this assumption, especially in soils exhibiting a large degree of variation. Thus, evaluation of pressure gradient variation through this theoretical analysis may provide some useful information on the pressure gradient in the natural soil.

For one-dimensional flow, the Fourier amplitude relationship between pressure gradient and pressure head is given as

$$dZ_j = ikdZ_h \tag{3.7.1}$$

Multiplying (3.7.1) by its complex conjugate and then taking its expected value results in the spectral relationship,

$$S_{jj} = k^2 S_{hh} = \frac{k^2 S_{ff}}{k^2 + \beta^2} \tag{3.7.2}$$

To evaluate the variance of j process, we integrate its spectrum. The variance σ_j^2, if the exponential covariance function is used, is

$$\sigma_j^2 = \frac{J^2\sigma_f^2}{\lambda\beta(1 + \lambda\beta)} \tag{3.7.3}$$

If the hole function is employed, the variance is

$$\sigma_j^2 = \frac{J^2\sigma_f^2}{(1 + \beta\eta)^2} \tag{3.7.4}$$

Similarly the variance of the pressure gradient resulting from the three-dimensional model is evaluated in Appendix F and can be expressed as

$$\sigma_j^2 = J^2\sigma_f^2\left[\frac{1}{2y} - \frac{1}{y^2} + \frac{2}{y^3} - \frac{5}{y^4} - \frac{1}{y^5}\left(\frac{y}{1+y} - 6\ln|1+y|\right)\right] \tag{3.7.5}$$

Where $y = \lambda\beta$. These results are shown in Figure (3.7.1).

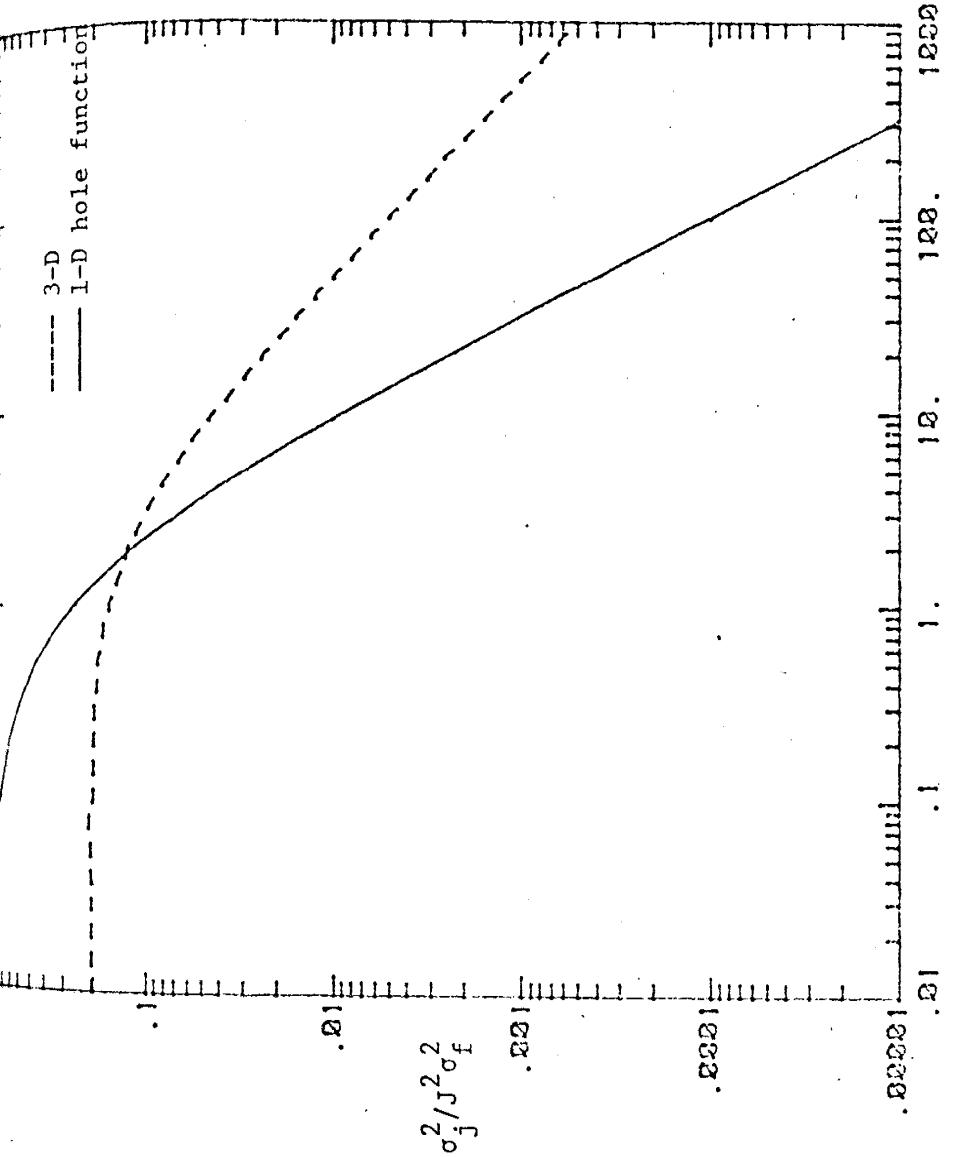

Figure 3.7.1: Comparison of one- and three-dimensional gradient variances, (3.7.4) and (3.7.5), respectively.

3.8 Summary and Discussion of the Results

One- and three-dimensional steady-state infiltration through unbounded media of statistically homogeneous and isotropic saturated hydraulic conductivity fields are investigated in this chapter. A simple exponential function is used to describe the relationship between unsaturated hydraulic conductivity and capillary pressure head. Assuming that the pore-size distribution parameter, α, is a deterministic constant, the head variances and covariance functions, effective hydraulic conductivities, variances of the hydraulic conductivity, flux variances, and variance of pressure gradient are determined by utilizing the spectral method. The results and their physical significance are discussed below.

Figure (3.2.2) shows the normalized head variance at J=1 as a function of the product of the pore-size distribution parameter and the correlation length scale, i.e., $\alpha\lambda$. To determine the effect of input covariance functions on the outputs, the length scale of the hole function in one-dimensional case is assumed to be 2.5 times that of the simple exponential covariance function in three-dimensional case, i.e. $\eta = 2.5\lambda$ (Bakr, et al 1978). Physically, α^{-1} can be considered as the thickness of capillary fringe of soil(Bouwer, 1958). Typical ranges for α^{-1} and λ (see Bouwer, 1975, and Bakr, 1976) are 0.2 to 2 m for both parameters; therefore the practical range of $\alpha\lambda$ would be from 0.1 to 10. Within that range, Figure (3.2.2) shows that the two one-

dimensional input covariance functions, the exponential and the hole functions, produce practically the same head variance. For a small value of $\alpha\lambda$, the head variance resulting from the exponential function approaches infinity as indicated by the one to one slope of the curve, whereas the hole function produces a finite head variance. In addition, the head variances obtained from the two input functions at the limit ($\alpha = 0$) are consistent with that of saturated flow (see Bakr et al., 1978). In fact, in this case, the flow equation (3.2.9) is equivalent to the saturated flow case of Bakr et al (1978). However, it is not appropriate to conclude that the head variance in the steady infiltration process should result in the same head variance as the saturated flow case. This is shown by (3.2.4a), where the product of α and head perturbation h does not necessarily vanish even though the mean capillary pressure head is zero. It means that the porous medium is not completely saturated due to the presence of the perturbation of the capillary pressure head. The assumption that $\alpha = 0$ bears no physical significance in practice. It simply brings about the mathematical equivalence of the equations at this particular case. It is also of interest to know that the governing one-dimensional steady state infiltration equation (3.2.7), in terms of capillary pressure head and log saturated conductivity perturbations, can be rearranged to:

$$\frac{d^2h}{dz^2} + \frac{dH}{dz}\frac{df}{dz} - 2\alpha\frac{dH}{dz}\frac{dh}{dz} + \left[\frac{df}{dz} - \alpha\frac{dh}{dz}\right] = 0 \qquad (3.8.1)$$

and can be compared to the horizontal absorption case:

$$\frac{d^2h}{dz^2} + \frac{dH}{dz}\frac{df}{dz} - 2\alpha\frac{dH}{dz}\frac{dh}{dz} = 0 \qquad (3.8.2)$$

The additional term on the left hand side of (3.8.1), then can be thought of the gravity term, which consists of the effects of the hydraulic conductivity and the capillary pressure head perturbation gradients, namely, $\frac{df}{dz}$ and $\frac{dh}{dz}$, respectively. The relationship between head variance and α becomes evident. When α becomes large, the resistance due to the variation in saturated conductivity is significantly reduced by the head perturbation gradient, which is amplified by the magnitude of α. In other words, the gravity term becomes dominant and the head variance is reduced.

The reduction of head variance at large values of $\alpha\lambda$ can be further elaborated through a "conditional analysis". Assume that soil formation is composed of a collection of soil columns: interaction between columns is neglected. Each individual column is assumed to be homogeneous. Darcy's law for each column, thus, can be written as:

$$q = K(\psi)\left(\frac{d\psi}{dz} + 1\right)$$

If $d\psi/dz$ is equal to 0, the above expression can be further simplified to:

$$q = K(\psi) = K_s e^{-\alpha\psi}$$

This equation yields the expression for the soil capillary pressure head:

$$\psi = \frac{\ln K_s}{\alpha} - \frac{\ln q}{\alpha}$$

Since the flux is constant, the variance of capillary pressure head is of the form:

$$\sigma_\psi^2 = \frac{\sigma_f^2}{\alpha^2}$$

Note that the head variance in the above equation is a result of variation in saturated hydraulic conductivity among soil column. Since each columns is homogeneous, and the correlation scale of the saturated hydraulic conductivity of each column is infinite.

This same result is found from the spatially variable stochastic anaylsis, (3.2.16), when $\beta\lambda=\alpha\lambda>>1$ with J=1; however this case could also be interpreted as one with fixed λ much smaller than the overall scale of the problem and $\alpha\lambda$ large because of the soil type. Both interpretations

demonstrated the head variance reduction when α is large. Note that when $\alpha\lambda >> 1$ the stochastic result, (3.2.16), shows the head variance to be independent of the correlation scale. This behavior is in contrast to the saturated flow case when the head variance increase as λ^2 (Bakr et al., 1978).

Figure (3.2.2) also shows that the head variance derived from the three- dimensional model approaches the saturated flow result as $\alpha\lambda$ becomes zero. For large values of $\alpha\lambda$, the one- and three- dimensional results are identical, indicating that the flow is predominantly one-dimensional under this condition. Comparing the one- and three- dimensional flow equations (3.2.9) and (3.3.5), it is clear that under this circumstance the gradient of the head perturbation terms in the z direction turns out to be more important in the flow system. Therefore, we may expect that the one-dimensional result may be appropriate for some field applications, especially for coarse texture soils which generally are associated with large values of α. Furthermore, soils are often horizontally stratified. However, for fine texture material, such as clay and silt, often characterized by small values of α, one-dimensional results may not be appropriate. The three-dimensional analysis produces a smaller head variance in this type of soil. Hence, for fine textured soils, significant errors could be introduced if results from a one-dimensional model are used to draw a conclusion on the effect of field heterogeneity on the flow

properties. The system, in fact, is inherently three- dimensional.

The head covariance functions resulting from one-dimensional analysis are illustrated in Figure (3.2.1) along with the dimensionless separation distance. It demonstrates that the mathematical filtering effect is directly related to the magnitude of $\alpha\lambda$. When its value is small, the head perturbations tend to correlate for a large distance. Conversely, the output covariance function tends to have the same correlation length scale as that of the input covariance when $\alpha\eta$ is large, although the magnitude of the variance is reduced. The hole effect (negative correlation) on the output also becomes evident. In Figure (3.3.2) the head covariance function of the three-dimensional model given by (3.3.16) is evaluated for several different values of the angle χ and $\alpha\lambda$. One should notice that the head perturbation in this case is anisotropic, even though the input log saturated hydraulic conductivity perturbation is isotropic. The perturbations of the head process in the direction perpendicular to the mean flow ($\chi = \pi/2$) have consistently higher correlation values than in the direction parallel to the mean flow, particularly for small values of $\alpha\lambda$. Yet, the difference in the correlation values in both directions diminishes as $\alpha\lambda$ becomes large. Furthermore the fluctuations in head in the direction parallel to the mean flow direction tend to exhibit the hole effect at large $\alpha\lambda$ values, when the exponential covariance function (3.3.9) is

used. This further confirms the finding that the infiltration process in coarse texture soils is simply a one-dimensional phenomenon. Conversely, in fine texture soils, water will dissipate laterally in response to the lateral head perturbation gradient and the process becomes three-dimensional.

The variance of log-unsaturated hydraulic conductivity as indicated by (3.4.5) and (3.4.7) is found to decrease with $\lambda\beta$. This is consistent with the previous finding on head variance in unsaturated flow.

The effective hydraulic conductivities determined from the one-and three-dimensional models are shown graphically in Figure (3.5.1). It is seen that the effective hydraulic conductivities approach the one- and three- dimensional saturated flow limits found by Gutjahr et al. (1978), as $\alpha\lambda$ becomes small. In addition, they are bounded by both the harmonic and arithmetic mean of saturated hydraulic conductivities. Note also that for large $\alpha\lambda$ both one- and three-dimensional effective hydraulic conductivities approach $K_G e^{-\alpha H}$. One of the interesting features of the effective hydraulic conductivity of unsaturated flow is its dependence on the magnitude of $\alpha\lambda$. This situation is not true in the saturated flow case. From (3.5.5), one can see that the increase of $\alpha\lambda$ reduces the value of $\sigma^2_{\ln K}$.

In the case of flow perpendicular to the bedding, Gutjahr et al. (1978) have found that the effective

hydraulic conductivity for the saturated flow situation is the harmonic mean of the saturated hydraulic conductivity. Similarly, equation (3.5.5) tells us in an unsaturated flow situation, the harmonic mean of the unsaturated hydraulic conductivity of layers is the equivalent effective hydraulic conductivity. However, the analog is not clear for three-dimensional unsaturated hydraulic conductivity.

The non-linear nature of unsaturated Darcy's flow is shown in Figure (3.5.2). The dependence of flux on the gradient in the three-dimensional case is insignificant as compared to that in the one-dimensional case. The non-linearity in the one-dimensional flux grows with $\alpha\lambda$. At large $\alpha\lambda$ values, the behavior of the Darcy's flux in both cases becomes erratic near J=1. This erratic behavior might be attributed to the neglect of product of perturbations in the analysis.

As expected, the variance of flux in the lateral direction diminishes relative to that in the direction of flow as the pore-size distribution parameter becomes large (Figure 3.6.1). This is also an indication of the dominance of gravitational flow in coarse-textured soil.

The variation of pressure gradient also can be related to $\alpha\lambda$ as illustrated in Figure (3.7.1). One-dimensional analysis produces a variance of the magnitude of $J^2\sigma_f^2$, and three-dimensional analysis results in a smaller capillary pressure gradient variation, which is about 2/5 of the one-dimensional result. As the value of $\alpha\lambda$ increases, the vari-

ance resulting from one-dimensional analysis is reduced rapidly as indicated by a two to one slope in the figure. However, the reduction rate of pressure variance in the three-dimensional result is linearly proportional to the magnitude of $\alpha\lambda$.

The results discussed above lead to a definitive conclusion that the variance of log-saturated hydraulic conductivity, its correlation scale, λ, the hydraulic gradient, and the pore-size distribution parameter are the essential elements controlling the effect of spatial variability of saturated hydraulic conductivity on the infiltration process. In addition, for large $\alpha\lambda$ the flow becomes essentially one-dimensional.

CHAPTER 4

FLOW IN STATISTICALLY ANISOTROPIC MEDIA WITH A DETERMINISTIC PORE-SIZE DISTRIBUTION PARAMETER

4.1 Introduction

In the previous chapter, we have analyzed unsaturated flow in statistically isotropic media. However, natural soils or geologic formations tend to exhibit bedding. It is therefore more realistic to assume the media are statistically anisotropic, especially the large scale media dealt with in this study.

In general, statistical anisotropy means that the correlation scales of a stochastic process are not equal in all directions. Hydraulic conductivity, for example, usually correlates at a longer distance in the direction parallel to bedding than in the direction perpendicular to bedding. Presently available data are adequate to quantify the anisotropy in natural soil formations. Smith (1980) measured the hydraulic conductivity of samples collected from both horizontal and vertical profiles of the Quadra Sand outcrop in Vancouver, B.C.. These data indicate that the correlation scale of hydraulic conductivity in the horizontal profile is an order of magnitude larger than that of vertical. Correlation scales of the mean diameter of Torrifluvent are examined by Gajem, (1980). He reports correlation scales obtained from two perpendicular transects in the horizontal plane to be 18 and 2 meters. Thus, these findings indicate

the necessity to extend the analysis to statistically anisotropic media.

This chapter deals mainly with the evaluation of head variance and effective hydraulic conductivity in statistically anisotropic media. The anisotropy is defined by the aspect ratio of the correlation scales of log-saturated hydraulic conductivity of the medium. Effects of the aspect ratio of the medium, which is the ratio of horizontal to vertical correlation scales, on the head variance and the effective hydraulic conductivity are determined for the case where the mean gradient is normal to stratification. The last section of this chapter examines the head variance and effective hydraulic conductivity of anisotropic media with arbitrarily oriented stratification.

4.2 Flow in Anisotropic Media with Flow Perpendicular to Bedding.

The general three-dimensional steady flow equation can be written as:

$$\frac{\partial}{\partial x_i}\left(K \frac{\partial \Phi}{\partial x_i}\right) = 0, \qquad i = 1,2,3 \tag{4.2.1}$$

where K is the hydraulic conductivity (assumed locally isotropic), and $\Phi = -x_1 - \Psi$. Here, the Einstein summation convention is used. Expanding and dividing by the nonzero conduc-

tivity, we can rewrite (4.2.1) as

$$\frac{\partial^2 \Phi}{\partial x_i^2} + \frac{\partial \ln K}{\partial x_i} \frac{\partial \Phi}{\partial x_i} = 0 \qquad (4.2.2)$$

By substituting $-x_1 - \Psi$ for Φ, one can obtain

$$\frac{\partial^2 \Psi}{\partial x_i^2} + \frac{\partial \ln K}{\partial x_1} + \frac{\partial \ln K}{\partial x_i} \frac{\partial \Psi}{\partial x_i} = 0 \qquad (4.2.3)$$

Then, the mean flow equation is derived by following the procedure used in the previous analysis (section 3.3).

$$\nabla^2 H + \frac{\partial (F - \alpha H)}{\partial x_1} + \nabla (F - \alpha H) \cdot \nabla H + \overline{\nabla (f - \alpha h) \cdot \nabla h} = 0 \qquad (4.2.4)$$

where the overbar denotes the expected value.

If we let

$$J_1 = 1 + \frac{\partial H}{\partial x_1}, \quad J_2 = \frac{\partial H}{\partial x_2}, \text{ and } J_3 = \frac{\partial H}{\partial x_3} \qquad (4.2.5)$$

and neglect terms involving the product of perturbations, the equation describing the relationship between head and saturated hydraulic conductivity perturbations is given as

$$\nabla^2 h + J_i \frac{\partial f}{\partial x_i} - 2\alpha J_i \frac{\partial h}{\partial x_i} + \alpha \frac{\partial h}{\partial x_1} = 0 \qquad (4.2.6)$$

By using the Fourier-Stieltjes representation, one can obtain the relationship between capillary pressure head and hydraulic conductivity Fourier amplitudes:

$$dZ_h = \frac{iJ_j k_j dZ_f}{[k^2 + i\alpha(2J_j k_j - k_1)]} \qquad (4.2.7)$$

To simplify the analysis, the mean hydraulic gradient is assumed to exist in the vertical direction x_1 only. ($J_1 \neq J_2 = J_3 = 0$). (4.2.7) thus can be transformed to the following expression in terms of the spectra of head and hydraulic conductivity perturbations:

$$S_{hh} = \frac{J_1^2 k_1^2 S_{ff}}{(k^4 + \beta^2 k_1^2)} \qquad (4.2.8)$$

where $\beta = \alpha(2J_1 - 1)$.

A three-dimensional anisotropic covariance function is selected for the saturated hydraulic conductivity random field to evaluate (4.2.8). This covariance function takes the form:

$$R_{ff}(\vec{\xi}) = \exp\left[- \left[\frac{\xi_1^2}{\lambda_1^2} + \frac{\xi_2^2}{\lambda_2^2} + \frac{\xi_3^2}{\lambda_3^2} \right]^{1/2} \right] \qquad (4.2.9)$$

where λ_1, λ_2, and λ_3 are the correlation scales in the x_1, x_2, and x_3, respectively. Figure (4.3.1) illustrates the ellipsoid resulting from such anisotropic correlation scales.

The corresponding spectrum S_{ff} of $\ln K_s$ is obtained by taking the inverse Fourier transform of R_{ff}, i.e.,

$$S_{ff} = \frac{1}{2\pi} \int_{-\infty}^{\infty} e^{-i\vec{k}\cdot\vec{\xi}} R_{ff}(\vec{\xi}) \, d\vec{\xi}$$

This results in

$$S_{ff} = \frac{\sigma_f^2 \lambda_1 \lambda_2 \lambda_3}{\pi^2 (1 + \lambda_1^2 k_1^2 + \lambda_2^2 k_2^2 + \lambda_3^2 k_3^2)^2}$$

The spectrum S_{hh} of fluctuations in capillary pressure head, therefore is:

$$S_{hh} = \frac{J_1^2 \sigma_f^2 \lambda_1 \lambda_2 \lambda_3 k_1^2}{\pi (k^4 + \beta^2 k_1^2)(1 + \lambda_1^2 k_1^2 + \lambda_2^2 k_2^2 + \lambda_3^2 k_3^2)^2} \qquad (4.2.10)$$

Further assume that the hydraulic conductivity

variation is isotropic in the horizontal plane, i.e., $\lambda_1 \neq \lambda_2 = \lambda_3 = \lambda$, for convenience. The capillary pressure head variance σ_h^2 is obtained by integrating the spectrum (4.2.10), (details are given in Appendix H). The general form of the head variance is:

$$\sigma_h^2 = J_1^2 \sigma_f^2 \lambda_1^2 \rho^4 \int_0^1 \frac{t^2\, dt}{[(\rho^2 - 1)t^2 + \rho^2 g t + 1]^2} \qquad (4.2.11)$$

where $\rho = \frac{\lambda}{\lambda_1}$; aspect ratio, $g = \lambda_1 \beta$; and $\beta = \alpha(2J_1 - 1)$. By integrating the right hand side of equation (4.2.11), the capillary pressure head variance is derived:

(A) if $[\rho^4 g^2 - 4(\rho^2 - 1)] \geq 0$

$$\sigma_h^2 = J_1^2 \sigma_f^2 \lambda_1^2 \rho^4 \left[\frac{(\rho^2 g + 2)}{[\rho^4 g^2 - 4(\rho^2 - 1)](\rho^2 + \rho^2 g)} + \frac{2}{[\rho^4 g^2 - 4(\rho^2 - 1)]^{3/2}} \right.$$

$$\left. \ln \left| \frac{[2(\rho^2 - 1) + \rho^2 g + [\rho^4 g^2 - 4(\rho^2 - 1)]^{1/2}]}{[2(\rho^2 - 1) + \rho^2 g - [\rho^4 g^2 - 4(\rho^2 - 1)]^{1/2}]} \right. \right.$$

$$\left. \left. \frac{[\rho^2 g - [\rho^4 g^2 - 4(\rho^2 - 1)]^{1/2}]}{[\rho^2 g + [\rho^4 g^2 - 4(\rho^2 - 1)]^{1/2}]} \right| \right] \qquad (4.2.11a)$$

(B) if $[\rho^4 g^2 - 4(\rho^2 - 1)] \leq 0$

$$\sigma_h^2 = J_1^2 \sigma_f^2 \lambda_1^2 \rho^4 \left\{ \frac{(\rho^2 g + 2)}{[4(\rho^2 - 1) - \rho^4 g^2](\rho^2 + \rho^2 g)} + \frac{4}{[4(\rho^2 - 1) - \rho^4 g^2]^{3/2}} \right.$$

$$\left. \left[\tan^{-1} \frac{-2\rho^2 - 2 + \rho^2 g}{[4(\rho^2 - 1) - \rho^4 g^2]^{1/2}} - \tan^{-1} \frac{\rho g}{[4(\rho^2 - 1) - \rho^4 g^2]^{1/2}} \right] \right\} \qquad (4.2.11b)$$

The effects of aspect ratio, ρ, on the variance of the capillary pressure head are shown in Figure (4.2.1).

To determine the effective hydraulic conductivity, it is necessary to evaluate $E[fh]$, and $E[f\partial h/\partial x_1]$ (see (3.5.9)). The previous analyses show that $E[fh]=(\beta/J)\sigma_h^2$ (see (3.4.4)). Using (4.2.9) for the hydraulic conductivity covariance function and following the procedure used in the previous chapter,

$$E[fj] = E\left[f\frac{\partial h}{\partial x_1}\right] = J_1 \sigma_f^2 \rho^2 \left[\frac{2\sigma_h^2}{\lambda_1^2 J_1^2 \sigma_f^2 \rho^4} - \frac{1}{\rho^2 (g+1)} \right] \qquad (4.2.12)$$

Details of the derivation of (4.2.12) are given in Appendix H. From (3.5.9), the effective hydraulic conductivity can be written in the form:

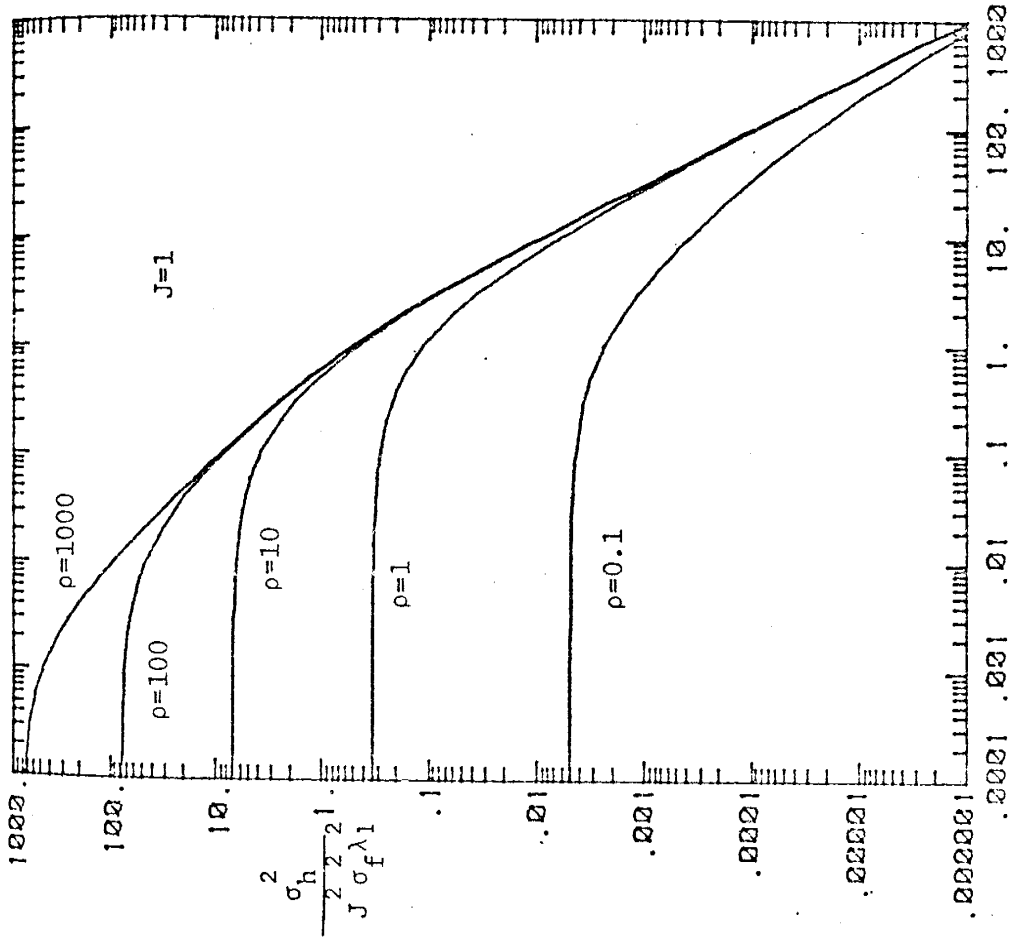

Figure 4.2.1: Variances of head perturbations resulting from three-dimensional anisotropic $\ln K_s$ field with different aspect ratios, $\rho = \lambda/\lambda_1$.

$$K_e=E[q_1]/J_1=K_m\left[1 + \frac{1}{2}[\sigma_f^2-2\alpha E[fh] + \alpha^2\sigma_h^2] + \frac{E[fj]}{J_1}\right] \qquad (4.2.13)$$

Substituting $\sigma_h^2\beta/J$ and (4.2.12) for E[fh] and E[fj], respectively, the effective hydraulic conductivity in the direction perpendicular to the bedding can be expressed as follows:

$$K_e = K_m\left[1 + \frac{1}{2}\left[\sigma_f^2\left(\frac{g-1}{g+1}\right) + \left[\alpha^2-\frac{2\alpha\beta}{J_1} + \frac{4}{J_1^2\lambda_1^2\rho^2}\right]\sigma_h^2\right]\right] \qquad (4.2.14)$$

If the exponential generalization is used, the effective hydraulic conductivity is given by:

$$K_e=K_G\exp\left[-\alpha H + \frac{1}{2}\left[\sigma_f^2\left(\frac{g-1}{g+1}\right) + \left[\alpha^2-\frac{2\alpha\beta}{J_1} + \frac{4}{J_1^2\lambda_1^2\rho^2}\right]\sigma_h^2\right]\right] \qquad (4.2.15)$$

The result of (4.2.15) is illustrated in Figure (4.2.2) together with several aspect ratios. Discussion of the significance of the result is given at the end of this chapter. Note that the principal effective hydraulic conductivity in the horizontal direction can not be evaluated directly in this case because of the uni-directional flow assumption.

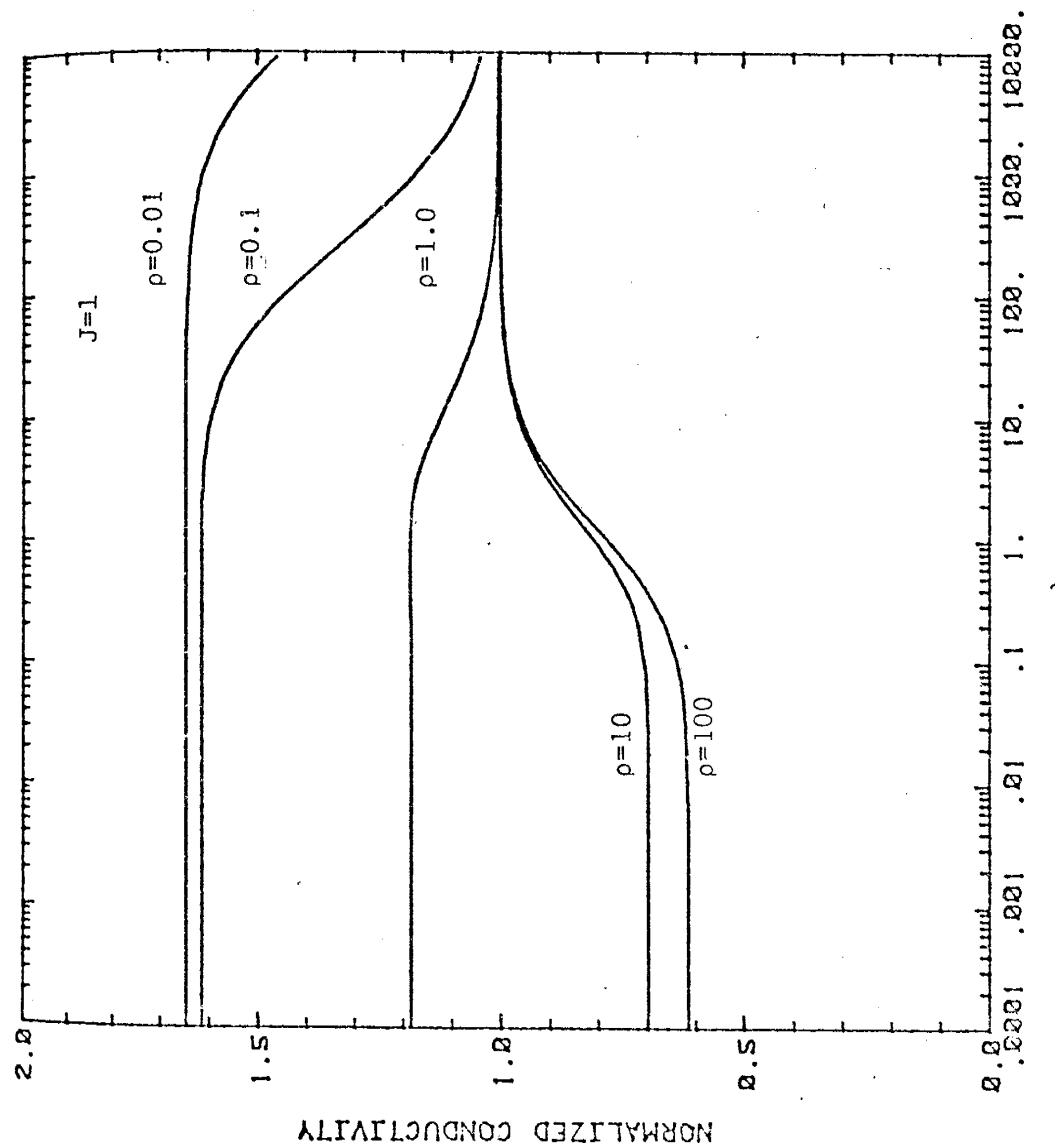

Figure 4.2.2: Effects of aspect ratio, ρ, on the effective hydraulic conductivity.

4.3 Flow in Anisotropic Media with Arbitrary Orientation of Stratification

The main objective of the analysis in this section is to define the properties of the effective hydraulic conductivity in statistically anisotropic porous media. As has been mentioned previously, the analysis in section 4.2 does not provide information about the effective hydraulic conductivity in the direction parallel to stratification, because the mean gradient exists only in the direction normal to the stratification. To allow us to carry out the analysis, we will examine the case where the principal directions of the hydraulic conductivity do not coincide with the coordinate axes. Only the special case where the soil formation is perfectly stratified (or the aspect ratio, $\frac{\lambda}{\lambda_1}$, is infinite.), will be investigated here to avoid complicated mathematics. A more general situation will be explored in a later section of this chapter.

Assuming local isotropy of the hydraulic conductivity, the Darcy's equation for a three-dimensional flow takes the form:

$$q_i = -K\frac{\partial \Phi}{\partial x_i}$$

$$= K_m\left\{\left[1 + (f-\alpha h) + \frac{(f-\alpha h)^2}{2} + \cdots\right]J_i + (f-\alpha h)\frac{\partial h}{\partial x_i}\right\} \quad (4.3.1)$$

Taking expected values of (4.3.1), dropping terms that are beyond the second-order and noting that $E[h\partial h/\partial x_i] = (1/2)\partial E(h)^2/\partial x_i = 0$,

$$E[q_i] = K_m\left\{\left[1 + \frac{E[(f - \alpha h)^2]}{2}\right] J_i + E\left[f\frac{\partial h}{\partial x_i}\right]\right\}$$

$$= K_m\left[\left[1 + \frac{(\sigma_f^2 - 2\alpha E[fh] + \alpha^2\sigma_h^2)}{2}\right]\delta_{ij} - F_{ij}\right] J_j \qquad (4.3.2)$$

$$= \bar{K}_{ij} J_j$$

where $E[f\partial h/\partial x_i] = F_{ij}J_j$, and δ_{ij} is the Kronecker delta. Thus even though local isotropy is assumed in the derivation of (4.3.2), the resulting equation produces a tensorial form of the mean Darcy's equation where $\bar{K}_{ij}$ is the effective hydraulic conductivity tensor.

Assume the direction of the stratification of the soil formation, x_2', is at an angle θ to the coordinate axis x_2 as shown in Figure (4.3.1). The unprimed (x_1, x_2, x_3) system is aligned in the direction of mean gradient so that $J_1 = J \neq 0$, and $J_2 = J_3 = 0$. Primed (x_1', x_2', x_3') system is oriented with the positive x_2' axis in the direction of stratification. Since the two coordinate systems are not identical, the mean hydraulic gradient vector may not coincide with the direction of the mean flow. The mean Darcy's equation (4.3.2) becomes

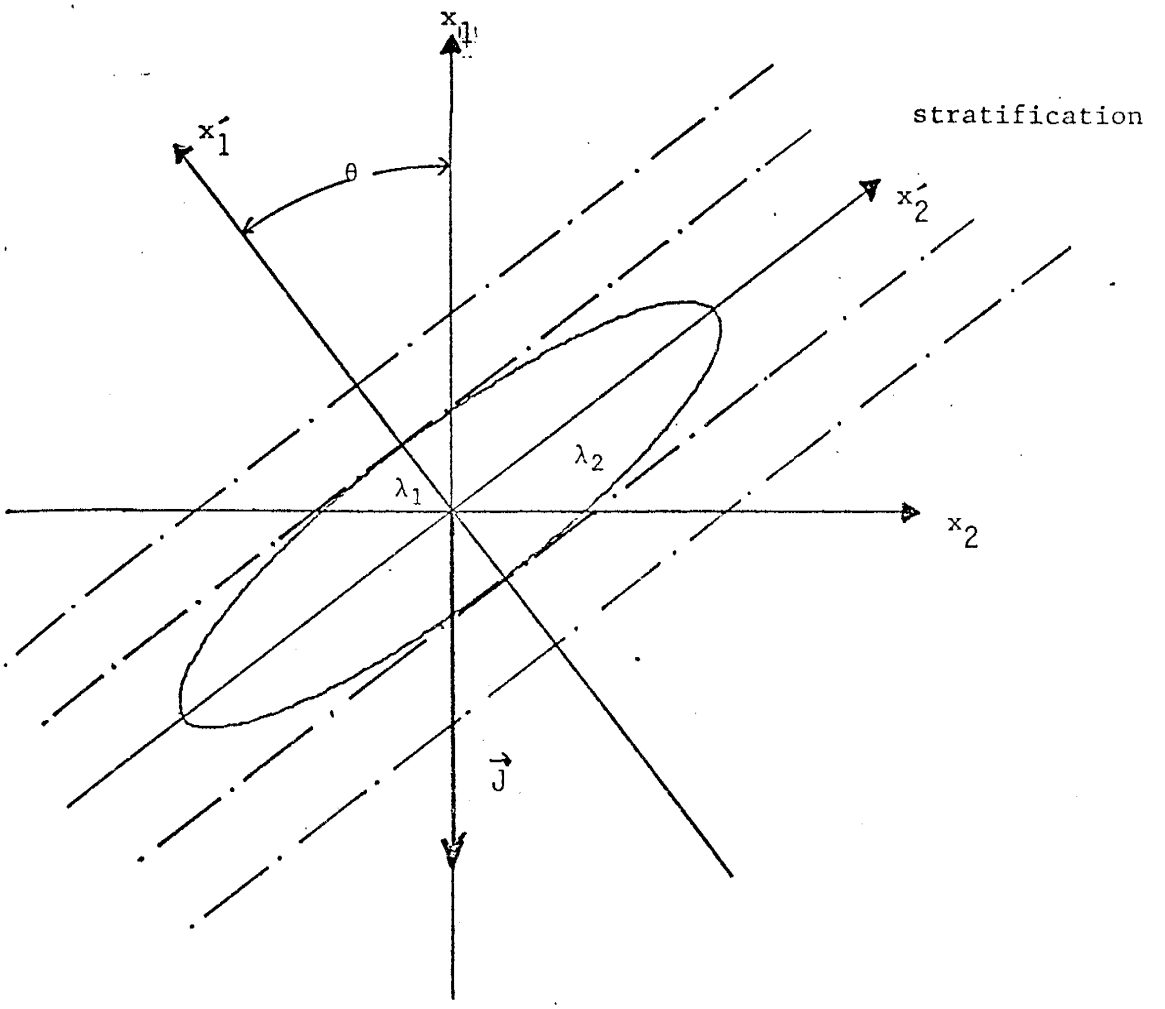

Figure 4.3.1: Coordinate system for the case of flow in anisotropic $\ln K_S$ media with arbitrarily oriented stratification.

$$\bar{q}_1 = \bar{K}_{11} J_1 \qquad (4.3.3a)$$

$$\bar{q}_2 = \bar{K}_{21} J_1 \qquad (4.3.3b)$$

correspondingly, the components of the mean hydraulic conductivity tensor, $\bar{K}_{11}$, and $\bar{K}_{21}$ can be assessed by $\bar{q}_1/J_1$ and $\bar{q}_2/J_2$, respectively. If the unsaturated hydraulic conductivity tensor is symmetric, the principal hydraulic conductivity can be calculated from these components. From (4.3.2), one can express $\bar{q}_2$ as:

$$E[q_2] = K_m\left\{\left[1 + \frac{E[(f-\alpha h)^2]}{2}\right]J_2 + E\left[f\frac{\partial h}{\partial x_2}\right]\right\} \qquad (4.3.4)$$

$$= K_m E\left[f\frac{\partial h}{\partial x_2}\right]$$

since $J_2 = 0$.

In order to evaluate the components of the hydraulic conductivity tensor, namely, $\bar{K}_{11}$, and $\bar{K}_{21}$, it is necessary to determine σ_h^2 and F_{ij} terms in (4.3.2). Since the stratification is at an angle θ to the x_2 axis of the unprimed coordinate system, the application of a coordinate transformation to (4.2.8), from unprimed to primed system, gives

$$S_{hh} = \frac{J_1^2 a_{n1} k'_n a_{m1} k'_m}{(\, k'^4 + a_{n1} k'_n a_{m1} k'_m \beta^2 \,)} S_{ff}(\vec{k}') \qquad (4.3.5)$$

where a_{nl} and a_{ml} are the directional cosines, and $S_{ff}(\vec{k}')$ is defined as

$$S_{ff}(\vec{k}') = \frac{\sigma_f^2 \lambda_1 \lambda_2 \lambda_3}{\pi^2 (1 + k_1'^2 \lambda_1^2 + k_2'^2 \lambda_2^2 + k_3'^2 \lambda_3^2)} \qquad (4.3.6)$$

Substituting (4.3.6) into (4.3.5), assuming $\lambda_2 = \lambda_3 = \lambda$, $\rho = \lambda/\lambda_1$, and $g = \lambda_1 \beta$, and integrating over the wave number vector (see Appendix I), the head variance of a perfectly stratified soil formation takes the form

$$\sigma_h^2 = \frac{J_1^2 \sigma_f^2 \lambda_1^2 a_{11}^2}{g\, a_{11}(1 + g\, a_{11})} \qquad (4.3.7)$$

Using Fourier-Stieljes representaion, the $F_{i1}J_1$ term becomes

$$F_{i1}J_1 = E\left[f\frac{\partial h}{\partial x_i} \right]$$

$$= \int_{\vec{k}} E\left[dZ_f(-ik_i)dZ_h^* \right]$$

$$= E\left[-\int_{\vec{k}} ik_i dZ_f\, dZ_h^* \right]$$

$$= -\int_{\vec{k}} \frac{J_i k_1 k_i}{(k^2 - ik_1\beta)} S_{ff}(\vec{k})$$

After the coordinate transformation, F_{il} may be further expressed as

$$F_{il} = \sigma_f^2 a_{ni} a_{ml} E_{mn}$$

where $a_{ni} = \cos(x'_n, x_i)$ and

$$E_{mn} = -\int_{\vec{k}'} \frac{k'_m k'_n}{(k'^2 - ia_{jl}k'_j\beta)} S_{ff}(\vec{k}')\, d\vec{k} \qquad j=1 \text{ and } 2. \qquad (4.3.8)$$

and where $E_{mn} = 0$, for $m \neq n$. The integral (4.3.7) is evaluated in Appendix I for the pertectly stratified case, $\rho \to \infty$. The results of the integration show

$$F_{11}J_1 = E\left[f\frac{\partial h}{\partial x_1}\right] = \frac{-J_1\sigma_f^2 a_{11}^2}{(1 + ga_{11})} \qquad (4.3.8a)$$

and

$$F_{21}J_1 = E\left[f\frac{\partial h}{\partial x_2}\right] = \frac{-J_1\sigma_f^2 a_{11}a_{12}}{(1 + ga_{11})} \qquad (4.3.8b)$$

Therefore, the components of the effective hydraulic conductivity tensor in the primed coordinate system are

$$\bar{K}_{11} = K_m\left[1 + \frac{\sigma_f^2}{2}\left[1 + \frac{N^2 J_1(2-3J_1)a_{11}^2}{ga_{11}(1+ga_{11})} - \frac{2a_{11}^2}{1+ga_{11}}\right]\right] \qquad (4.3.9a)$$

$$\text{and} \qquad \bar{K}_{21} = -K_m a_{11} a_{12} \sigma_f^2\left[\frac{1}{1+ga_{11}}\right] \qquad (4.3.9b)$$

where $N = \alpha\lambda_1$; $g = \alpha\beta$; $\beta = \alpha\lambda_1(2J-1)$.

Assuming the unsaturated hydraulic conductivity is a symmetric tensor, the hydraulic conductivity in the x_2 direction can be determined via the application of the Mohr Circle principle. From this principle, one can obtain the relationships among $\bar{K}_{22}$, $\bar{K}_{11}$, and $\bar{K}_{21}$.

$$\begin{aligned}\bar{K}_{22} &= \bar{K}_{11} - 2\bar{K}_{21}\cot 2\theta \\ &= \bar{K}_{11} - 2\bar{K}_{21}\left[\frac{a_{11}^2 - a_{12}^2}{a_{11}a_{12}}\right]\end{aligned} \qquad (4.3.9c)$$

where $a_{11} = \cos\theta$, and $a_{12} = \sin\theta$. Using the above relationship, $\bar{K}_{22}$ is given as

$$\bar{K}_{22} = K_m\left[1 + \frac{\sigma_f^2}{2}\left[1 + \frac{N^2 J_1(2-3J_1)a_{11}^2}{ga_{11}(1+ga_{11})} - \frac{2a_{12}^2}{1+ga_{11}}\right]\right] \qquad (4.3.10)$$

The principal hydraulic conductivities aligned with the primed coordinate system are determined by using the following relationships:

$$\bar{K}'_{11} \text{ or } \bar{K}'_{22} = \frac{\bar{K}_{11} + \bar{K}_{22}}{2} \pm \left\{ \left[\frac{\bar{K}_{11} - \bar{K}_{22}}{2} \right]^2 + \bar{K}_{21}^2 \right\}^{1/2} \qquad (4.3.11)$$

The resultant principal hydraulic conductivities in the x'_1, x'_2, and x'_3 directions are

$$\bar{K}'_{11} = K_m \left\{ 1 + \frac{\sigma_f^2}{2} \left[1 + \frac{N^2 J_1 (2-3J_1) a_{11}^2}{g a_{11} (1 + g a_{11})} - \frac{2}{1 + g a_{11}} \right] \right\} \qquad (4.3.12a)$$

and

$$\bar{K}'_{22} = \bar{K}'_{33} = K_m \left\{ 1 + \frac{\sigma_f^2}{2} \left[1 + \frac{N^2 J_1 (2-3J_1) a_{11}^2}{g a_{11} (1 + g a_{11})} \right] \right\}, \qquad (4.3.12b)$$

respectively. The exponential generalization of (4.3.12a) and (4.3.12b) leads to the general expressions of the principal hydraulic conductivities which are

$$\bar{K}'_{11} = K_m \exp\left\{\frac{\sigma_f^2}{2}\left[1 + \frac{N^2 J_1 (2-3J_1) a_{11}^2}{g a_{11}(1 + g a_{11})} - \frac{2}{1 + g a_{11}}\right]\right\} \qquad (4.3.13a)$$

and

$$\bar{K}'_{22} = \bar{K}'_{33} = K_m \exp\left\{\frac{\sigma_f^2}{2}\left[1 + \frac{N^2 J_1 (2-3J_1) a_{11}^2}{g a_{11}(1 + g a_{11})}\right]\right\} \qquad (4.3.13b)$$

To simplify the above expressions, the gradient is assumed to be unity. Thus, the corresponding principal hydraulic conductivities become

$$\bar{K}'_{11} \simeq K_m \exp\left[\frac{-\sigma_f^2}{2(1 + g a_{11})}\right] \qquad (4.3.14a)$$

$$= K_m e^{-\sigma^2_{\ln K}/2} \quad \text{and}$$

$$\bar{K}'_{22} = \bar{K}'_{33} \simeq K_m \exp\left[\frac{\sigma_f^2}{2(1 + g a_{11})}\right] \qquad (4.3.14b)$$

$$= K_m e^{\sigma^2_{\ln K}/2}$$

From (3.4.6), one can show that $\sigma^2_{\ln K} = \sigma_f^2/(1+g a_{11})$. Therefore, $\bar{K}'_{11}$, and $\bar{K}'_{22}$ correspond respectivily to the harmonic and arithematic means of unsaturated hydraulic conductivi-

ties. The principal hydraulic conductivities, (4.3.14a) and (4.3.14b), are depicted in Figure (4.3.2) to demostrate the effects of $\alpha\lambda_1$ and the orientation of the stratification, θ, on the principal effective hydraulic conductivities.

Using (4.3.14a) and (4.3.14b), the hydraulic conductivity anisotropy of the media, $\bar{K}'_{22}/\bar{K}'_{11}$, is given as:

$$\bar{K}'_{22}/\bar{K}'_{11} = \exp(\sigma^2_{\ln K}) = \exp\left[\frac{\sigma_f^2}{(1+ga_{11})}\right] \qquad (4.3.14)$$

The effects of $\alpha\lambda_1$ and θ on the anisotropy ratio are shown in Figure (4.3.3).

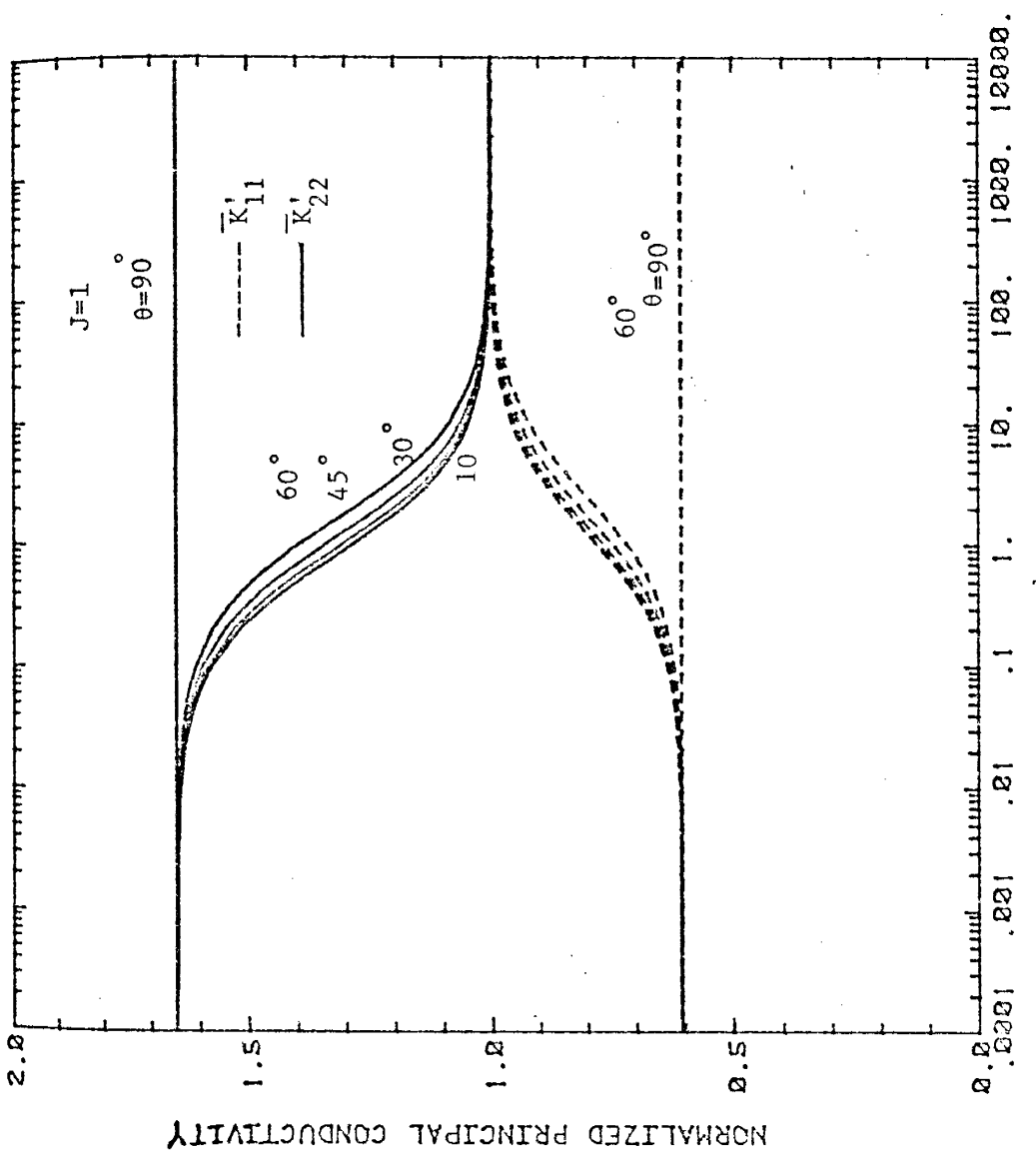

Figure 4.3.2: Principal effective hydraulic condutivities as functions rotation angle, θ, and $\alpha\lambda_1$.

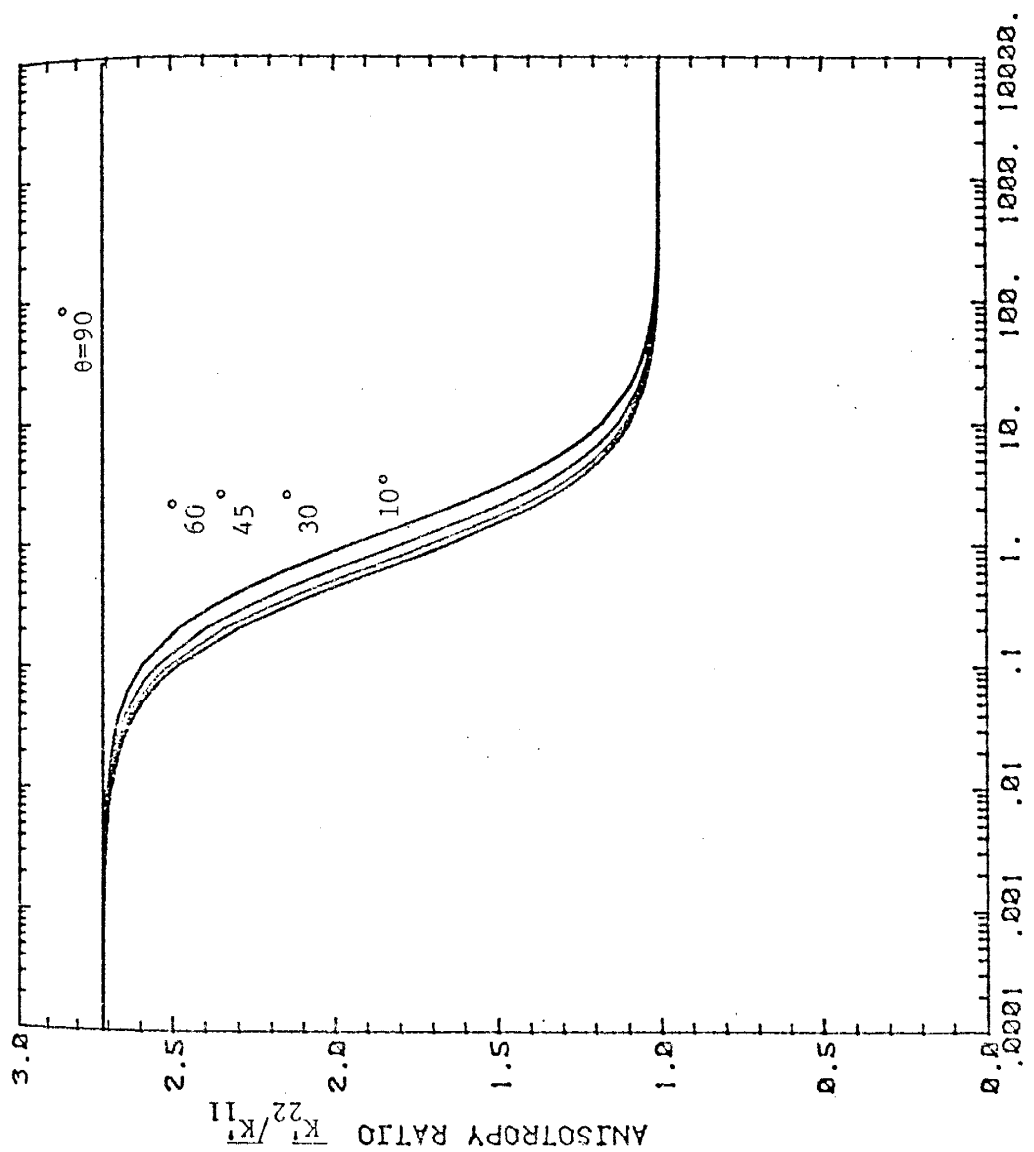

Figure 4.3.3: Ratios of principal hydraulic conductivities as functions of rotation angle, θ, and $\alpha\lambda_1$.

4.4 Multidirectional Flow Analysis

In this section, we investigate the effective hydraulic conductivity in a more generalized case where the gradient is not restricted to be unidirectional as assumed in the previous analysis. In other words, the mean gradient vector $\vec{J}$ inclines to the axes of the original coordinate system (unprimed system) x_1, x_2, and x_3 with angles γ_1, γ_2, and γ_3, respectively. The stratification is aligned in the horizontal axis of the primed coordinate system. The angle between the direction of stratification and the ordinate of the unprimed system, x_2, is θ. Thus, the mean gradient vector is composed of three gradient components; J_1, J_2, and J_3 in the direction of x_1, x_2, and x_3, respectively (see Figure 4.4.1). Since J_1, J_2, and J_3 are not zero, the flow becomes multi-directional. The objective is to derive a more generalized tensorial form for the effective hydraulic conductivity of this type of porous media.

To achieve this goal, the assumptions described in section (4.3) are again used. They are

(1) The soil formation is perfectly stratified; the aspect ratio $\frac{\lambda}{\lambda_1} \to \infty$.

(2) The hydraulic conductivity of the media is isotropic at the local scale.

(3) The log-hydraulic conductivity covariance function is assumed exponential (4.3.6).

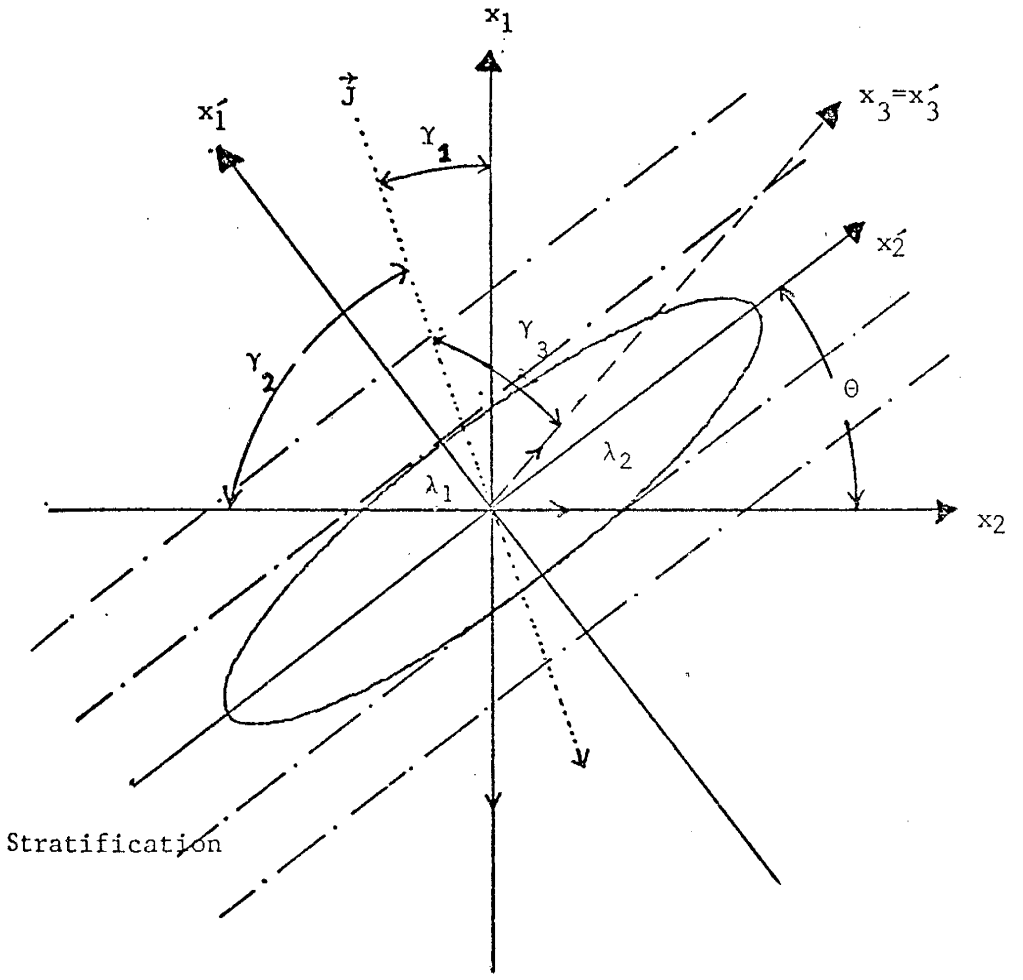

Figure 4.4.1: Coordinate systems for the case of flow in anisotropic $\ln K_s$ media with arbitrarily oriented stratification and mean gradient.

From the relationship of capillary pressure head and hydraulic conductivity Fourier amplitudes (4.2.7), the head spectrum can be related to the hydraulic conductivity spectrum by

$$S_{hh} = \frac{J_i k_i J_j k_j}{(k^4 + 4\alpha^2 P_i P_j k_i k_j)} S_{ff} \qquad (4.4.1)$$

where $P_i = J_i - (\delta_{il}/2)$, and δ_{ij} is the Kronecker delta. Application of the transformation rule, $k_i = a_{ni} k'_n$, and substitution of the hydraulic conductivity covariance function (4.3.6), the head spectrum in the primed system takes the form

$$S_{hh}(k') = \frac{\sigma_f^2 J_i J_j a_{mi} a_{nj} k'_m k'_n \lambda_1 \lambda_2 \lambda_3}{\pi^2 [k'^4 + 4\alpha^2 P_i P_j a_{mi} a_{nj} k'_m k'_n](1 + k'^2_j \lambda^2_j)} \qquad (4.4.2)$$

Integration over the wave number vector, $\vec{k}$, (see Appendix J), results in the capillary pressure head variance.

$$\sigma_h^2 = \frac{\sigma_f^2 \lambda_1^2 (J_1 a_{11} + J_2 a_{12})^2}{e(1 + e)} \qquad (4.4.3)$$

where $e = \alpha\lambda_1[(2J_1 - 1)a_{11} + 2J_2 a_{12}]$. Again the term $E[f\partial h/\partial x_i]$ has to be evaluated in order to determine the effective hydraulic conductivity. For this generalized

case, the cross-spectrum of f and j is

$$S_{fj_i} = E[-ik_i dZ_f dZ_h^*]$$
$$= \frac{-J_j k_j k_i [k^2 + i2\alpha k_n P_n] S_{ff}}{[k^4 + (2\alpha J_j k_j - \alpha k_1)^2]} \qquad (4.4.4)$$

where n,m = 1 and 2. Using the exponential covariance function (4.3.6), and transforming (4.4.4) to the primed coordinate system, the generalized spectrum relation becomes:

$$S_{fj_i}(k') = - \frac{\sigma_f^2 [J_j a_{mi} a_{nj} k'_m k'_n k'^2] \lambda_j \lambda_1 \lambda_2 \lambda_3}{\pi^2 [k'^4 + 4\alpha^2 P_i P_j a_{mi} a_{nj} k'_m k'_n](1 + k'^2_j \lambda^2_j)} \qquad (4.4.5)$$

The integration of (4.4.5) is given in the appendix E. It results in

$$E\left[f \frac{\partial h}{\partial x_i}\right] = \frac{-a_{1i} a_{1j} J_j \sigma_f^2}{(1 + e)} \qquad (4.4.6)$$

Therefore the mean fluxes in the x_1 and x_2 directions can be obtained by substituting (4.4.3) and (4.4.6) into (4.3.2). The term E[fh] is evaluated by the relationship provided in (3.4.4). Consequently, the mean fluxes in the x_1 and x_2 directions in the unprimed coordinate system are:

$$E[q_1] = K_m\left[\left[1 + \frac{\sigma_f^2}{2}\left[1 + \frac{N^2(2a_{11}-3J')J'}{e(e+1)} - \frac{2a_{11}^2}{1+e}\right]\right]J_1 + \left[\frac{-\sigma_f^2 a_{11}a_{12}}{1+e}\right]J_2\right] \tag{4.4.7}$$

$$E[q_2] = K_m\left[\left[\frac{-\sigma_f^2 a_{11}a_{12}}{1+e}\right]J_1 + \left[1 + \frac{\sigma_f^2}{2}\left[1 + \frac{N^2(2a_{11}-3J')J'}{e(e+1)} - \frac{2a_{12}^2}{1+e}\right]\right]J_2\right]$$

where $J' = J_1a_{11}+J_2a_{12}$; and $N = \alpha\lambda_1$. It becomes obvious that the hydraulic conductivity tensor in the unprimed system can be written as follow:

$$\bar{K}_{11} = K_m\left[1 + \frac{\sigma_f^2}{2}\left[1 + \frac{N^2(2a_{11}-3J')J'}{e(e+1)} - \frac{2a_{11}^2}{1+e}\right]\right] \tag{4.4.8a}$$

$$\bar{K}_{22} = K_m\left[1 + \frac{\sigma_f^2}{2}\left[1 + \frac{N^2(2a_{11}-3J')J'}{e(e+1)} - \frac{2a_{12}^2}{1+e}\right]\right] \tag{4.4.8b}$$

$$\bar{K}_{12} = K_m\left[\frac{-\sigma_f^2 a_{11}a_{12}}{1+e}\right] \qquad (4.4.8c)$$

$$\bar{K}_{21} = K_m\left[\frac{-\sigma_f^2 a_{11}a_{12}}{1+e}\right] \qquad (4.4.8d)$$

This result demonstrates that $\bar{K}_{ij}$ is a symmetric tensor of rank two. It should be recognized that $\bar{K}_{11}$ and $\bar{K}_{22}$ are functions of J_1 and J_2, respectively. The principal effective hydraulic conductivities become:

$$\bar{K}'_{11} = K_m\left[1 + \frac{\sigma_f^2}{2}\left[1 + \frac{N^2(2a_{11}-3J')J'}{e(e+1)} - \frac{2}{1+e}\right]\right] \qquad (4.4.9a)$$

and

$$\bar{K}'_{22} = \bar{K}'_{33} = K_m\left[1 + \frac{\sigma_f^2}{2}\left[1 + \frac{N^2(2a_{11}-3J')J'}{e(e+1)}\right]\right] \qquad (4.4.9b)$$

After the exponential generalization, the principal hydraulic conductivities take the form:

$$\bar{K}'_{11} = K_m \exp\left[\frac{\sigma_f^2}{2}\left[1 + \frac{N^2(2a_{11}-3J')J'}{e(e+1)} - \frac{2}{1+e}\right]\right] \qquad (4.4.10a)$$

$$\bar{K}'_{22} = \bar{K}'_{33} = K_m \exp\left[\frac{\sigma_f^2}{2}\left[1 + \frac{N^2(2a_{11}-3J')J'}{e(e+1)}\right]\right] \qquad \text{In}$$

The above hydraulic conductivities yield an anisotropy ratio:

$$\frac{\bar{K}'_{22}}{\bar{K}'_{11}} = \exp\left[\frac{\sigma_f^2}{(1+e)} \right] \qquad (4.4.11)$$

Note that (4.4.11) is similar to (4.3.14) with the exception that $e=\alpha\lambda_1[(2J_1-1)a_{11}+2J_2a_{12}]$. Consider the case where $J_1\neq 0$, and $J_2=J_3=0$, then (4.4.11) is the smae as (4.3.14). In addition, (4.4.11) shows that the anisotropy ratio of the hydraulic conductivity depends on not only σ_f^2, $\alpha\lambda$, and θ, but also the magnitue and orientation of the mean hydraulic gradient vector, $\vec{J}$.

4.5 Summary and Discussion of Results

The head variance and effective hydraulic conductivity of heterogeneous unsaturated media are investigated in this chapter. A statistically anisotropic saturated hydraulic conductivity field and a uniform pore-size distribution parameter portray the heterogeneous nature of the medium.

Results from the analysis of Section 4.2 reveal that the head variance resulting from a steady-state infiltration in anisotropic media is proportional to the statistical properties of the media: σ_f^2, λ_1, λ_2, and mean gradient, J. The effect of the aspect ratio of the medium on the head variance is shown in Figure (4.2.1). For flow normal to the bedding of a perfectly stratified soil formation of which the aspect ratio is infinite, the head variance grows infinitely. This result agrees with the result of one-dimensional flow where the exponential covariance function is used. Conversely, head variance vanishes at a zero aspect ratio, which represents the situation where flow is parallel to the bedding of a perfectly stratified soil formation.

Effective hydraulic conductivity in the direction of the mean gradient is derived in Section 4.2. Figure (4.2.2) illustrates the relationship between unsaturated hydraulic conductivity and the aspect ratio. Generally, the effective unsaturated conductivity follows the well-known behavior of saturated flow in a deterministic medium. The hydraulic conductivity tends to be the arithmetic mean, if the medium

has a small aspect ratio, which represents the case of flow parallel to the stratification. In a medium with a large aspect ratio representing the case of flow normal to the stratification, the effective hydraulic conductivity becomes the harmonic mean. However, the effective hydraulic conductivity becomes less sensitive to the aspect ratio as the correlation scale and pore-size distribution parameter of the medium increase. In this case, it approaches the geometric mean.

The principal unsaturated hydraulic conductivities in a perfectly stratified medium of arbitrary orientation are depicted in Figure (4.3.2) as a function of $\alpha\lambda$. The effective unsaturated hydraulic conductivities in the directions parallel and normal to the stratification are found to be the arithmetic mean and harmonic mean, respectively. They converge to the geometric mean as $\alpha\lambda$ becomes large.

The effect of orientation of stratification on the anisotropy ratio of unsaturated hydraulic conductivity is illustrated in Figure (4.3.3). As indicated in this figure, the orientation effect is significant at intermediate values of $\alpha\lambda$, and it is irrelevant at other possible ranges of $\alpha\lambda$. Overall, the anisotropy ratio of unsaturated hydraulic conductivity is smaller than that of saturated hydraulic conductivity. This can be ascribed to the assumption of a uniform pore-size distribution and the effect of the non-linear nature of unsaturated flow. This theoretical anisotropy ratio may not represent the anisotropy ratio of the natural

soils, because the parameter α may vary significantly.

The multidirectional flow analysis in Section 4.4 substantiates unsaturated hydraulic conductivity as a symmetric tensor of rank two and derives the full tensor of the effective hydraulic conductivity. The analysis also shows the degree of anisotropy to be dependent on σ_f^2, $\alpha\lambda$, the magnitude and the direction of the gradient, and orientation of the stratification. A large gradient, pore-size distribution parameter, and correlation scale can reduce the anisotropy ratio.

CHAPTER 5

FLOW IN AN ANISOTROPIC MEDIUM WITH A RANDOM PORE-SIZE DISTRIBUTION PARAMETER

5.1 Introduction

As expected, the results of the analyses based on the assumption that the heterogeneity of the medium can be represented by a random saturated hydraulic conductivity field and a deterministic pore-size parameter does not necessarily provide realistic information on the behavior of unsaturated flow in any natural porous media. As a result of this assumption, the previous analyses have demonstrated both the head variance and the anisotropy of the effective hydraulic conductivity are independent of the mean capillary pressure head. This outcome however can be easily conceived if one compares the K-ψ relation curves illustrated in both figure (2.4.1) and (2.4.2). To be more pragmatic, one has to extend the analysis to the case where the saturated hydraulic conductivity and pore-size distribution parameter are considered random.

This chapter begins with the analysis of head variance and effective hydraulic conductivity resulting from one-dimensional flow in a porous medium of isotropic random-saturated hydraulic conductivity and pore-size distribution parameter. This section is followed by the analysis of three-dimensional flow in an anisotropic random field.

subsquently, the head variance and the effective hydraulic conductivity of the porous medium of such anisotropic media is explored.

5.2 One-Dimensional Flow With Random Saturated Hydraulic Conductivity and Pore-size Distribution Parameter.

If the pore-size distribution parameter α is assumed to be a statistically homogeneous stochastic process, it then can be decomposed to mean and perturbation components,

$$\alpha = A + a \qquad (5.2.1)$$

where $E[\alpha] = A$ and $E[a] = 0$. Substituting (5.2.1) into (3.2.5a), and neglecting the products of the perturbations, the logarithmatic unsaturated hydraulic conductivity can be expressed in terms of means and perturbations as follows:

$$\ln K = F + f - AH - Ah - aH \qquad (5.2.2)$$

Replacing the lnK in the (3.2.3) with the above expression (5.2.2), and assuming the mean saturated hydraulic conductivity and the pore-size distribution parameter are independent of z, the mean flow equation, after neglecting the second order terms, can be derived as

$$\frac{d^2H}{dz^2} - AJ\frac{dH}{dz} + \overline{(\frac{df}{dz} - A\frac{dh}{dz} - a\frac{dH}{dz} - H\frac{da}{dz})\frac{dh}{dz}} = 0 \qquad (5.2.3)$$

where J is 1+dH/dz. The governing flow equation in terms of the perturbations becomes

$$\frac{d^2h}{dz^2} - A(2J - 1)\frac{dh}{dz} + J\frac{df}{dz} - J(J - 1)a - JH\frac{da}{dz} = 0 \qquad (5.2.4)$$

The last two terms are the results of the stochastic representation of the pore-size distribution parameter, α. If it is assumed that the mean capillary pressure head changes gradually, application of Fourier-Stieltjes representation for the f, h (see 3.2.10), and a:

$$a = \int_{-\infty}^{\infty} e^{ikz} dZ_a(k) \qquad (5.2.5)$$

leads to the Fourier amplitude relations of h, f, and a stochastic processes:

$$dZ_h = \frac{-J(J - 1)dZ_a + iJk(dZ_f - HdZ_a)}{[k^2 + iA(2J - 1)k\ ]} \qquad (5.2.6)$$

Furthermore, the spectral density function of the head process is given by

$$S_{hh} = \frac{J^2[(J-1)^2 S_{aa} + 2(J-1)kQ_{af}}{[k^4 + A^2(2J-1)^2k^2]} + \frac{k^2(S_{ff} - 2HCo_{af} + H^2Saa)]}{[k^4 + A^2(2J-1)^2k^2]} \qquad (5.2.7)$$

where Co_{af} and Q_{af} are the cospectrum and quadspectrum components of the cross-spectral density function ,S_{af} , of a and f processes. For the special case considered below the quadspectrum is alway zero. Thus, we can rewrite (5.2.7) to

$$S_{hh} = \frac{J^2[(J-1)^2 S_{aa} + k^2(S_{ff} - 2HCo_{af} + H^2 S_{aa})]}{[k^4 + A^2(2J-1)^2k^2]} \qquad (5.2.8)$$

In order to evaluate the head spectrum S_{hh}, knowledge of spectra of a and f processes is necessary. The cross-spectral density function of a and f processes has to be known beforehand as well. If the cross-covariance of these two processes is known, the cospectrum can be determined. However, no data and information are available for this purpose. Since a and f are not necessarily perfectly correlated with each other, such a cross-covariance function would not rise to the maximum at the origin. Therefore, it is difficult to assume an arbitrary function for the cross-covariance function without any definite justification.

Hydraulic conductivity and capillary pressure head relation curves of several different types of soil obtained

from Mualem's soil catalog (1976) are plotted in Figure (5.2.1). These data illustrate that the parameter α varies among the soils and with capillary pressure. However, no clear relationship between K_s and α is evident. Any conclusion on the behavior of such a correlation requires a significant amount of field data.

Since no justifiable cospectrum and the spectrum of a process are available, the analysis is carried out with the following assumptions:

(1) The auto-correlation functions of a and f processes are assumed to be equivalent.
(2) The a and f processes have the same correlation length scale for the sake of simplicity.
(3) The relation of a and f will be considered as either statistically independent or perfectly correlated.

In the following analysis, we will refer to the case where the saturated hydraulic conductivity and pore-size distribution parameter are perfectly correlated as Case I, and where the saturated hydraulic conductivity and pore-size distribution parameter are independent as Case II.

(I) Case I: α and K_s are perfectly correlated.

If perfect correlation between α and K_s is considered,

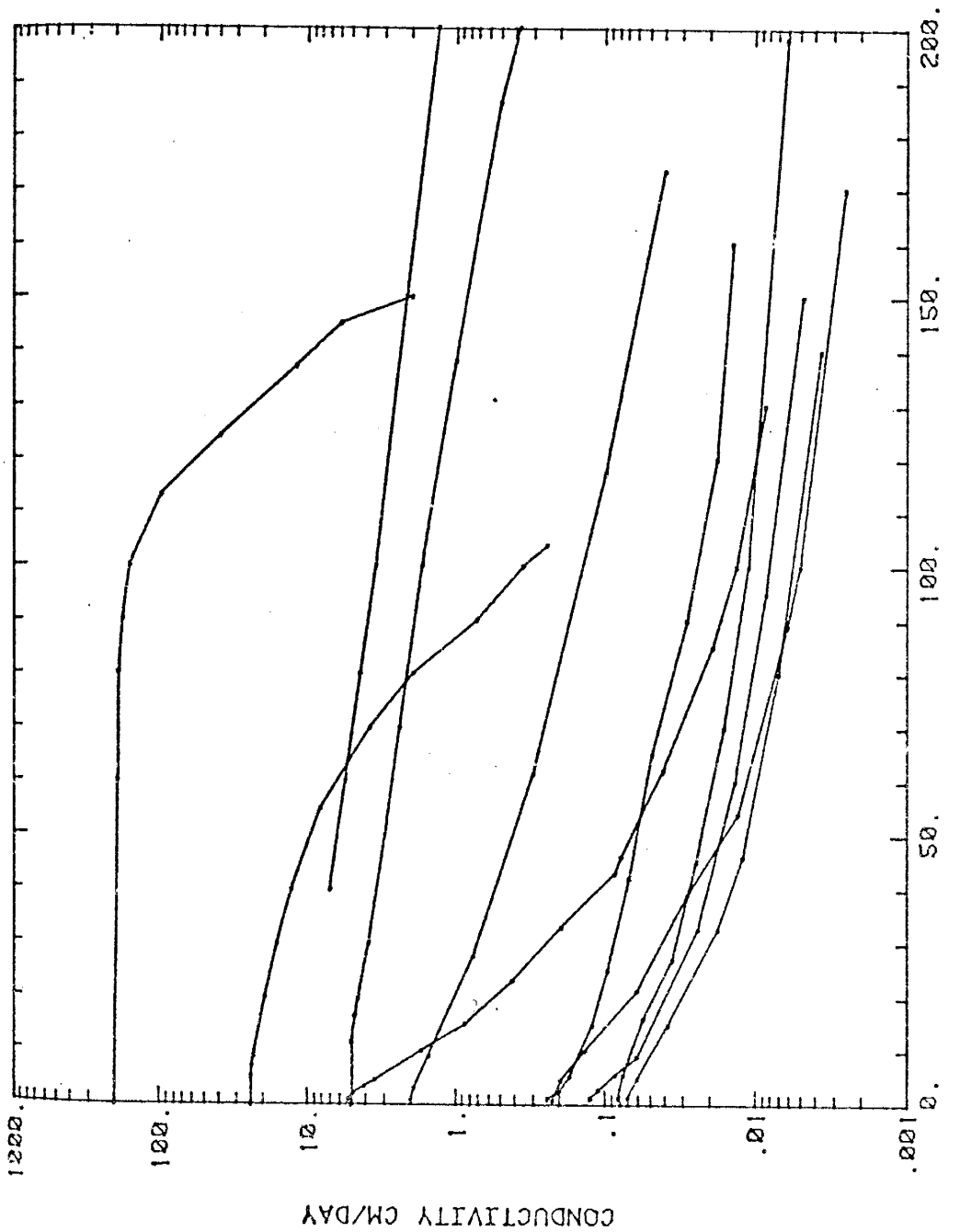

Figure 5.2.1: K-ψ relationships of some soils from Mualem's soil catalog.

one can express K_s in terms of α as

$$K_s = \frac{\alpha}{\zeta} \tag{5.2.9}$$

Therefore, $\zeta f = a$

Making use of Fourier-Stieltjes representation theorem, the spectrum of a process is related to f by

$$S_{aa} = \zeta^2 S_{ff} \tag{5.2.10}$$

and the cross-spectrum, consequently, becomes

$$S_{af} = \zeta S_{ff} \tag{5.2.11}$$

which is real so that $Co_{af} = S_{af}$ and $Q_{af} = 0$.

As a result of substituting (5.2.10), and (5.2.11) into (5.2.8), the head spectrum for this particular case is

$$S_{hh} = \frac{J^2[(J-1)^2\zeta^2 + k^2(1-H\zeta)^2]S_{ff}}{k^2[k^2 + A^2(2J-1)^2]} \tag{5.2.12}$$

From the above expression for S_{hh}, it is evident that the exponential covariance function (3.2.13) will result in an infinite head variance, since the first term of the right hand side of (5.2.12) will produce a singularity at origin.

However, if J = 1, this term will vanish. Thus, for a generalized situation, J ≠ 1, the hole function (3.2.17) is used to represent the covariance functions of a and f stochastic processes.

The capillary pressure head covariance function derived from the exponential function (when J = 1) in terms of the variance of f and a is given as:

$$R_{hh}(\xi) = \frac{\sigma_f^2(1 - \zeta H)^2\lambda^2}{(1 - A\lambda)}\left[\frac{e^{-A\lambda|\xi|/\lambda}}{A\lambda} - e^{-|\xi|/\lambda}\right] \quad (5.2.13)$$

Note that $\sigma_a^2 = \zeta^2\sigma_f^2$. Let $\xi = 0$, the head variance is

$$\sigma_h^2 = \frac{\sigma_f^2\lambda^2(1 - \zeta H)^2}{A\lambda(1 + A\lambda)} \quad (5.2.14)$$

When J is not equal to unity, the hole function is used. The head covariance function of one-dimensional flow is evaluated in Appendix K as

$$R_{hh}(\xi) = \frac{J^2\sigma_f^2(1-\zeta H)^2\eta^2}{(1-\beta^2\eta^2)^2}\left[(1-\beta^2\eta^2)(1+|\xi|/\eta)e^{-|\xi|/\eta} + 2\beta^2\eta^2 e^{-|\xi|/\eta} - 2\beta\eta e^{-\beta|\xi|}\right] + \frac{J^2(J-1)^2\sigma_f^2\zeta^2\eta^4}{(\beta^2\eta^2-1)^2}\left\{\frac{-2}{\beta\eta}e^{-\beta|\xi|} + \left[3-\beta^2\eta^2+(1-\beta^2\eta^2)|\xi|/\eta\right]e^{-|\xi|/\eta}\right\} \quad (5.2.15)$$

Correspondingly, the head variance is

$$\sigma_h^2 = \frac{J^2\eta^2\sigma_f^2}{(1+\beta\eta)^2}\left[(1-\zeta H)^2 - (J-1)^2\eta^2(\beta\eta + 2)\right] \quad (5.2.16)$$

In the case where J=1, the head variance is

$$\sigma_h^2 = \frac{\sigma_f^2(1 - \zeta H)^2\eta^2}{(1 + A\eta)^2} \quad (5.2.17)$$

The results of the above analysis show the mean capillary pressure head, H, dependence of the head variance.

(II) Case II: α and K_s are statistically independent.

If a and f are statistically independent, the cross-spectrum of a and f is zero. Thus, the cospectrum term, Co_{af}, in (5.2.8) vanishes. The head covariance correspond-

ing to the exponential covariance function and J=1 is

$$R_{hh}(\xi) = \frac{(\sigma_f^2 + H^2\sigma_a^2)\lambda^2}{(1 - A\lambda)}\left[\frac{e^{-A\lambda|\xi|/\lambda}}{A\lambda} - e^{-|\xi|/\lambda}\right] \quad (5.2.18)$$

Let $\xi = 0$, the head variance is

$$\sigma_h^2 = \frac{(\sigma_f^2 + H^2\sigma_a^2)\lambda^2}{A\lambda(1 + A\lambda)} \quad (5.2.19)$$

Similarily, the covariance function of head process resulting from the hole function input is given as

$$R_{hh}(\xi) = \frac{J^2(\sigma_f^2 + H^2\sigma_a^2)\eta^2}{(1-\beta^2\eta^2)^2}\left[(1-\beta^2\eta^2)(1+|\xi|/\eta)e^{-|\xi|/\eta} + 2\beta^2\eta^2 e^{-|\xi|/\eta} - 2\beta\eta e^{-\beta|\xi|}\right] + \frac{J^2(J-1)^2\sigma_a^2\eta^4}{(\beta^2\eta^2-1)^2}\left\{\frac{-2}{\beta\eta}e^{-\beta|\xi|} + \left[3 - \beta^2\eta^2 + (1-\beta^2\eta^2)|\xi|/\eta\right]e^{-|\xi|/\eta}\right\} \quad (5.2.20)$$

Correspondingly, the head variance is

$$\sigma_h^2 = \frac{J^2(\sigma_f^2 + H^2\sigma_a^2)\eta^2}{(1+\beta\eta)^2}\left[(\sigma_f^2+H^2\sigma_a^2) - (J-1)^2\sigma_a^2\eta^2(\beta\eta + 2)\right] \quad (5.2.21)$$

In the case where J=1, the head variance is

$$\sigma_h^2 = \frac{(\sigma_f^2 + H^2\sigma_a^2)\eta^2}{(1 + A\eta)^2} \qquad (5.2.22)$$

Comparing the head variance derived in this chapter for the case when J=1, namely; (5.2.14), (5.2.17), (5.2.19), and (5.2.22) to those obtained in Chpater 3, (3.2.16) and (3.2.20), the effect of the randomness of α on the head variance becomes clear. The randomness of α simply brings in the contributions of mean capillary pressure head and the variance of α in addition to σ_f^2 itself as in (3.2.16) and (3.2.20). Thus, the head variance increases with its mean, indicating that the pressure head process is a nonstationary process.

To evaluate the effective hydraulic conductivity, one can substitute (5.2.2) into Darcy's flow equation to obtain

$$q=K_m\left[1 + (f-Ah-aH) + \frac{(f-Ah-aH)^2}{2} + \cdots\right]\left[\frac{dH}{dz} + \frac{dh}{dz} + 1\right] \qquad (5.2.23)$$

The mean flux thus becomes

$$E[q]=K_m\left\{1 + E\left[\frac{(f-Ah-aH)^2}{2}\right]\right\}J + K_m E\left[(f-Ah-aH)\frac{dh}{dz}\right] \qquad (5.2.24)$$

The squared term on the right hand side of (5.2.24), $E[(f-Ah-aH)^2]$, expands to

$$\sigma_f^2 + A^2\sigma_h^2 + H^2\sigma_a^2 - 2A\ E[fh] - 2H\ E[af] + 2AH\ E[ah] \quad (5.2.25)$$

The remaining term on the right hand side can also be expanded to

$$E\left[f\frac{dh}{dz}\right] - A\ E\left[h\frac{dh}{dz}\right] - H\ E\left[a\frac{dh}{dz}\right] \quad (5.2.26)$$

However, the second term of (5.2.26) is always zero.

Following the procedures employed in the previous analyses, the cross-spectra of the cross-covariances in (5.2.25, and 5.2.26) can be expressed in terms of input spectra, S_{ff} and S_{aa}, and the cross-spectrum of the inputs, S_{af}. The results are summarized in Table (5.2.1). Assuming appropriate input spectra for a and f, the integration of the spectral relationships results in the cross-covariances for each term. These are also included in Table (5.2.1) for the case when J=1, and the exponential and hole function input covariance functions are used. Most of these results are similar to those obtained in Chapter 3 with the exception that σ_f^2 is replaced by either $\sigma_f^2(1-H\zeta)$ or $(\sigma_f^2+\sigma_a^2H)$ depending on the relationship between α and $\ln K_s$. Therefore, details of the derivation of each term in Table (5.2.1) are omitted.

When J = 1 and the input covariance function is an exponential function, the effective hydraulic conductivity derived from the assumption that a and f are statistically

Table 5.2.1: A summary of spectral relationships, variances, and cross-covariances used in one-dimensional analysis of flow through $\ln K_s$ and α random fields.

	SPECTRAL RELATIONSHIP			a, & f INDEPENDENT $Co_{af} = 0$	a & f PERFECTLY CORRELATED $S_{aa} = \zeta^2 S_{ff}$
S_{fh}	$\frac{J\beta S_{ff} - J[(J-1)+H\beta]S_{af}}{(k^2+\beta^2)}$	E[fh]	exp. J=1	$\frac{\sigma_f^2\lambda}{(1+A\lambda)}$	$\frac{\sigma_f^2\lambda(1-H\zeta)}{(1+A\lambda)}$
			hole	$\frac{J\sigma_f^2\eta^2\beta}{(1+\beta\eta)^2}$	$\frac{J\sigma_f^2\eta^2}{(1+\beta\eta)^2}[\beta-(J-1+H\beta)\zeta]$
S_{ah}	$\frac{J\beta S_{af} - J[(J-1)+H\beta]S_{aa}}{(k^2+\beta^2)}$	E[ah]	exp. J=1	$\frac{-\sigma_a^2\lambda H}{(1+A\lambda)}$	$\frac{\sigma_f^2\lambda(1-H\zeta)\zeta}{(1+A\lambda)}$
			hole	$\frac{-J\sigma_a^2\eta^2}{(1+\beta\eta)^2}(J-1+H\beta)$	$\frac{J\sigma_f^2\eta^2\zeta}{(1+\beta\eta)^2}[\beta-(J-1+H\beta)\zeta]$
S_{fj}	$\frac{-Jk^2S_{ff} + J(Hk^2-\beta(J-1))S_{af}}{(k^2+\beta^2)}$	E[fj]	exp. J=1	$\frac{-\sigma_f^2}{(1+A\lambda)}$	$\frac{-\sigma_f^2(1-H\zeta)}{(1+A\lambda)}$
			hole	$\frac{-J\sigma_f^2}{(1+\beta\eta)^2}(1+2\beta\eta)$	$\frac{-J\sigma_f^2}{(1+\beta\eta)^2}[(H\zeta-1)(1+2\beta\eta)-(J-1)\zeta\beta\eta^2]$
S_{aj}	$\frac{-Jk^2S_{af} + J(Hk^2-\beta(J-1))S_{aa}}{(k^2+\beta^2)}$	E[aj]	exp. J=1	$\frac{\sigma_a^2H}{(1+A\lambda)}$	$\frac{-\sigma_f^2\zeta(1-H\zeta)}{(1+A\lambda)}$
			hole	$\frac{\sigma_a^2J}{(1+\beta\eta)^2}[H(1+2\beta\eta)-(J-1)\beta\eta^2]$	$\frac{J\sigma_f^2\zeta}{(1+\beta\eta)^2}[-(1-H\zeta)(1+2\beta\eta)-(J-1)\zeta\beta\eta^2]$
S_{hh}	$\frac{J^2(J-1)^2S_{aa}+J^2k^2(S_{ff}-2HCo_{af}+H^2S_{aa})}{(k^4+A^2(2J-1)^2k^2)}$	σ_h^2	exp. J-1	$\frac{(\sigma_f^2+H^2\sigma_a^2)\lambda^2}{(1+A\lambda)\lambda A}$	$\frac{\sigma_f^2\lambda^2(1-H\zeta)^2}{(1+A\lambda)\lambda A}$
			hole	$\frac{J^2\eta^2(\sigma_f^2+\sigma_a^2H^2)}{(1+\beta\eta)^2} + \frac{J^2(J-1)^2\sigma_a^2\eta^4(\beta\eta-2)}{(1+\beta\eta)^2\beta\eta}$	$\frac{J^2\sigma_f^2(1-H\zeta)^2\eta^2}{(1+\beta\eta)^2} + \frac{J^2(J-1)^2J^2\sigma_f^2\eta^4(\beta\eta+2)}{(1+\beta\eta)^2\beta\eta}$

independent is

$$K_e = K_G e^{-AH}\left[1 - \frac{(\sigma_f^2 + \sigma_a^2 H^2)}{(1 + A\lambda)}\right] \qquad (5.2.27)$$

Note that the E[af] term in the (5.2.25) is zero in this case.

If a and f processes are perfectly correlated, the effective hydraulic conductivity becomes

$$K_e = K_G e^{-AH}\left[- \frac{\sigma_f^2 (H\zeta - 1)^2}{2(1 + A\lambda)}\right] \qquad (5.2.28)$$

Since a and f are perfectly correlated, the term E[af] is $\zeta\sigma_f^2$, instead of zero.

These results are a first order approximation. To avoid obtaining negative hydraulic conductivity values, we can express (5.2.27) and (5.2.28) in a generalized exponential form:

$$K_e = K_G e^{-AH + \gamma} \qquad (5.2.29)$$

where γ is equal to

$$\gamma = \frac{-(\sigma_f^2 + \sigma_a^2 H^2)}{2(1 + A\lambda)}$$

for the case when a and f are statistically independent, and

$$\gamma = \frac{-\sigma_f^2 (H\zeta - 1)^2}{2(1 + A\lambda)}$$

for the case when a and f are perfectly correlated.

In more generalized situations where $J \neq 1$, the hole covariance function is required to obtain the effective hydraulic conductivity. This is achieved by making use of the results in Table (5.2.1) and (5.2.24). However, the effective hydraulic conductivity for this case will not be presented due to the complexity of the equation.

5.3 Three-dimensional Flow in a Perfectly Stratified Soil Formation

The results of one-dimensional flow analysis in the previous section have demonstrated the importance of the stochastic representation of both the saturated hydraulic conductivity and the pore-size distribution parameter. The one-dimensional analysis, however does not necessarily provide realistic information on flow in natural soil formations, since flow in natural soil formations is an inherently three-dimensional phenomenon.

In the following analysis, the natural soil formation is replaced by three-dimensional statistically anisotropic f and a fields. The anisotropy of the medium is characterized by the aspect ratio.

Taking advantage of equations (4.2.3) and (5.2.2), the governing mean flow equation for an arbitrarily oriented mean gradient becomes

$$\frac{\partial^2 H}{\partial x_i^2} + \frac{\partial (F-AH)}{\partial x_1} + \frac{\partial (F-AH)}{\partial x_i}\frac{\partial H}{\partial x_i} + \overline{\frac{\partial ah}{\partial x_1} + \frac{\partial (f-Ah-aH-ah)}{\partial x_i}\frac{\partial h}{\partial x_i}} = 0 \quad (5.3.1)$$

Then, the corresponding perturbation equation for the flow is:

$$\frac{\partial^2 h}{\partial x_i^2} - A(2J_i-\delta_{1i})\frac{\partial h}{\partial x_i} - J_i(J_i-\delta_{1i})a + J_i\left[\frac{\partial f}{\partial x_i} - H\frac{\partial a}{\partial x_i}\right] = 0 \quad (5.3.2)$$

The above equation shows that the stochastic representation of pore-size distribution parameter in the three-dimensional flow situation also brings in additional terms in the perturbation equation as in the one-dimensional flow analysis. One of the additional terms is the product of mean capillary pressure head and the perturbation gradient, $\partial a/\partial x_i$. Thus, the effects of the mean capillary pressure head on the results is perceivable.

Again using Fourier-Stieljes integral representation for the random processes, the Fourier amplitude relation of the capillary pressure head h, saturated hydraulic conductivity, f, and pore-size distribution parameter a is given by:

$$dZ_h = \frac{iJ_n k_n (dZ_f - H dZ_a) - (J_n J_n - J_1) dZ_a}{[k^2 + iA(2J_n k_n - k_1)]} \qquad (5.3.3)$$

Multiplying both sides by the complex conjugate of the Fourier amplitude dZ_h, taking mean values and using the spectral representation theorem results in the spectral relationship:

$$S_{hh} = \frac{J_n^2 k_n^2 (S_{ff} - 2HCo_{af} + H^2 S_{aa}) - 2J_n k_n (J_n^2 - J_1) Q_{af} +}{[k^4 + A^2 (2J_n k_n - k_1)^2]} \qquad (5.3.4)$$

$$\underline{(J_n J_n - J_1)^2 S_{aa}}$$

where Q_{af} and Co_{af} again are the quadspectrum and cospectrum components of the cross-spectral density function, S_{af}, respectively. For the two special cases of perfectly correlated (I) or uncorrelated (II) α and $\ln K_s$, the quadspectrum is always zero. The selection of autocovariance functions or spectra for the saturated hydraulic conductivity and pore-size distribution parameter fields however requires additional consideration in this case. This is due to the presence of the last term, $(J_n J_n - J_1)^2 S_{aa}$, in equation (5.3.4). If the three-dimensional anisotropic exponential autocovariance equation (4.2.9) is used for the random process, the resulting head variance is infinite due to singularity of this term at the origin. However, this mathematical difficulty can be circumvented if a modified exponential autocovariance function, (Naff, 1978; Gelhar and Axness, 1981)

$$R_{f\,f}(\vec{\xi}) = \sigma_f^2[1 - \xi^2/\lambda_1^2 s]\exp[-s] \qquad (5.3.5)$$

where $s^2=\xi_1^2/\lambda_1^2+\xi_2^2/\lambda_2^2+\xi_3^2/\lambda_3^2$, is used, or the mean gradient is restricted only in the x_1 direction and assumed to be a unit gradient. The assumption of the uni-directional unit gradient simply eliminates the singularity. In the following analysis, results for the head variance and the effective hydraulic conductivity are obtained with the exponential autocovariance for both a and f processes with the uni-directional unit gradient assumption.

The resultant head variance is similar to that obtained in section 4.2 with the exception that the σ_f^2 in equation (4.2.11) is replaced by $\sigma_f^2(1-\zeta H)^2$ and $(\sigma_f^2+\sigma_a^2H^2)$ for case (I) and case (II), respectively. Therefore, the head variance for case (I) can be expressed by:

$$\sigma_h^2=J_1^2\sigma_f^2(1-H\zeta)^2\lambda_1^2\rho^4\int_0^1\frac{t^2\,dt}{[(\rho^2-1)t^2+\rho^2gt+1]} \qquad (5.3.6a)$$

Similarly, the head variance for case (II) is given by

$$\sigma_h^2=J_1^2(\sigma_f^2+\sigma_a^2H^2)\lambda_1^2\rho^4\int_0^1\frac{t^2\,dt}{[(\rho^2-1)t^2+\rho^2gt+1]} \qquad (5.3.6b)$$

To derive the expression for the effective hydraulic conductivity tensor, we again assume the hydraulic conductivity at local scale is homogeneous and isotropic, and the medium is perfectly stratified. Thus, the mean Darcy's equation is

$$q_i = -K\frac{\partial\Phi}{\partial x_i} \qquad i=1,2, \text{ and } 3.$$

Utilizing the expression for lnK, (5.2.2):

$$q_i = K_m\left[1 + (f - aH - Ah) + \frac{(f - aH - Ah)^2}{2} + \cdots\right]\left[J_i + \frac{\partial h}{\partial x_i}\right] \qquad (5.3.7)$$

where $K_m = K_G e^{-AH}$. the mean flux in the x_i direction is

$$E[q_i] = K_m\left\{1 + E\left[\frac{(f - aH - Ah)^2}{2}\right]\right\}J_i + K_m E\left[(f - aH - Ah)\frac{\partial h}{\partial x_i}\right] \qquad (5.3.8)$$

Similarly, the expectations on the right hand side of equation (5.3.8) can be expanded as those in equations (5.2.25) and (5.2.26). The spectral or cross-spectral relationships needed to evaluate the variances or covariances in equation (5.3.8) for the case where $J_1 = 1$, and $J_2 = J_3 = 0$ are summaried in Table (5.3.1).

Since the mean gradient only exists in x_1 direction, to obtain a complete description of the hydraulic conductivity tensor we have to examine the case where the stratification of the soil formation does not coincide with the principal direction. Thus, a coordinate transformation of the spectal relationship as that employed in Chapter 4 should be used. After the transformation and the integration over the wave number, the variances and covariances for case (I) and case (II) are listed in Table (5.3.1).

Substituting the results in Table (5.3.1) into (5.3.8), the mean flux in the x_1 direction with $J_1 = 1$ becomes

TABLE 3.3.1: A summary of spectral relationships, variances, and cross covariances used in three-dimensional analysis of flow through anisotropic $\ln K_s$ and α random fields.

	SPECTRAL RELATIONSHIP		CASE (I)	CASE (II)
S_{hh}	$\frac{k_1^2(S_{ff}-2HS_{af}+H^2S_{aa})}{(k^4+A^2k_1^2)}$	σ_h^2	$\frac{a_{11}^2\sigma_f^2(1-H\zeta)^2\lambda_1^2}{e(1+e)}$	$\frac{a_{11}^2(\sigma_f^2+\sigma_a^2H^2)\lambda_1^2}{e(1+e)}$
S_{fh}	$\frac{k_1^2A(S_{ff}-HS_{af})}{(k^4+A^2k_1^2)}$	$E[fh]$	$\frac{a_{11}^2\sigma_f^2(1-H\zeta)\lambda_1^2A}{e(1+e)}$	$\frac{a_{11}^2\sigma_f^2A\lambda_1^2}{e(1+e)}$
S_{ah}	$\frac{k_1^2A(S_{af}-HS_{aa})}{(k^4+A^2k_1^2)}$	$E[ah]$	$\frac{a_{11}^2\sigma_f^2(1-H\zeta)\lambda_1^2A\zeta}{e(1+e)}$	$\frac{-a_{11}^2\sigma_a^2\lambda_1^2AH}{e(1+e)}$
S_{fj_m}	$\frac{-k_1k^2k_m(S_{ff}-HS_{af})}{(k^4+A^2k_1^2)}$	$E[fj_m]$	$\frac{-a_{11}a_{1m}\sigma_f^2(1-H\zeta)}{(1+e)}$	$\frac{-a_{11}a_{1m}\sigma_f^2}{(1+e)}$
S_{aj_m}	$\frac{-k_1k^2k_m(S_{af}-HS_{aa})}{(k^4+A^2k_1^2)}$	$E[aj_m]$	$\frac{-a_{11}a_{1m}\sigma_f^2(1-H\zeta)\zeta}{(1+e)}$	$\frac{-a_{11}a_{1m}\sigma_a^2H}{(1+e)}$

*where m=1 or 2, and $e=A\lambda_1a_{11}$

$$E[q_1] = K_m\left[1 + \frac{\sigma_f^2(1-H\zeta)^2}{2}\left[\frac{1-2a_{11}}{1+ga_{11}}\right]\right]J_1 \qquad (5.3.9)$$

for case (I), and

$$E[q_1] = K_m\left[1 + \frac{(\sigma_f^2+H^2\sigma_a^2)}{2}\left[\frac{1-2a_{11}}{1+ga_{11}}\right]\right]J_1 \qquad (5.3.10)$$

for case (II).

Since the mean gradient only exists in the x_1 direction, $J_2 = 0$. The mean flux equation in the x_2 direction for case (I) becomes:

$$E[q_2] = K_m E\left[f\frac{\partial h}{\partial x_2}\right] = K_m[\sigma_f^2(1-H\zeta)^2]\left[\frac{-J_1 a_{11} a_{12}}{(1+ga_{11})}\right] \qquad (5.3.11)$$

, and

$$E[q_2] = K_m E\left[f\frac{\partial h}{\partial x_2}\right] = K_m(\sigma_f^2+\sigma_a^2H^2)\left[\frac{-J_1 a_{11} a_{12}}{(1+ga_{11})}\right] \qquad (5.3.12)$$

for case (II).

Correspondingly, the effective hydraulic conductivity tensor components can be written as follows:

Case (I): a and f are perfectly correlated

$$\bar{K}_{11} = \frac{E[q_1]}{J_1} = K_m\left\{1+ \frac{\sigma_f^2(1-H\zeta)^2}{2}\left[\frac{1-2a_{11}}{1+ga_{11}}\right]\right\}$$

$$\bar{K}_{21} = \frac{E[q_2]}{J_1} = K_m\sigma_f^2(1-H\zeta)^2\left[-\frac{a_{11}a_{12}}{(1 + ga_{11})}\right] \qquad (5.3.13)$$

Case (II): a and f are statistically independent

$$\bar{K}_{11} = \frac{E[q_1]}{J_1} = K_m\left\{1+\frac{(\sigma_f^2+H^2\sigma_a^2)}{2}\left[\frac{1 - 2a_{11}}{1+ga_{11}}\right]\right\}$$

$$\bar{K}_{21} = \frac{E[q_2]}{J_1} = K_m(\sigma_f^2+\sigma_a^2H^2)\left[\frac{-a_{11}a_{12}}{(1 + ga_{11})}\right] \qquad (5.3.14)$$

Since the effective hydraulic conductivity is a symmetric second-ranked tensor, the hydraulic conductivity in the x_2 direction in the unprimed system, $\bar{K}_{22}$, can be obtained through the relationships between $\bar{K}_{11}$ and $\bar{K}_{21}$, as shown in (4.3.9c). Finally, the effective hydraulic conductivity tensor, $\bar{K}_{ij}$ in the unprimed coordinate system are:

Case (I): a and f are perfectly correlated

$$\bar{K}_{11} = K_m\left[1 + \frac{\sigma_f^2}{2}(1-H\zeta)^2\frac{(1 - 2a_{11})}{1+ga_{11}}\right]$$

$$\bar{K}_{22} = \bar{K}_{33} = K_m\left[1 + \frac{\sigma_f^2}{2}(1-H\zeta)^2\frac{(1 - 2a_{12})}{1+ga_{11}}\right] \qquad (5.3.15)$$

$$\bar{K}_{21} = K_m\sigma_f^2(1-H\zeta)^2\left[\frac{-a_{11}a_{12}}{(1 + ga_{11})}\right]$$

Case (II): a and f are statistically independent.

$$\bar{K}_{11} = K_m\left[1+\frac{(\sigma_f^2+\sigma_a^2H^2)}{2}\frac{(1 - 2a_{11})}{1+ga_{11}}\right]$$

$$\bar{K}_{22} = \bar{K}_{33} = K_m\left[1+\frac{(\sigma_f^2+\sigma_a^2H^2)}{2}\frac{(1 - 2a_{12})}{1+ga_{11}}\right] \qquad (5.3.16)$$

$$\bar{K}_{21} = \bar{K}_{12} = K_m(\sigma_f^2+\sigma_a^2H^2)\left[\frac{-a_{11}a_{12}}{(1 + ga_{11})}\right]$$

The principal effective hydraulic condutivities thus can be derived by using equation (4.3.11). The results are given as follows:

$$\bar{K}'_{11} = K_m\left[1 - \frac{\sigma_f^2(1-H\zeta)^2}{2(1+ga_{11})}\right] \simeq K_m \exp\left[\frac{-\sigma_f^2(1-H\zeta)^2}{2(1+ga_{11})}\right]$$

$$\bar{K}'_{22} = \bar{K}'_{33} = K_m\left[1 + \frac{\sigma_f^2(1-H\zeta)^2}{2(1+ga_{11})}\right] \simeq K_m \exp\left[\frac{\sigma_f^2(1-H\zeta)^2}{2(1+ga_{11})}\right] \qquad (5.3.18a)$$

and

$$\bar{K}'_{11} = K_m\left[1 - \frac{(\sigma_f^2+\sigma_a^2H^2)}{2(1+ga_{11})}\right] \simeq K_m \exp\left[\frac{-(\sigma_f^2+\sigma_a^2H^2)}{2(1+ga_{11})}\right]$$

$$\bar{K}'_{22} = \bar{K}'_{33} = K_m\left[1 + \frac{(\sigma_f^2+\sigma_a^2H^2)}{2(1+ga_{11})}\right] \simeq K_m \exp\left[\frac{(\sigma_f^2+\sigma_a^2H^2)}{2(1+ga_{11})}\right] \qquad (5.3.18b)$$

for case (I) and case (II), respectively. Therefore, anisotropy ratio of the principal horizontal to the vertical hydraulic conductivity is

$$\frac{\bar{K}'_{22}}{\bar{K}'_{11}} = \exp\left[\frac{\sigma_f^2(1-H\zeta)^2}{1+ga_{11}}\right] \qquad (5.3.19a)$$

and

$$\frac{\bar{K}'_{22}}{\bar{K}'_{11}} = \exp\left[\frac{(\sigma_f^2+\sigma_a^2H^2)}{1+ga_{11}}\right] \qquad (5.3.19b)$$

for case (I) and case (II), respectively.

CHAPTER 6
RESULTS AND APPLICATIONS

6.1 Summary of Results

In Chapter 3, steady-state infiltration in unbounded large scale heterogeneous media is investigated. A simple exponential model, (2.2.1), defines the relationship between unsaturated hydraulic conductivity and capillary pressure head at local scale. The characteristics of the heterogeneous porous medium are represented by a stochastic log-saturated hydraulic conductivity and a constant pore size distribution parameter α. The results of this analysis show that variances of capillary pressure head resulting from one and three-dimensional random media are in a form similar to the head variance of saturated flow (Bakr et al., 1978). Both head variances of saturated and unsaturated flow depend on the gradient, the variance of log-saturated hydraulic conductivity, and the correlation scale. Due to the non-linear nature of unsaturated flow, the head variance of unsaturated flow is generally less than the head variance of saturated flow. This result is manifested by the presence of the product term of pore-size distribution parameter, correlation scale, and gradient in (3.2.16), (3.2.20), and (3.3.13).

Head variances of one- and three-dimensional flow are equivalent at large values of $\alpha\lambda$, which correspond to either coarse-textured material or perfectly correlated medium. Reduction of head variance due to higher dimensionality is

significant only for small $\alpha\lambda$ values.

Generally, the effective hydraulic conductivity of unsaturated media, unlike saturated media, is dependent on the capillary pressure gradient, pore-size distribution parameter, and correlation length scale of the media. This association demonstrates the non-linear Darcy flow behavior of the infiltration process. Effective hydraulic conductivities of one- and three-dimensional models are bounded by the harmonic and arithmetic mean, and approach the geometric mean as $\alpha\lambda$ grows. The variance of log-unsaturated hydraulic conductivity decreases with $\alpha\lambda$, and depends on the pressure gradient.

Chapter 4 examines unsaturated flow in more realistic stratified porous media. Again, the heterogeneity of the medium is represented by a stochastic log-saturated hydraulic conductivity. However, a three-dimensional anisotropic covariance function defines the spatial correlation structure of the medium. The vertical scale, λ_1, is assumed to be less than the horizontal scales: λ_2, and λ_3. The horizontal scales are considered to be isotropic ($\lambda_2 = \lambda_3 = \lambda$). The head variance is evaluated as a function of the aspect ratio, $\rho=\lambda/\lambda_1$. As the ratio becomes large, corresponding to the case of flow perpendicular to a perfectly stratified soil, the head variance approaches infinity. This result is equivalent to the one-dimensional

result. In contrast, the head variance approaches zero when the ratio approaches zero. This satisfies the condition for which flow is parallel to a perfectly stratified soil formation.

Effective hydraulic conductivity in the vertical direction in this case strongly depends on the aspect ratio. The analysis yields a harmonic mean and arithmetic mean for $\rho \to \infty$ and $\rho = 0$, respectively. However, the effective hydraulic conductivity of the medium, which is associated with large $\alpha\lambda$ values, tends to become the geometric mean regardless of the magnitude of the aspect ratio.

Flow in an arbitrarily oriented anisotropic random medium is analyzed in Section 4.3. In this case, the bedding is at an angle to the mean gradient as illustrated in Figure (4.3.1). Assuming that the unsaturated hydraulic conductivity is a second rank symmetric tensor, effective hydraulic conductivities in principal directions are derived. For the special case where $\rho \to \infty$ (perfectly stratified soil formation) and the mean gradient is a unity and in the vertical direction, the principal effective hydraulic conductivities are $K_v = K_m \exp(-\sigma^2_{\ln K}/2)$ and $K_h = K_m \exp(\sigma^2_{\ln K}/2)$. These conductivities correspond to the harmonic and arithmetic means of the unsaturated conductivities, respectively.

Further investigation on the effective hydraulic conductivity is carried out for a similar case, but the direction of the mean gradient is arbitrary. The arbitrarily oriented mean gradient yields a multi-gradient flow situation as shown in Figure (4.4.1). For a perfectly stratified soil formation ($\rho \to \infty$), the effective hydraulic conductivity is substantiated to be a symmetric tensor of rank two ((4.4.8a) to (4.4.8d)). If the mean gradient is fixed only in the vertical direction, the results are identical to those obtained in Section 4.3 where the conductivity is assumed to be a symmetric tensor of rank two. The result confirms the assumption of tensorial properties of unsaturated hydraulic conductivity. The principal conductivities of the hydraulic conductivity tensor can be written in general form as $\bar{K}'_{11}(H) = K_G \exp(-AH-\sigma^2_{lnK}/2)$ and $\bar{K}'_{22}(H) = \bar{K}'_{33}(H) = K_G \exp(-AH+\sigma^2_{lnK}/2)$ where K_G is the geometric mean of saturated hydraulic conductivity, and A and H are the mean of pore-size distribution parameters and capillary pressure heads, respectively. The anisotropy ratio $\bar{K}'_{22}/\bar{K}'_{11}$, is given by $\exp[\sigma^2_f/(1+e)]$, where $e = \alpha\lambda_1[(2J_1-1)a_{11}+2J_2a_{12}]$. The degree of anisotropy depends on the magnitude of e whcih are related to $\alpha\lambda_1$, orientation of the stratification, θ, and the magnitude and the direction of the gradient. For large values of e, the medium tends to be isotropic. In contrast, the anisotropy ratio increases with a decreasing e value. However, when

α = 0, the maximum anisotropy ratio is equal to that of saturated flow .

In Chapter 5, one dimensional infiltration through a heterogeneous medium is reinvestigated by considering both the log-saturated hydraulic conductivity and the pore-size distribution parameter of the medium as stochastic processes in space. Exponential and hole covariance functions are used in one-dimensional analyses. Since the exponential covariance function does not yield a finite head variance in a general case where J≠1 (see (5.2.12)), the hole function is used. Because of the consideration of α as a stochastic process, knowledge of the cross-covariance function between a and f processes is necessary in order to evaluate the head variance. To simplify the analysis, two cases are considered; Case (I): α and $\ln K_s$ are perfectly correlated, and Case (II): α and $\ln K_s$ are statistically independent. When J=1, both cases yield similar forms of head variance as those derived with the deterministic pore-size distribution parameter assumption. However, the head variance under this circumstance is proportional to $\sigma_f^2(1-\zeta H)^2$ or $(\sigma_f^2 + \sigma_a^2 H^2)$, instead of only σ_f^2 as in previous chapters; ζ is the constant of proportionality relating α to $\ln K_s$. Thus, the head variance can be significantly large depending on the magnitude of the mean capillary pressure, especially for soils with a large variance of the pore-size distribution parameter, σ_a^2.

The effective hydraulic conductivity resulting from the one-dimensional analysis with the assumption that $\ln K_s$ and α are stochastic processes is of the same form as that derived from the analysis based on a deterministic α and random $\ln K_s$; i.e., $K_e = K_G \exp(-AH-\sigma^2_{\ln K}/2)$. However, the variance of $\ln K$, $\sigma^2_{\ln K}$, is replaced by either $(\sigma_f^2+\sigma_a^2H^2)/[(1+A\lambda]$ or $\sigma_f^2(1-H\zeta)^2/[(1+A\lambda)]$, instead of $\sigma_f^2/[(1+A\lambda)]$, depending on the correlation between α and $\ln K_s$. The results for the head variance and effective hydraulic econductivity obtained show that the variation of the pore-size distribution parameter is the essential element which causes a significant head variation and a reduction of effective hydraulic conductivity.

Finally, three-dimensional flow in a perfectly stratified soil formation with an arbitrary angle to a unit gradient is analyzed in section 5.3. Again, similar effects on the head variance and effective hydraulic conductivity as in one-dimensional flow are evident. The most significant effect of variation of the pore-size distribution parameter is on the anisotropy ratio of hydraulic conductivity. Variation of this parameter reveals that the ratio can be strongly dependent on the mean capillary pressure. The ratio also depends on the magnitude and direction of the mean gradient, the products of correlation scale and the mean pore-size distribution parameter, and the orientation of the stratification. In other words, the anisotropy of unsa-

turated hydraulic conductivity is dependent on moisture content and hydraulic gradient dependent.

6.2 Comparison of Observed and Calculated Variance of Soil Moisture Content

To illustrate the predictive capability of the theoretical result on the head variance, the theoretical result, (5.3.6b), is applied to a field situation where some of the necessary parameters have been observed. Nielsen et al. (1973) have observed a large number of hydraulic conductivity-soil moisture relationships and soil-water retention data over a 150-hectare field in Fresno, California. The soil is generally classified as the Panoche soil series, which has uniform profiles but a wide range of textures including: loam, clay loam, silty clay, and silty clay loam. Although measurements were taken from 20 plots at 6 different depths (1 foot intervals) over the entire area, only data collected in the silty clay loam (9 plots, 6 depths) are used in the calculation of soil moisture variation. The statistical homogeneity assumption employed in the theoretical analysis restricts the use of the entire data set.

In order to apply the model to the field situation, estimates of the parameters, σ_f^2, σ_a^2, λ_I, and λ have to be calculated from the available data set. Since the hydraulic conductivity data are measured in terms of soil moisture content θ, a translation of K-θ to K-ψ is necessary for this calculation. This translation is carried out by a direct conversion of θ to ψ according to the soil-water retention curve observed at each depth of each plot. By fitting the

exponential hydraulic conductivity model, (2.2.1), to the converted $\ln K$-ψ relation data, the α (slope) and $\ln K_s$ (intercept) of each K-ψ curve are determined. Estimates of σ_f^2, σ_a^2, and mean A of this soil are 2.467, 0.000067 cm^{-2}, and 0.0294 cm^{-1}, respectively. The data are not adequate to estimate the correlation scales of this particular field. To circumvent this difficulty, the horizontal and vertical scales are assumed to be 40 m and 1.0 m, respectively, based on information reported by Bakr (1976) and Vieira et al. (1981).

Head variance is predicted by utilizing the theory (5.3.6b) and the estimated parameters. To obtain a direct comparison of observed data to the calculated result, the calculated head variance is related to the variance of soil-moisture content by considering a simple linear relationship:

$$\theta = c\psi + d + \epsilon$$

where θ= moisture content, ψ= capillary pressure head, and ϵ is a normally distributed random variable with mean zero and variance σ_ϵ^2. Based on the above linear model, a regression analysis was carried out for the 54 soil-water retention curves at pressure ranges, 0.0 to 200.0 cm of water. The value for c is found to be -0.0006. The correlation coefficient for the regression line is 0.7022 with σ_ϵ=0.0387. Therefore, the variance of capillary pressure head, σ_h^2, is

related to the variance of moisture content, σ_θ^2 by:

$$\sigma_\theta^2 = c^2\sigma_h^2 \qquad (6.2.2)$$

The results are illustrated in Figure (6.2.1), where the standard deviations of calculated moisture contents at different mean capillary pressure heads are plotted along with the standard deviations of observed moisture data. Results obtained for other values of the vertical scale λ_1, and λ_2 (same aspect ratio) are also illustrated in figure (6.2.1). The theoretical calculations are subjective because λ_1, λ_2, and correlation between a and f processes of this field are not known. In addition, the exponential model does not accurately describe the K-ψ relation for each observed data set at the entire range of pressure head. The assumption of a linear model for capillary pressure head and moisture content could further misrepresent actual behavior of the relation. Since these retention curves vary spatially, the linear model merely describes the average behavior of actual capillary pressure and moisture relation. In fact, the variation of these retension curves are significant as indicated by σ_ϵ. However, it is interesting that the theory predicts the observed magnitudes of σ_θ with reasonable value of λ_1, and λ_2. Moreover, the theory predicts the general trend of variation of moisture contents. The general trend follows the relation that the variation of moisture content increases with mean capillary pressure. The predicted trend

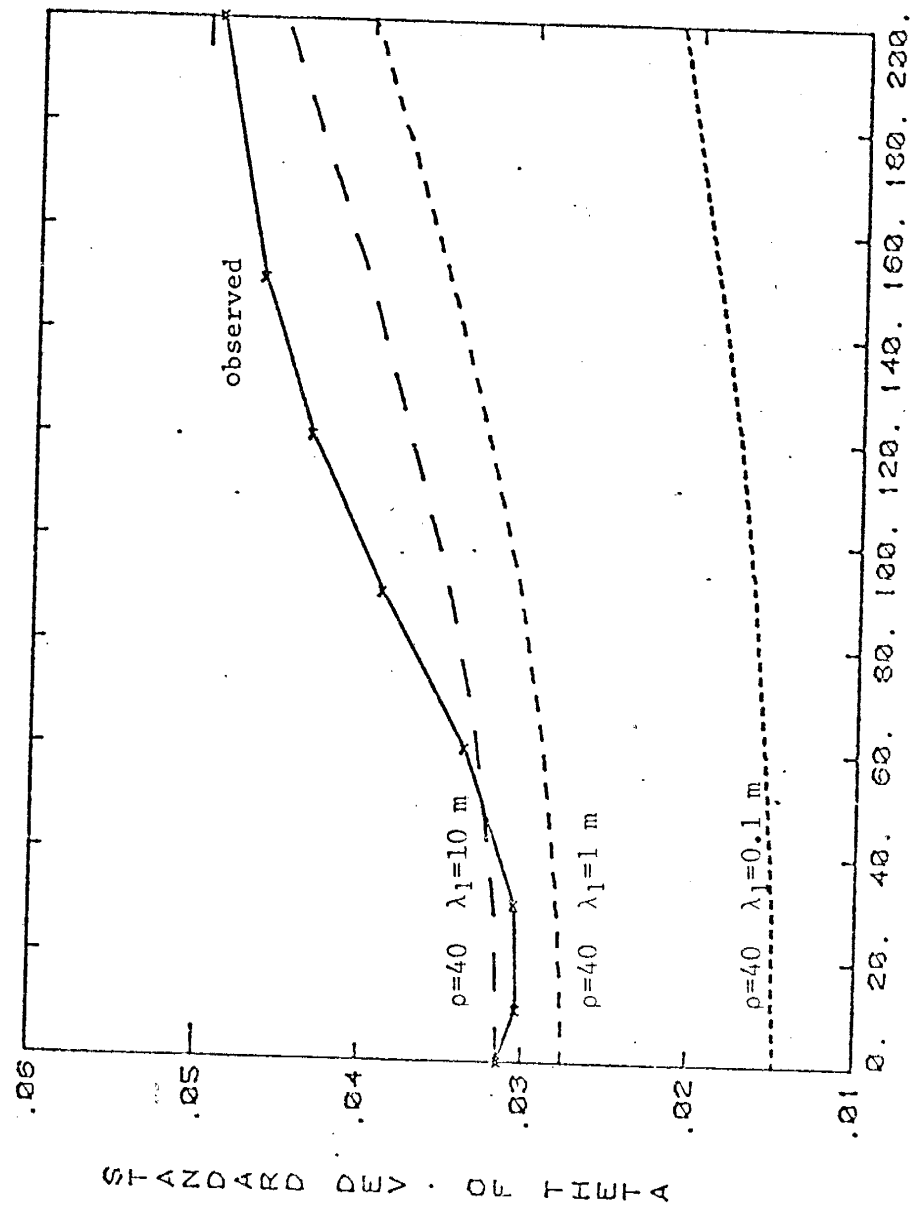

Figure 6.2.1: Comparison of observed and calculated standard deviation of moisture content as a function of mean capillary pressure.

is also in reasonable agreement with the observed trend.

To further illustrate mean dependence of capillary pressure variation, capillary pressure measurements collected by Fritten (1981) in a 2-hectare corn field are analyzed. Estimated variances of the capillary pressure head are listed in Table (6.2.1) along with its mean values. Similar information obtained from data collected by the author (see appendix A) in an alfalfa field is also included in the table. Both observed variations of capillary pressure confirm the theoretical result that the head variance grows with the mean capillary pressure. In other words, the drier the soil is, the higher the capillary pressure head variance.

Table 6.2.1: Variances and means of soil capillary pressure in some fields.

Fritton		Author	
MEAN (BAR)	STANDARD DEV.	MEAN (CM)	STANDARD DEV.
1.2	4.7	162	22
2.0	10.0	185	33
4.4	28.0	186	35
8.5	48.0	187	36
		325	80
		334	137
		336	95
		402	170

6.3 Examples of Field Anisotropy of Unsaturated Hydraulic Conductivity

The theory developed in Chapter 5 predicts that unsaturated conductivity anisotropy is a function of mean capillary pressure. What is the magnitude of anisotropy in a realistic soil formation at low saturation? To answer this question, the anisotropy ratios of two soils- Panoche silty clay loam (Nielsen et al. 1974) and Maddock sandy loam (Carvallo et al. 1974)- are evaluated by using the theoretical model for the special case where gradient J=1. Representative behavior of the hydraulic conductivity of the two soils as a function of capillary pressure head is shown in Figures (6.3.1) and (6.3.2). Note that the variation of α (slope) of the $\ln K$-ψ curves of the sandy loam is more drastic as compared to Panoche silty clay loam.

The procedure used in estimating the required parameters of Maddock sandy loam for this analysis is essentially the same as the previous example for Panoche soil. However, the number of data points available in this case is much less (2 plots and 7 depths). Table (6.3.1) includes the estimated values of the parameters of the two soils needed to evaluate the anisotropy. The variances of $\ln K_s$, α, and mean of α for the sandy loam are significantly greater than those of the silty clay loam. The value of σ_f^2 for the sandy loam is unusually large. This large variation can be attributed to extrapolation of the unsaturated conductivity to

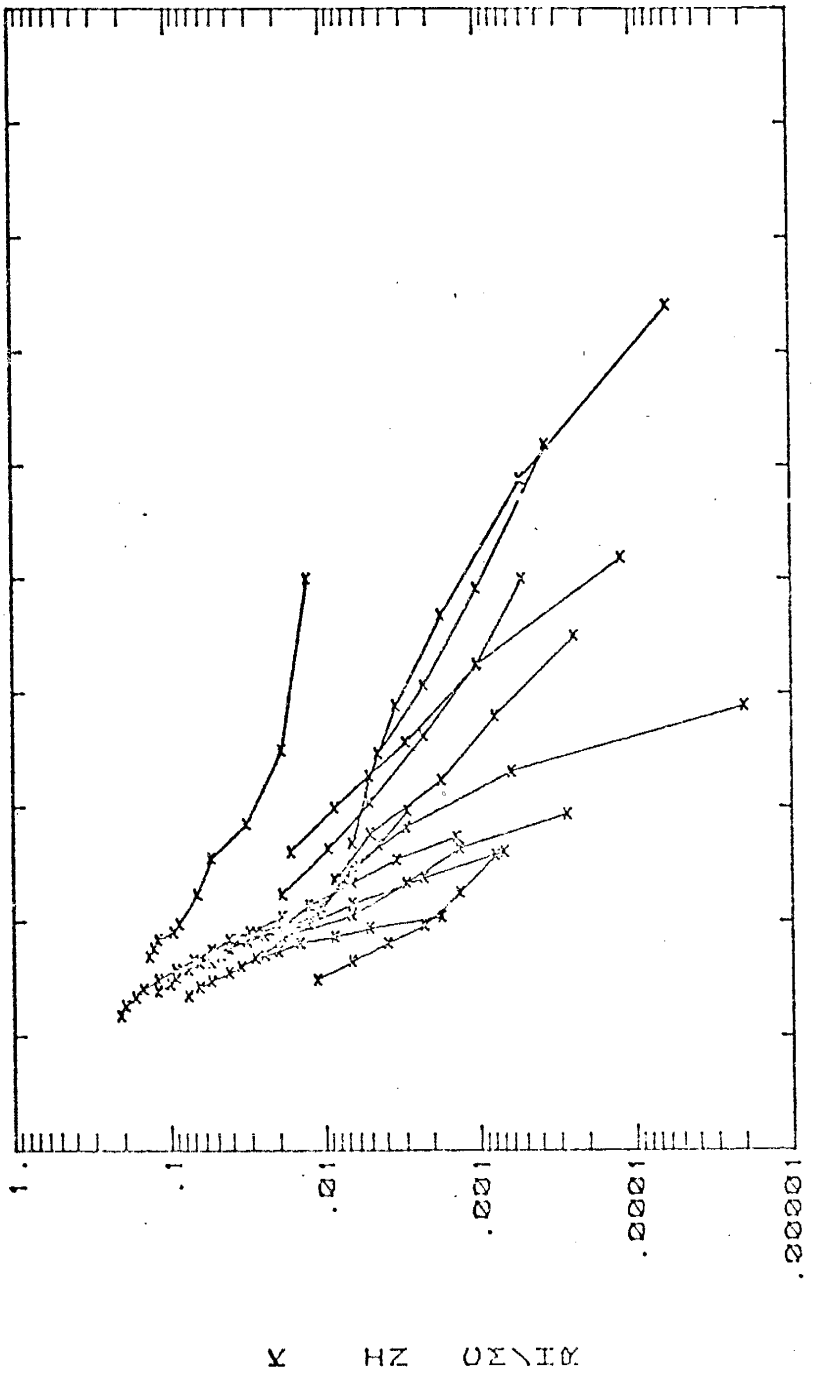

Figure 6.3.1: K-ψ relationships of Maddock sandy loam.

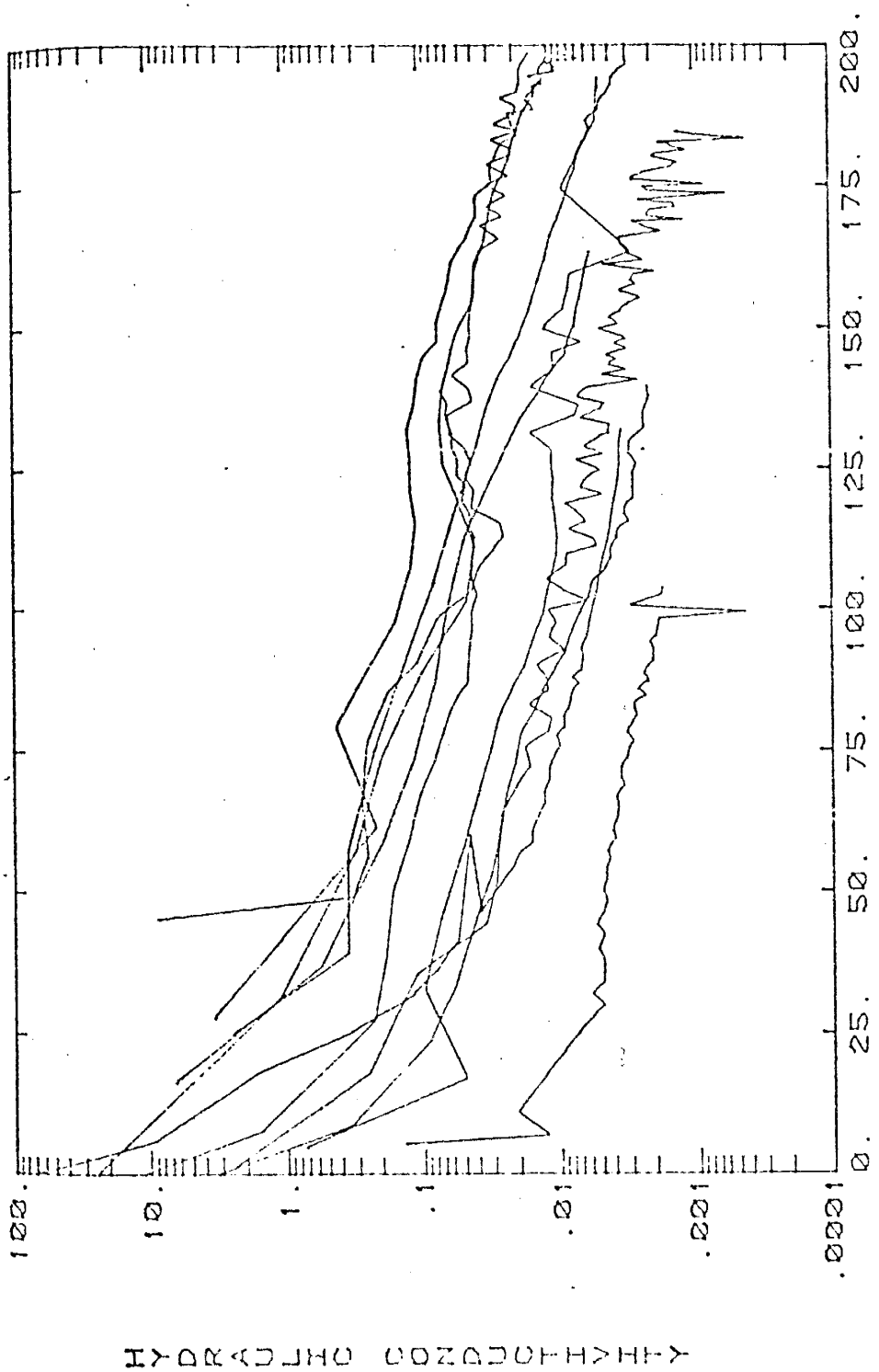

Figure 6.3.2: K-ψ relationships of Panoche silty clay loam.

Table 6.3.1 Estimated parameters for the evaluation of hydraulic conductivity anisotropy in Maddock sandy loam and Panoche silty clay loam.

SOIL TYPE	σ_f^2	σ_a^2 CM^{-2}	A CM^{-1}	ρ	SOURCE
Maddock Sandy loam	7.45	0.0076	0.147	40	Carvallo et al. 1974
Panoche Silty Clay loam	2.48	0.000067	0.0294	40	Nielsen et al. 1973

the saturated condition based on the simple exponential conductivity model. However, the effect of the large variation of f on the results is not significant for high mean capillary pressures, since the contribution from the mean pressure head is much greater than the variance of saturated hydraulic conductivity. To be more precise, one should consider σ_f^2 as the variance of conductivity at a reference capillary pressure head in the range where the exponential relation holds.

The anisotropy ratios for these two soils with ρ=40 are derived by using (5.3.8) in which the variance and the cross-covariances terms are evaluated numerically (details of this numerical evaluation is given in Appendix L). Figure (6.3.3) illustrates the mean capillary pressure dependence of the anisotropy ratio of these two soils. The figure shows the anisotropy of Maddock sandy loam is far more significant, as mean capillary pressure increases, than the anisotropy of the Panoche silty clay loam. This difference can be conceived easily if one examines the anisotropy formula (5.3.19b) derived from the theory for the special case where J_1=1, J_2=J_3=0; θ=0, and $\rho \to \infty$. (5.3.19b) indicates that the anisotropy grows exponentially with the exponent $(\sigma_f^2+\sigma_a^2H^2)/(1+A\lambda)$. As a result of a large value of σ_a^2 in sandy loam (about 2 orders of magnitude larger than that of silty clay loam), the conductivity anisotropy of sandy loam grows rapidly as mean capillary pressure increases. On the other hand, the rate of growth of the anisotropy of Panoche

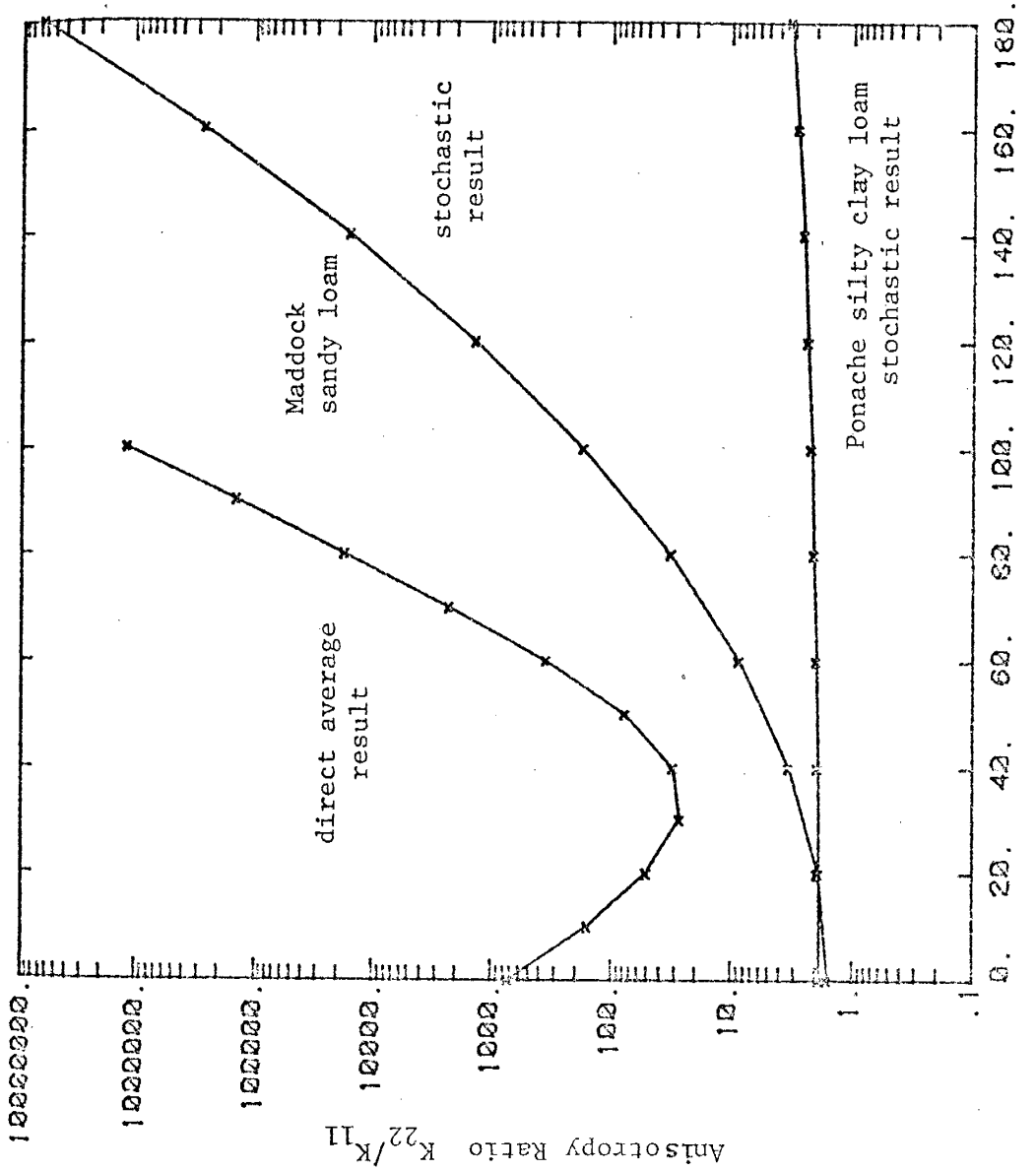

Figure 6.3.3: Comparison of the anisotropy ratios obtained by the stochastic and the direct average methods for the sandy loam and the silty clay loam.

silty clay loam is insignificant at this pressure range. This phenomenon is clarified if one considers the sandy loam as a medium consisting of soils of two distinct textures: clay and sand. One of the possible situations is that of sand overlying clay layer. In such a situation, after a steady-state infiltration is established, a perched water table can develop in the sand, just above the boundary with the less permeable clay layer. Thus, the lateral hydraulic conductivity can be greater than the vertical hydraulic conductivity.

The opposite case is infiltration into a profile with a clay layer over a sand layer. As illustrated in Figure (2.2.1), at some pressure ranges the unsaturated conductivity of clay is always greater than that of sand. Vertical movement of water from the clay layer can be restricted because of the infinitesimally small conductivity of sand at this pressure range. Thus, water is confined to the clay layer and tends to disperse in the lateral direction instead of downward direction. As pressure increases, the conductivity of sand is further reduced, and the conductivity of the clay may remain relatively constant. Hence, the anisotropy becomes more significant. In contrast, the silty clay loam has a uniformly textured material throughout the profile which is evident from Figure (6.3.2). The contrast in unsaturated hydraulic conductivity of each layer is relatively small for the whole range of capillary pressure. Water easily can propagate downward and lateral movement of

moisture would be limited.

Since similar behavior of the anisotropy can be produced by any deterministic model for layered soil, the importance of considering spatial correlation structure in determining the effective unsaturated conductivity should be discussed.

One plausible way to estimate the effective conductivity anisotropy is to take the ratio of arithmetic mean and harmonic mean of conductivity values. The arithmetic mean represents effective conductivity in the direction parallel to the bedding of a composite medium, whereas the harmonic mean represents that in the direction normal to the bedding. This has been proved to be valid (Bear, 1972; Gutjhar et al., 1978; Gelhar and Axness, 1981) for saturated flow. By applying this simplistic concept, the hydraulic conductivities of each soil, reconstructed from the previously estimated parameters and the exponential conductivity model, are arithmetically averaged at each pressure to obtain a mean K-ψ curve that represent the unsaturated conductivity in the directions parallel to the beddings. Similarly, the harmonic mean of the hydraulic conductivities at each pressure head is used to represent the mean hydraulic conductivity in the direction normal to the beddings at that perticular pressure. Thus, each soil has two K-ψ curves to describe the unsaturated hydraulic conductivities in two principle directions. We will refer to this method as the "direct average method". The two curves obtained by this

method are plotted in Figure (6.3.4) as a function of capillary pressures. The anisotropy ratio, which is the ratio of the two curves, is depicted in Figure (6.3.3) along with the ratio derived from the theory. The anisotropy ratio obtained by the direct average method behaves in a similar manner as that by the stochastic theory. Both results show the dependence of anisotropy ratio on the mean capillary pressure. But the direct average method yields a consistently higher anisotropy in the range of interest.

To explain the discrepancy, note that, assuming lnK to be normally distributed, the harmonic mean and the arithmetic mean can be expressed in general forms as:

$$K_h = K_m \exp(-\sigma^2_{lnK}/2) \text{ and } K_a = K_m \exp(\sigma^2_{lnK}/2)$$

in which σ^2_{lnK} is the variance of the unsaturated conductivity, and K_m is the geometric mean of the unsaturated hydraulic conductivity. The theory behind the direct average method can be unravelled from the evaluation of σ^2_{lnK}. From (3.2.4), lnK can be expressed as

$$lnK = \bar{K}+k = F+f -(A+a)\psi \qquad (6.3.2)$$

if ψ is considered to be non-random. Subtracting the mean equation of (6.3.2) from (6.3.2), the perturbation equation becomes:

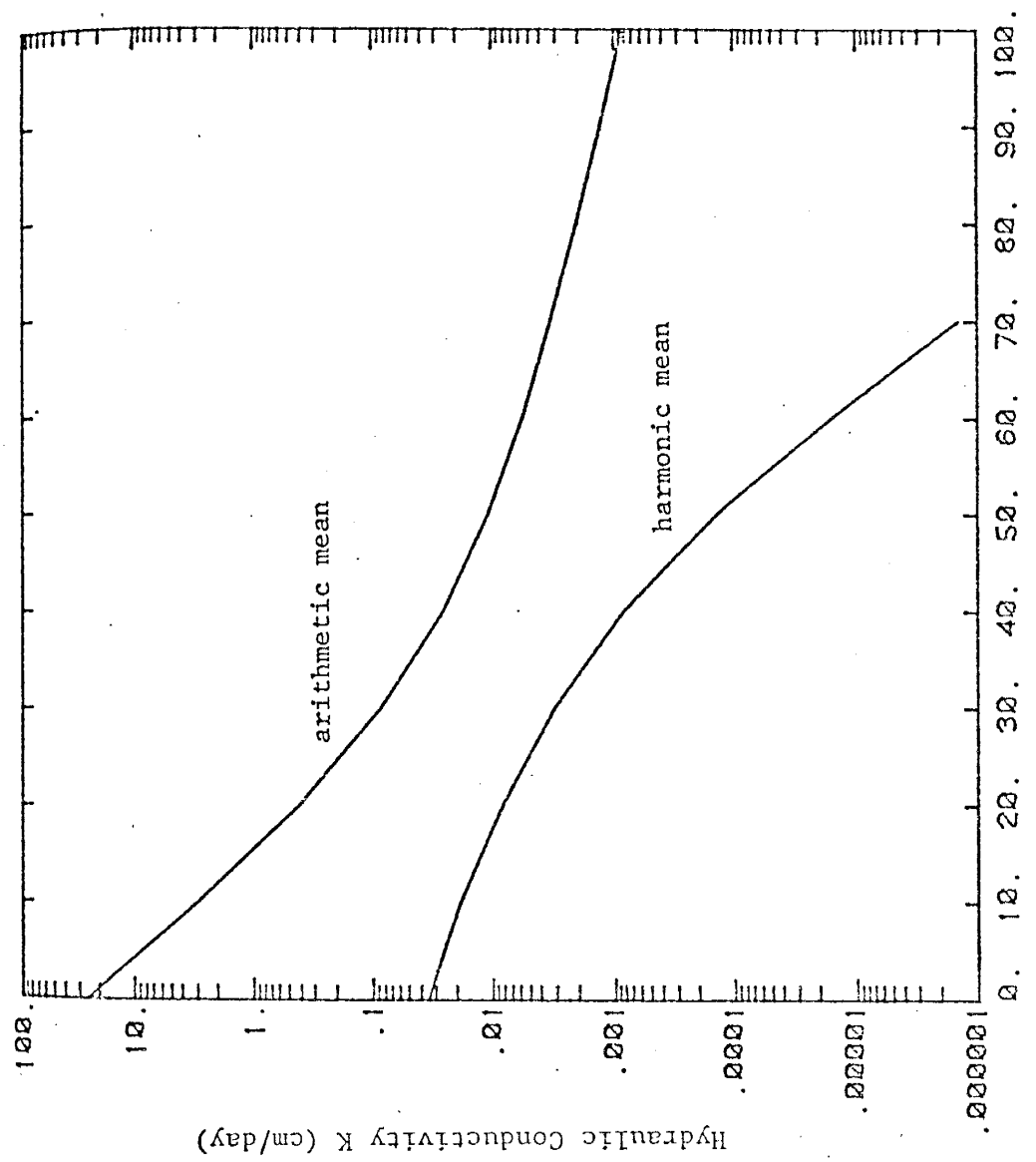

Figure 6.3.4: Mean K-ψ relation curves of Maddock sandy loam obtained by the direct average method.

$$\ln K - E[\ln K] = f - a\psi$$

correspondingly,

$$\sigma^2_{\ln K} = E[(f - a\psi)^2]$$
$$= \sigma^2_f - 2\mathrm{cov}(a,f)\psi + \sigma^2_a\psi^2$$

The above expression can be further reduced to

$$\sigma^2_{\ln K} = \sigma^2_f + \sigma^2_a\psi^2,$$

if we assume a and f are uncorrelated. Thus, the anisotropy ratio is determined as

$$\frac{K_a}{K_h} = \exp(\sigma^2_{\ln K}) = \exp(\sigma^2_f + \sigma^2_a\psi^2) \qquad (6.3.3)$$

By comparing (6.3.3) with (5.3.19b),

$$\frac{K_{22}}{K_{11}} = \exp[(\sigma^2_f + \sigma^2_a H^2)/(1+A\lambda)]$$

which is the result for the special case where J=1, θ=0, and $\rho\to\infty$, the reason that the direct average method overestimates the anisotropy ratio becomes clear. This is because the stochastic theory produces a smaller $\sigma^2_{\ln K}$ due to the pres-

ence of the denominator $(1+A\lambda)$ than the direct average method. The direct average method assumes that capillary pressure head is a deterministic variable. In reality, ψ is a stochastic process, as has been observed in field studies (see Section 2.3). Furthermore, ψ is directly related to the flow regime, which is subject to the influence of the correlation scale of the soil property. Therefore, without solving the governing flow equation, the direct average method fails to provide a more realistic result. The unsaturated anisotropy of a heterogeneous medium depends not only on the mean pressure but also on gradient and correlation scales.

Field data for a quantitative comparison on anisotropy with the theoretical anisotropy results are not available. However, some field observations of moisture movement in unsaturated zones do indicate qualitative confirmation of the saturation dependence of unsaturated anisotropy. Crosby et al. (1968, 1971a, and 1971b) reported findings of comprehensive field observations of pollutant migration in glacial outwash deposits at Spokane Valley, Washington. One of the pollutant sources in the area is a septic tank drain field serving a local nursing home. Results of soil sample analysis indicate that chemical pollutants travel with moisture fronts. However, they report that moisture is limited to the upper 20 to 25 feet, approximately a quarter of the thickness of the unsaturated zone in the area. To explain the extremely dry condition at the depth below 25 feet, they state that " the drain field waters quite obviously must be

dispersing laterally in the finest interbed in response to capillary gradients exceeding the gravitational potential". This lateral flow postulation seems consistent with the anisotropy derived from the theory.

In the loess-loam area north of Beer-Sheba, field observations (Sinai et al, 1974) reveal a similar phenomenon- rain infiltrates the soil to a limited depth, so that there was no net recharge of the groundwater. A lateral flow effect within the unsaturated soil was suggested.

Direct evidence of the saturation dependent anisotropy was reported by Corey and Rathjens (1956). In their Figure 4, relative permeability of oil and gas measurements on the Berea sandstone core demonstrate that anisotropy is a function of oil saturation. They stated that ".....Berea sandstone which, when dry or fully saturated, appears to be homogeneous and isotropic. When the material is partially desaturated, however, thin and regular spaced strata are apparent. Moreover, the air permeability of the dry core is almost twice as great paralled to the bedding planes as perpendicular to them. Evidently the material is quite uniform, but it is not isotropic. the effect of the anisotropy is to increase greatly the critical gas and to make the oil relative permeability curve steeper when flow is across the bedding planes". Although the scale of the core sample is relatively smaller than the scale the theory considers, the observation supports the theoretical result.

Zaslavsky and Sinai (1981 IV and V) explore the concept

of the anisotropy of unsaturated flow in a stratified soil formation. Based on a theoretical study of steady-state infiltration in a two-layered soil, they conclude that the soil actually behaves as an anisotropic medium. The anisotropy is found to increase with the rate of vertical flow. The horizontal component of the hydraulic conductivity can be several times the vertical one. To show the similarities between the stochastic theory and their results on anisotropy, the stochastic result is applied to their study. Their model considers only a two-layered deterministic system, but it does provide a direct comparison of the anisotropy derived from the stochastic analysis.

A medium consisting of two homogeneous soil layers is considered (Zaslavsky and Sinai, 1981 IV). The thickness of these two layers are D_1 and D_2, respectively. Their saturated conductivities are K_{s1}, and K_{s2}, respectively. The relationship of unsaturated conductivity and capillary pressure head is also assumed to be exponential. The pore-size distribution parameters are a_1 and a_2 for the upper and lower soil layers, respectively. The anisotropy of the effective unsaturated conductivity of this composite medium is derived from the analysis of steady-state infiltration to the medium with an inclination angle of θ. No lateral capillary pressure gradient was assumed. For small values of a_1D_1 or $a_2D_2\cos\theta$, the anisotropy coefficient, $U=(K_{22}/K_{11}-1)$, as a function of rain intensity P of the layers, in which $K_{s2}/K_{s1}=10$, $a_2/a_1=6$, and $D_2/D_1=10/6$ is illustrated in Figure

(6.3.5). Assuming the composite medium has a bimodal distribution, the theoretical result for the case where J=1, and $\rho \to \infty$ is directly applied to the example. The variance of log-saturated hydraulic conductivity is evaluated to be σ_f^2=1.32. Since mean capillary pressure is zero at saturation (Pr=2.28), and the correlation scale, λ of the situation is estimated to be 4.0, the mean slope A = 0.05 is obtained via (5.3.19a) in which $\rho \to \infty$, θ=0, and J=1 are assumed. The knowledge of A and a_2/a_1 =6 yields values of a_1 and a_2; 0.014 and 0.086, respectively. Correspondingly, the variance of the pore-size distribution parameter σ_a^2 is given as 0.0013. The two-layered deterministic system can be thought of as one with α and $\ln K_s$ perfectly correlated, with $a_1 \neq a_2$, the K-ψ curves of these two soil should cross at a specific capillary pressure H^*. The perfect correlation between a and f implies that $\sigma_f - \sigma_a H^*$ in the theoretical model should be equal to zero at H^*. Since σ_f and σ_a are known, H^* is determined to be 31.9 cm, which is equivalent to Pr=0.63 in their result. Provided that these estimated parameters are comparable to their case, the anisotropy ratio is evaluated through the correlated model (5.3.19a). The result is illustrated in Figure (6.3.5). This figure shows an excellent agreement in the results of the two models. However, it may not be appropriate to make such a statement since the estimated parameters are not necessarily representative of the situation. For example, the angle of inclination is unknown in their analysis so that the theoretical analysis

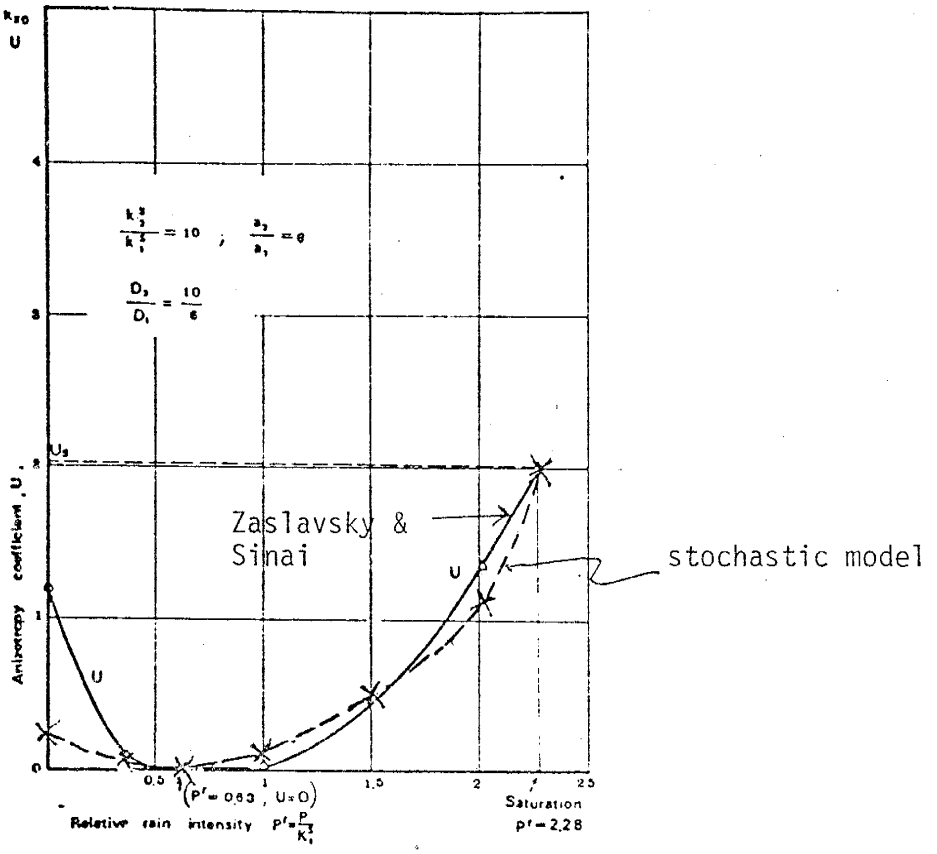

Figure 6.3.5: Comparison of anisotropy ratios derived from the stochastic result and a deterministic analysis.

assumes an angle of zero. However, it does demonstrate that both models derive the same general behavior of the anisotropy of unsaturated conductivity.

6.4 Practical Implication of The Results

The most important result arising from the theoretical analysis is the anisotropy of unsaturated hydraulic conductivity. The unique nature of the anisotropy, which depends on the degree of soil saturation, may have been postulated in the past. However, conclusive results on this aspect of unsaturated conductivity have not been reported in the literature. The practical implication of the anisotropy is significant. Such a moisture dependent anisotropy virtually causes a strong lateral flow component in unsaturated media. The magnitude of the lateral flow is not immaterial, and it can not be neglected for practical purposes.

One of the immediate impacts of the lateral flow concept on hydrology is the groundwater recharge from open channel. In the classic approach, seepage from open channel is analyzed either by the "saturated approach" (Glover, 1961; Bouwer, 1964; and others) or by Green-Ampt's one-dimensional unsaturated flow approach (Bouwer, 1964 and others). Recent studies (Jeppson and Nelson, 1970 and Vaclin et al., 1979) show that these approaches do not adequately describe the actual flow system in the field due to the presence of strong lateral capillary pressure gradients. Multidimensional unsaturated flow analysis is suggested.

Since most soils exhibit bedding, the non-uniformity and stratification of the soils produce a moisture-dependent anisotropy in which the horizontal hydraulic conductivity can be many times the vertical, depending on the saturation

of the soils. Thus, the vertical flow component is no longer dominant. A three-dimensional flow situation with large lateral flow components develops. Such a three-dimensional phenomenon can not be adequately depicted by any classic three-dimensional flow model with isotropic conductivity or anisotropic conductivities of a constant ratio (Freeze, 1971). The lateral flow resulting from the moisture-dependent anisotropy may restrict vertical movement of water to the groundwater. Consequently, water may be confined to a shallow depth so that the net recharge to groundwater systems is much less than that predicated by the classic approach.

Thus, application of the classic methods to estimate net groundwater recharge would be erroneous without a careful consideration of the complexity of the infiltration process.

The saturation dependent anisotropy plays an important role in the study of pollutant migration. According to theoretical results the horizontal unsaturated hydraulic conductivity of a perfectly stratified soil formation could be several orders of magnitude greater than the vertical unsaturated hydraulic conductivity. The vertical conductivity decreases considerably as mean capillary pressure increases. As the soil becomes drier, the horizontal hydraulic conductivity increases relative to the vertical conductivity. The increase in the lateral flow component causes migration of water in the horizontal direction.

When pollutants escape from a landfill or a waste depository site into a geologic formation where interbedded clay and sand are dominant, the plume of pollutants can migrate a substantial horizontal distance in the unsaturated zone before reaching the water table. Since pollutants migrate a substantial horizontal distance before reaching the water table, this new concept of unsaturated anisotropy may shed some light on solving some waste isolation problems.

Field observations confirm the lateral migratory path of polluted water in the vadose zone. Crosby et al. (1968) found that pollutants discharging from a septic tank drain field in a glacial outwash plain of Spokane Valley, Washington, tend to travel with moisture. The soil moisture in this area is restricted to a depth of approximately 25 feet, and the water table is about 90 feet to 125 feet below the land surface. According to Crosby et al. (1968), during the summer season, much of the water in the upper 25 feet is ultimately removed by evapotranspiration causing an increase in the concentration of pollutants in this zone. They also suggested the continuous built-up of pollutants in the upper 25 feet of unsaturated zone could reduce the permeability of the soil, and restrict the downward migration of water.

The theoretical results and field observations suggest a method for wastewater disposal. The use of controlled application rates of wastewater in a stratified unsaturated soil formation would be an appropriate and inexpensive way to isolate wastewater. Since migration of pollutants in

this type of environment is predominantly in lateral direction, wastewater applied on the surface would be confined to the unsaturated zone. Hence, the pollutant plume tends to spread to a greater extent laterally because of this reduction of vertical movement. Thus, the danger of polluting groundwater resources may be reduced.

Another practical application of the anisotropy of unsaturated media can be illustrated in the design of geologic environments using the unsaturated hydraulic conductivity properties of soils for waste storage facilities in the shallow subsurface. Under unsaturated conditions, a gravel lens will cause lateral flow in a finer-textured material situated above the gravel. Corey and Horton (1969) refer to this phenomenon as the "wick effect". Frind et al. (1976) revealed the potential usefulness of the wick effect in the design of a waste storage facility.

The basic design of the storage facility is illustrated in Figure (6.4.1). The waste container situated above the water table is enclosed in a gravel layer with a sloping surface at the top. Finer-grained material overlying the gravel layer forms the wick layer. Due to drastic contrasts in the unsaturated hydraulic conductivity of the two layers, water is confined in the finer-textured material. The sloping interface creates lateral hydraulic gradients in finer-grained material and forms a protective "umbrella" for the waste container.

A more desirable material for this protective umbrella

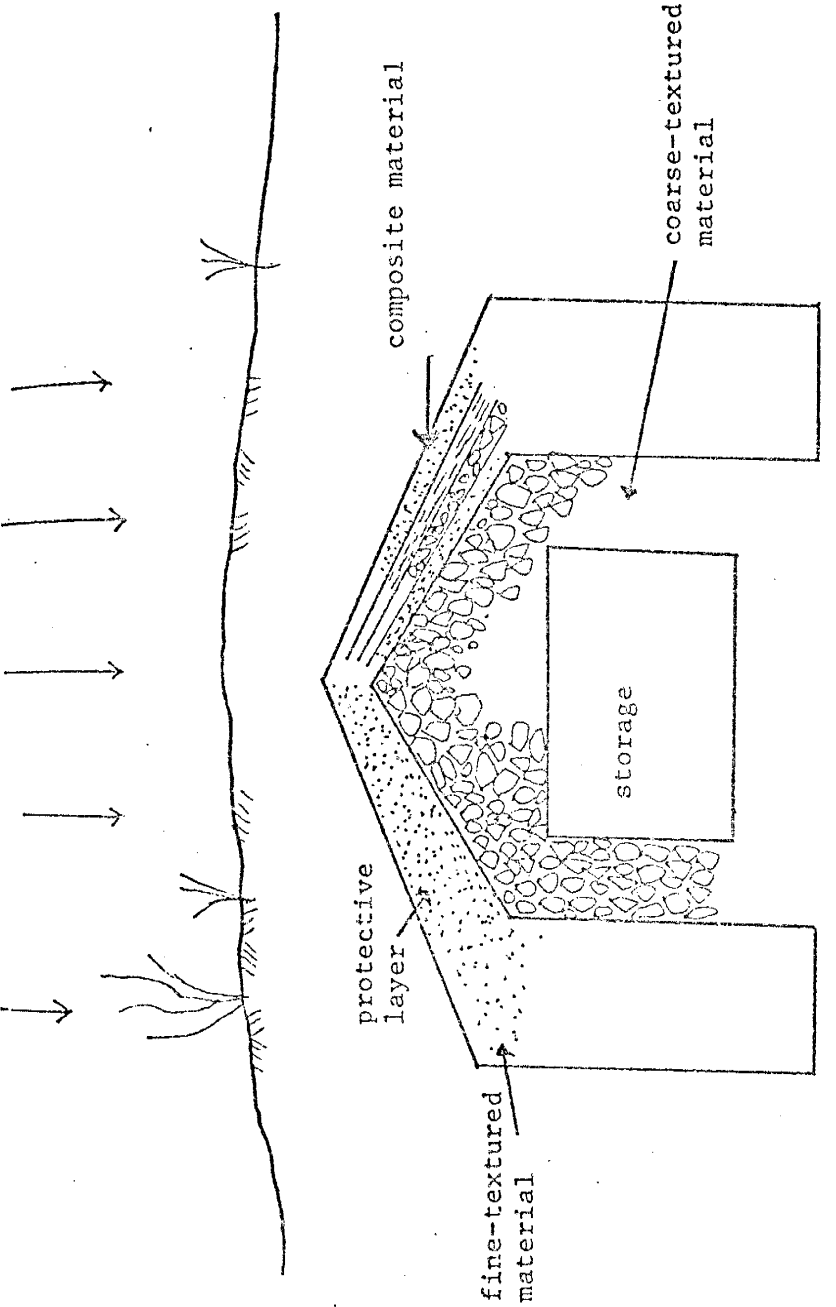

Figure 6.4.1: Configuration of the shallow underground waste storage facility.

is a medium with a larger conductivity in the horizontal versus vertical direction. In this way, the vertical flow of water can be further eliminated. According to the anisotropy ratio formula derived from the theory, a protective layer having a large conductivity anisotropy can be produced by an appropriate arrangement of different textured materials.

Consider the case where a perfectly stratified soil is inclined at an angle θ to the gradient, J=1, as illustrated in Figure(6.4.2). The flux parallel to the stratification can be expressed as (see (5.3.18a)):

$$q_s = K_s J\sin\theta = K_m \exp\left[\frac{(\sigma_f^2 + \sigma_a^2 H^2)}{2(1+Na_{11})}\right] J\sin\theta$$

where $N=\alpha\lambda_1$. Similarly, the flux in the vertical direction, q_z parallel to the gradient, is given by (see (5.3.16)):

$$q_z = K_z J = K_m \exp\left[\frac{(\sigma_f^2 + \sigma_a^2 H^2)(1-2a_{11}^2)}{2(1+Na_{11})}\right] J$$

The ratio of q_s to q_z becomes:

$$\frac{q_s}{q_z} = \frac{K_s}{K_z}\sin\theta = \sin\theta \exp\left[\frac{(\sigma_f^2 + \sigma_a^2 H^2)\cos^2\theta}{(1+N\cos\theta)}\right] \qquad (6.4.1)$$

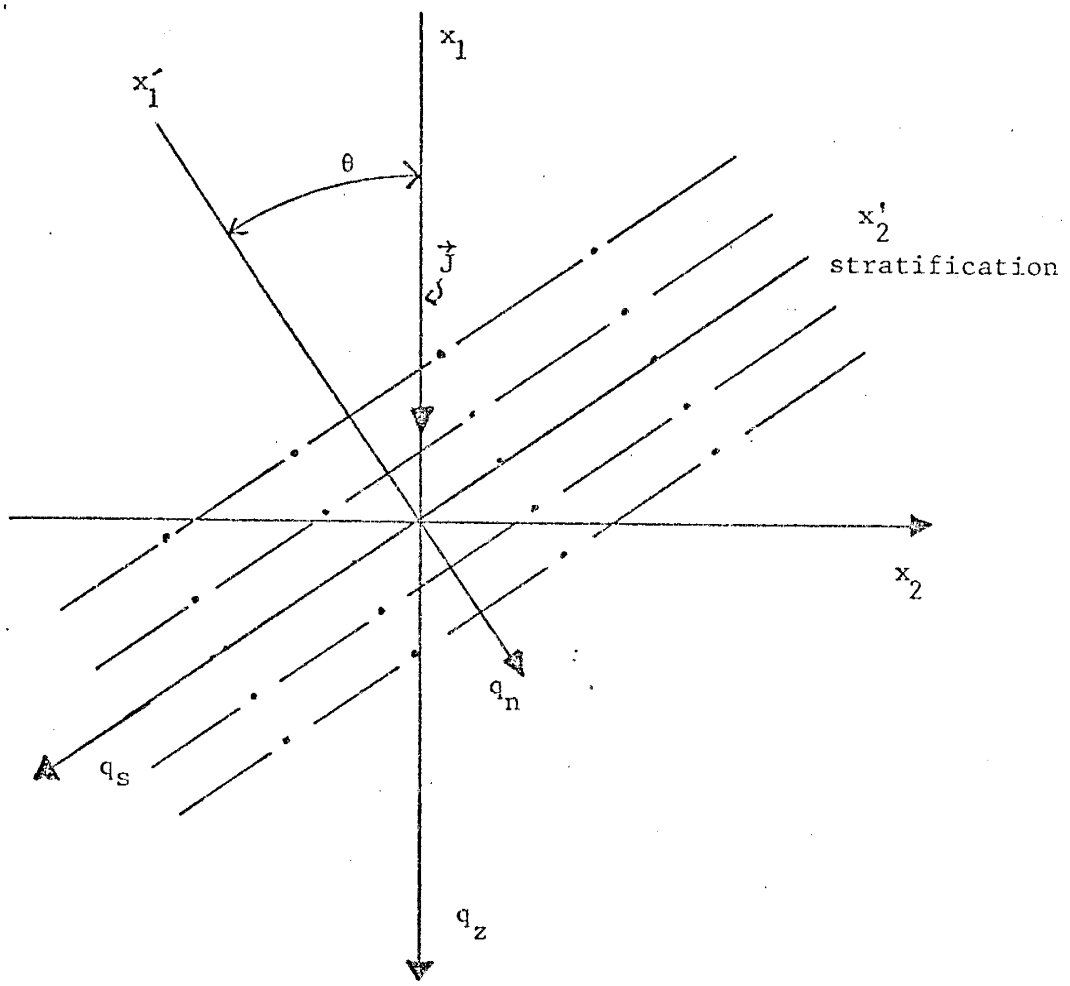

Figure 6.4.2: Coordinate systems for the analysis of fluxes in the design of the protective layer of the underground waste storage facility.

To achieve a maximum contrast in q_s and q_z, (6.4.1) suggests that the material overlying the gravel layer should be perfectly stratified and possess a large variance of $\ln K_s$ and pore-size distribution parameter. This equation implies that it is more advantageous to use a composite medium consisting of a mixture of layers of fine- and coarse-textured material than a single uniform homogeneous fine-grained material. If the correlation scale can be regarded as the average thickness of the layers, the above formula also indicates that the thickness of each layer in the composite medium be as small as possible. An optimum slope of the interface can be determined from the above analysis as well. For a demonstration purpose, the ratios of q_s to q_z for Maddock sandy loam at various interface slopes and mean capillary pressures are illustrated in Figure (6.4.3). The results demonstrate that with the proper selection of slope, a favorable anisotropy can be maintained in all possible ranges of soil moisture conditions. This information facilitates a better design of a waste storage facility. Comprehensive computer modeling and experimental investigation is still needed to verify the adequacy of the design.

Other consequences of the saturation-dependent anisotropy lies in its implications in surface hydrology. Zaslvasky and Sinai (1981, I-VI) have a detailed discussion on this subject. Briefly, they found that the anisotropy of unsaturated soils and the slope of the land surface can produce a lateral flow component. This horizontal flow, in

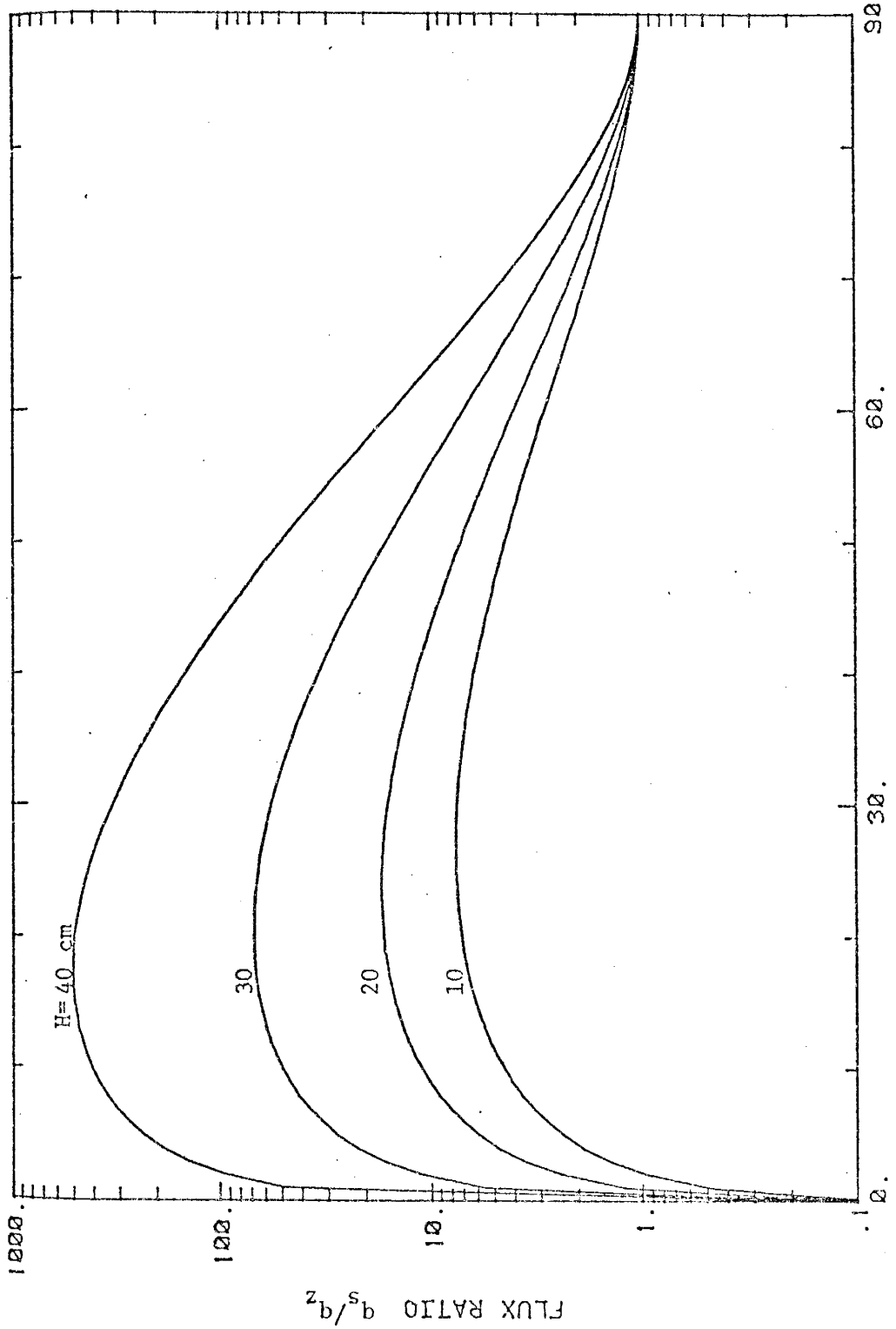

Figure 6.4.3: The relationship between the flux ratio, q_s/q_z, and the slope of the protective layer at different mean capillary pressures, H.

turn, causes moisture accumulation in concave parts of the landscape to the point of saturation. Concentration of water in concave areas explains some rainfall-runoff and erosion phenomena that were previously unexplained by classical concepts of infiltration. Revision of watershed hydrology and erosion mechanisms is necessary to improve the ability to solve hydrologic problems.

6.5 Discussion

The key findings of the theoretical analysis are summarized as follows:

(1) In order to obtain more realistic estimates of the statistical properties of unsaturated flow behavior, one has to take the correlation structure into account.

(2) As pore-size distribution parameter, α, becomes large (corresponds to coarse-textured material), the result of this analysis show that one- and three-dimensional head variance are equivalent, indicating that the flow is predominantly one-dimensional under this condition.

(3) Capillary pressure head variance grows with the mean capillary pressure, (i.e. the drier the soil is, the higher the capillary pressure head variance).

(4) Analysis of the effective hydraulic conductivity demonstrates that unsaturated hydraulic conductivity is a symmetric tensor of rank two.

(5) In general, the effective unsaturated hydraulic conductivity of one- and three-dimensional models are bounded by the harmonic and arithmetic mean. However, they approach the geometric mean as $\alpha\lambda$ grows.

(6) the anisotropy ratio of horizontal to vertical unsaturated hydraulic conductivity is found to increase with mean capillary pressure. This ratio is also a function of the magnitude and direction of hydraulic gradient, pore-size distribution parameter, the correlation scales and the orientation of the stratification. This is mainly

attributed to the variation of pore-size distribution parameter and the anisotropy in the correlation scale.

It is of importance to recognize the limitations and assumptions employed in this study. The theoretical analysis is carried out with the assumption that σ_f^2 and σ_a^2 are small. The validity of omitting some terms in developing the perturbation equations may be subjected to some criticism, since no exact solutions are available for comparative purposes. This assumption does not lead to any loss of generality of the results. The need is recognized for exact solutions in order to evaluate the adequacy of the assumption. Similar arguments also apply to the exponential generalization of the effective hydraulic conductivity approximations. A more detailed discussion of this aspect is offered in Gelhar and Axness (1981).

The exponential relationship between the conductivity and capillary pressure head assumed in the analysis merely simplifies the mathematics involved. Other functions can be adopted to obtain similar results. In fact, the exponential relationship has been widely used in many practical studies of unsaturated flow. One of the disadvantages of the exponential relationship is that this relationship does not correctly describe the behaviors of unsaturated conductivity of some soils as a function of pressure, especially coarse-textured soils.

In the development of spectral relationships of capillary pressure head, log-saturated hydraulic conductivity, and pore-size distribution parameter (equation (5.3.3)), stationarity of the head process was assumed in order to use the Fourier-Stieltjes representation theorem. The stationarity of head process is often observed in many field steady-state infiltration studies. However, for a more general case, a gradually varied mean gradient is required.

The assumption that both the pore-size parameter and log-saturated hydraulic conductivity have the same correlation scale and covariance function is a convenience in the analysis. Similar analysis can be carried out for more complex problems where the statistical properties of the two parameters are not necessarily equal. General behavior of the results should remains similar.

The cross-covariance function of α and $\ln K_s$ may be critical in field application of the stochastic results. Analyses have shown that the difference between the results of case (I) and case (II) are significant only at low capillary pressure ranges. The results of these two cases should provide the upper and lower limits of the results of any realistic problem.

It should be pointed out again that the stochastic results are in the sense of ensemble average or ensemble variance. In order to apply the results of the stochastic analysis to a field situation, it is necessary to invoke the

ergodic hypothesis. This hypothesis implies that the scale of the problem under study has to be many times larger than the correlation scale of the input process. Thus, an equivalence between ensemble average and space average can be achieved.

Applications of the theoretical results to field situations requires information on the statistical properties of the processes, $\ln K_s$ and α. These statistical parameters include σ_f^2, σ_a^2, λ_1, λ_2, λ_3, and their autocorrelation functions and cross-covariance function. Information on the statistical properties of saturated hydraulic conductivity is relatively easy to obtain for any field sites. Gelhar and Axness (1981) suggested several possible ways to obtain the estimates of these parameters. Difficulties lie in the determination of the statistical properties of the pore-size distribution parameter. Estimates of these properties of α can be determined only after a large number of K-ψ curves are obtained. In general, the measurements of K-ψ relationship is time-consuming and laborious. To obtain reasonable estimates of the properties may be a formidable task. However, the instantaneous profile method (Nielsen et al., 1973) may provide a relatively simple solution to this problem.

Finally, much work relating to unsaturated flow is still needed, especially work related to careful and systematic field observations of soil hydrologic properties.

The results of the present theoretical study leads us to recognize some important features of unsaturated flow in heterogeneous media that have been ignored for the past decades. In order to improve our capability to predict water movement in unsaturated soils and geologic formations, more rigorous theoretical analyses are necessary. Research of unsaturated flow in heterogeneous media deserves much attention in the future.

REFERENCES

Bakr, A. A., Stochastic analysis of the effect of spatial variations in hydraulic conductivity on groundwater flow, Ph. D. dissertation, New Mexico Institute of Mining and Technology., Socorro, July, 1976.

Bakr, A. A., L. W. Gelhar, A. L., Gutjar, and J.R. MacMillan, Stochastic analysis of spatial variability in subsurface flows, 1, Comparison of one-and three-dimensional flows, Water Resour. Res. 14, 263-271, 1978.

Bear, J., Dynamics of Fluids in Porous Media, 746 pp., Elsevie, New York, 1972.

Bouwer, H., Unsaturated flow in ground-water hydraulics, J. Hydraulic Div., Amer. Soc. Civil Eng., 90(HY5), 121-144, 1964.

Bouwer, H., Groundwater hydrology, 480pp, McGraw-Hill, 1978.

Carvallo, H. O., D. K. Cassel, J. Hammond, and A. Bauer, Spatial variability of in situ unsaturated hydraulic conductivity of maddock sandy loam, Soil Sci., 121(1), 1-8, 1976.

Coelho, M. A., Spatial variability of water related soil physical properties, Ph.D., Dissertation, 1974, Univ.of Ariz., Tucson.

Corey, A. T. and C. H. Rathjens, Effect of stratification on relative permeability, J. Petr. Tech., 69, Dec. 1956.

Crosby, J. W., D. L. Johnstone, C. H. Drake, and R. L. Fenston, Migration of Pollutants in a glacial outwash environment, 1,Water Resour. Res., 4(5), 1095-1113, 1968.

Crosby, J. W., D. L. Johnstone, C. H. Drake, and R. L. Fenston, Migration of Pollutants in a glacial outwash environment, 2, Water Resour. Res., 7(1), 204-208, 1971.

Crosby, J. W., D. L. Johnstone, C. H. Drake, and R. L. Fenston, Migration of Pollutants in a glacial outwash environment, 3, Water Resour. Res., 7(3), 713-720, 1971.

Dagan, G., Models of groundwater flow in statistically homogeneous porous formations, Water Resour. Res., 15(1), 47-63, 1979.

Dagan G. and E. Bresler, Solute dispersion in unsaturated heterogeneous soil at field scale,I, Theory, Soil Sci. Soc. Amer. J., Vol., 43, 461-466, 1979.

Delhomme, J. P., Spatial variability and uncertainty in groundwater flow parameters: A geostatistical approach,

Water Resour. Res., 15(2), 269-280, 1979

Dwight, H. B., Tables of integrals and other mathematical data, 336 pp, MacMillan, 1961.

Freeze, R. A., Three-dimensional, transient, saturated- unsaturated flow in a groundwater basin, Water Resour Res., 347-366, 1971.

Freeze, R. A., A stochastic-conceptual analysis of one-dimensional groundwater flow in nonuniform homogeneous media, Water Resour. Res., 11(5), 725-741, 1975.

Freeze, R. A., A stochastic-conceptual analysis of rainfall-runoff processes on a hillslope, water Resour. Res.16(2), 391-408,1980.

Frind, E. O., R. W. Gillham, and J. F. Pickens, Application of unsaturated flow properties in the design of geologic environments for radioactive waste storage facilities, Proceedings of the first international Conference on Finite Elements in Water Resources at Princeton University, U.S.A. in July, 1976, "Finite Elements in Water Resources", Pentech Press, 1977.

Fritton, D. D., Variability of soil physical properties in a corn field, AGU Chapman conference on spatial variability in hydrologic modeling, July 21-23, 1981.

Gajem, Y. M., Spatial structure of physical properties of a typic torrifluvent, Master thesis, 125 pp., Univ. of Ariz. Tucson.

Gardner, W. R., Some steady state solution of the unsaturated moisture flow equation with application to evaporation from a water table, Soil Sci. 85, 228-232, 1958.

Gelhar, L. W., Effects of hydraulic conductivity variations on groundwater flows, in Proceedings of the Second International IAHR Symposium on stochastic hydraulic, int. Ass. of Hydrauli. Res., Lund, Sweden, 1976.

Gelhar, L. W. and C. L. Axness, Stochastic analysis of macrodispersion in three-dimensionally heterogeneous aquifers, Hydrology Research Report No. H-8, New Mexico Institute of Mining and Technology, August, 1981.

Glover, R. E., Mathematical derivations as pertain to groundwater recharge, report 81pp., U. S. Dept of Agr., Agr., Res. Serv., Fort Collins, Colo., 1961.

Gutjahr, A. L., L. W. Gelhar, A. A., Bakr, and J. R. MacMillan, Stochastic analysis of spatial variability in subsurface flows, 2, Evaluation and application, Water Resour. Res.

14, 953-959, 1978.

Hillel, D., Soil and water, 288p, Academic Press, 1971.

Jenkins, G. M., and D. G. Watts, Spectral analysis and its applications, 525 pp, Holden Day, 1968.

Jeppson, R. and R. Nelson, Inverse formulation and finite difference solution to partially saturated seepage from canals, Soil Sci. Soc. Amer. Proc., 34, 9-14, 1970.

Lumley, J. L., and H. A. Panofsky, The structure of Atmospheric Turbulences, 239 pp., John Wiley, New York, 1964.

Marthaler, H. P., W. Vogelsanger, and S. Richard, A digital syringe manometer for field tensiometers, Soil Sci. Soc. Amer. J., submitted for publication.

Mizell, S. A., A. L. Gutjahr, and L. W. Gelhar, Stochastic analysis of spatial variability in two-dimensional steady groundwater flow assuming stationary and nonstationary heads, Water Resour. Res. in print.

Mualem, Y., A catalogue of the hydraulic properties of unsaturated soils, "Development of methods, tools and solutions for unsaturated flow with application to watershed hydrology and other fields.", Research Project 442, Technion Israel Institute of Technology, 100 pp, 1976.

Naff, R. L., A continuum approach to the study and determination of field longitudinal dispersion coefficients, Ph. D. dissertation, 176 pp., New Mexico Institute of Mining and Technology, Socorro, NM, June, 1978.

Nielsen, D. R., J. W. Biggar, and K. T. Erh, Spatial variability of field measured soil-water properties, Hilgardia 42 (7), 215-260, 1973.

Peck, A. J., P. A. Yendle, and F. E. Batini, Hydraulic conductivity of deeply weathered materials in the Darling Range, Western Australia, Aust. Jour. Soil Res. 31, 1980.

Philip, J. R., Field heterogeneity: Some basic issues, Water Resour. Res., 16(2), 443-448, 1980.

Rogowski, A. S., Watershed physics: Soil Variability criteria, Water Resour. Res., 8(4), 1015-1023, 1972.

Russo D. and E. Bresler, Soil hydraulic properties as stochastic processes:I-An analysis of field spatial variability, Soil Sci. Soc. Amer. J., 45, 682-687, 1980.

Sinai, G., D. Zaslavsky, and P., Golany, Influence of Anisotropy in Soil, Permeability on Surface Runoff Publication 232,

Faculty of Agricultural Engineering, Technion, Haifa, Israle, 1974.

Sisson J. B. and P. J. Wierenga, Spatial variability of steady-state infiltration rates as a stochastic processes, Soil Sci. Soc. Amer. J. 45, 699-704, 1981.

Smith, L., A stochastic analysis of steady-state groundwater flow in a bounded domain, Ph.D. thesis, 325 pp., Univ. of B. C., Vancouver, 1978.

Smith, L., and R. A. Freeze, Stochastic analysis of groundwater flow in a bounded domain, 1, One-dimensional simulations, Water Resour. Res. 15(3), 521-528, 1979.

Smith, R. E. and R. H. B. Hebbert, A monte carlo analysis of the hydrologic effects of spatial variability of infiltration, Water Resour. Res., 15(2), 419-429, 1979.

Stockton, J. G. and A. W. Warrick, Spatial Variability of unsaturated hydraulic conductivity, Soil Sci. Soc. Am. Proc. 35, 847-848, 1977.

U. S. Geological Survey, Definitions of selected ground-water terms- Revisions and conceptual refinements, Water-Supply Paper 1988, 21 pp., 1972.

Vaclin, M., D. Khanji., and G. Vachaud, Experimental and numerical study of a transient, two-dimensional unsaturated-saturated water table recharge problem, Water Resour Res., 15(5), 1089-1101, 1979.

Vieira, S. R., D. R. Nielsen, and J. W. Biggar, Spatial variability of field-measured infiltration rate, Soil Sci. Soc. Am. J., 45, 1040-1048, 1982.

Warrick, A. W., Areal predictions of soil water flux in the unsaturated zone, Proceedings of National Conference, irrifation return flow quality management, EPA and Colorado State University., May 16-19, 1977a.

Warrick, A. W., G. J. Mullen, and D. R. Nielsen, Scaling field-measured soil hydraulic properties using a similar media concept. Water Resour. Res., 13(2), 355-362, 1977b.

Warrick, A. W. and D. R. Nielsen, Spatial variability of soil physical properties in the field in Hillel, "Applications of Soil Physics", Academic Press, p319-344, 1980.

Wierenga, P. J., C. Duffy, R. Kselik, R. Senn, and W. Strong, Impacts of irrigrated agriculture on water quality in the Rio Grande below Albuquerque, Dept of Agronomy, New Mexico State University, Las Crusas, NM, Feb. 1979.

Zaslavsky, D., and G. Sinai, Surface hydrology: I-Explanation of phenomena, J. Hydr. Div., Amer. Soc. Civil Eng., 107(HY1), 1-16, 1981.

Zaslavsky, D., and G. Sinai, Surface hydrology: IV-Flow in sloping layered soil, J. Hydr. Div., Amer. Soc. Civil Eng., 53-64, 107(HY1), 1981.

APPENDIX A

FIELD OBSERVATION OF SOIL CAPILLARY PRESSURE SPATIAL VARIATION

A.1 Introduction

The flow equations employed in this theoretical analysis are expressed in terms of capillary pressure head. The capillary pressure head is a stochastic process since it is a direct product of the stochastic flow equation. Numerous soil scientists have observed the field variability of a variety of soil hydrologic properties in recent years. Only a few of them have dealt with the variability of soil capillary pressure. Therefore, one of the purposes of this chapter is to demonstrate the stochastic nature of the soil capillary pressure. Achievement of this goal requires a large number of simultaneous observations of soil capillary pressure. Conventional capillary pressure monitoring devices; namely, mercury-water manometer, jet filled, and quick-draw type tensiometers, in general, are either slow in response or inconvenient in installation. Furthermore, the conventional devices, due to their slow responses, may observe temporal variation in addition to the spatial variation of the pressure, if a large number of measurements are required. Thus, a technique for a "simultaneous" measurement of soil capillary pressures in a large area is developed to minimize temporal variation of the pressures.

A.2 Monitoring Device

The measurement device consists of a tensiometer, a transducer, and a digital readout device (Marthaler, et al. 1982). The tensiometer consists of a porous ceramic cup glued to a one-foot PVC pipe of 7/8" OD and a 2.5 inch long clear plexiglas of 5/8" OD and 1/2" ID connected to the other end of the PVC pipe. The tensiometer is then filled with water (up to about 1" below the top). A serum rubber stopper which allows insertion of hypodermic needles seals the top of the tensiometer unit.

The transducer and pressure indicator are the products of Druck Incorporated. The part numbers of the transducer and pressure indicator are DPCR10/F and DPI201, respectively. The transducer has ± 0.1 % BSL non-linearity and hysteresis with a pressure range of 0.0 to ± 1.0 bar in gauge pressure. Its temperature error band is about ± 0.5 %. The digital readout device (pressure indicator) has ± 0.1 % FS. linearity and hysteresis for a range from 0.0 to 70 bars. Both of the two units are powered by a rechargable battery.

The transducer is screwed on a brass housing on which a hypodermic needle of 0.019" OD is mounted. The housing is designed in such a way that a minimal clearance (about 0.005 cc of volume) between the bottom of the housing and the top

of the diaphragm in the transducer is obtained.

A.3 Principle Involved in Operation of This Device

When the tensiometer is placed in soil, water in the system comes into hydraulic contact with soil-water through the pores in the ceramic wall. Unsaturated soil, being generally at negative pressure, starts to draw out a certain amount of water from the ceramic cup. As water is sucked from the unit, a partial vacuum is created at the top of the tensiometer. Water in the unit flows out until the vacuum created in the tensiometer equilibrates with the capillary pressure in the surrounding soil and the weight of water remaining in the system. This vacuum in the tensiometer is then measured by inserting the hypodermic needle through the serum rubber stopper. This hypodermic needle is connected to a pressure transducer. Thus, the vacuum pressure is directly transmitted and excites the diaphragm which sends out signals to the digital readout device. The pressure displayed on the readout device is expressed in terms of centimeters of water. It is then corrected for the hydrostatic pressure of the water column remaining in the tensiometer.

Since a large number of tensiometer are installed in the ground prior to measurement, they have equilibrated with the pressure in the surrounding soil at the time of measure-

ment. The device developed here can determine the vacuum pressure in the individual tensiometer in a matter of seconds. Therefore, a large numbers of soil capillary pressure measurements can be attained in a short period time.

A.4 Some Theoretical Considerations

The vacuum pressure in the tensiometer, before the insertion of the hypodermic needle, is equal to the sum of the soil suction and the hydrostatic pressure of the water column in the tensiometer. Once the hypodermic needle is inserted into the system, a small amount of air (the amount of air residing in the hypodermic needle and the space between the housing and the transducer) is introduced into the tensiometer. This amount of air can cause an increase of the pressure in the unit. As a response to the increase of pressure, an amount of water has to flow out to reach a new equilibrium. The volume of water is equal to the product of change in pressure head and the area of the tensiometer tube. The response time (time to a new equilibrium) depends on the amount of water discharged from the unit, the conductivity of the ceramic cup, and the permeability of surrounding soil. If the change of pressure is large, a relatively large volume of water has to be discharged through the ceramic wall. Thus, the initial soil condition is disturbed. The response time of the system can be several hours.

To determine the magnitude of disturbance caused by the insertion the hypodermic needle to the tensiometer, a simple theoretical analysis based on the ideal gas law is carried out.

Assuming the amount of air initially in the tensiometer is V_i, the volume of the air at an equilibrium V_e is determined by

$$V_e = \frac{P_a V_i}{P_e} \qquad (a.1)$$

where P_a is the air pressure (1 atmosphere: 1 bar), and P_e is the pressure at equilibrium, which consists of the actual soil capillary pressure and the hydrostatic pressure of water in the tensiometer.

As the needle is inserted, an amount of air V_h is added to the system. The new equilibrium pressure P_{ne} in the system after the insertion would become:

$$P_{ne} = \frac{P_e V_e + P_a V_h}{V_e + V_h} = \frac{P_e + \frac{V_h}{V_e}}{1 + \frac{V_h}{V_e}} \qquad (a.2)$$

Equation (a.2) indicates that the difference between the pressure P_{ne} and P_e can be negligible, if the ratio of V_h/V_e is small. Since the pressure difference is small, the

amount of water discharged through the ceramic wall will be small. The initial soil condition is preserved.

A direct application of equation (a.2) to the tensiometer system used in this study can serve as a test of the adequacy of the design. The initial air volume V_i in the tensiometer is about 3.2 cc. At 0.5 bar of P_e the initial volume of air increase to V_e is about 6.4 cc, according to equation (a.1). The volume of air in the transducer unit is estimated to be 0.05 cc. These conditions result in a value of 0.504 bar for P_{ne}. Similarly, at 0.95 bar of soil suction, the corresponding P_{ne} is 0.9507 bar. The changes of pressure in these cases are relatively small. Thus, it is confirmed that the present design of the tensiometer system is adequate to monitor the spatial variation of the soil capillary pressure.

A.5 Procedures

All the assembled tensiometers are tested for leaks. The test is carried out by submerging each tensiometer into water, and applying positive pressure up to 1.5 bars to the tensiometer. If any leak occurs at this pressure range, the tensiometer is considered as defective. All the intact tensiometers, then, are filled with water up to 1 inch below the top and are sealed with the rubber stoppers. This leaves a volume of air of 30.0 cc in the tensiometer. This amount of air is essential because it can compensate the

change of pressure due to insertion of the hypodermic needle.

Hole of 7/8 inches in diameter and one-foot depth is prepared by a coring tool. A slurry made of water and cored soil is poured into the hole before installing the tensiometer. Thus, a tight contact between the ceramic wall and surrounding soil can be obtained. This tight contact is important to make a correct soil capillary pressure measurement.

Before measurements are taken, the transducer and readout unit are calibrated with air-mercury and water-mercury manometers to compensate for the fluctuation of atmospheric pressure and temperature effects. However, in most cases, the calibration is not necessary because variation due to temperature is insignificant.

Leaks in the rubber stopper may occur after the rubber stopper has been punctured several times. This kind of leakage is evident when a significant drop of water level in the tensiometer is observed after measurements. To prevent leaking air through the rubber stopper, silicon rubber is used to seal the punctured rubber stopper.

A.6 Results and Discussions

Ninety four tensiometers are installed along a transect at an alfalfa field, San Acacia, New Mexico. Location of

the transect and associated soil permeability map are shown in Figure (A.1). The interval between two tensiometers is ten feet. Each tensiometer is inserted into the soil to a depth of one foot.

Measurements began a week after installation. This period of time allows the slurry to dry out and allows the tensiometer to equilibrate with the surrounding soil. Four space series are obtained in a period of two weeks. The first measurements were carried out on December 2, 1981, two days after a rain of 1.35 cm (data collected at Socorro weather station by Dr. Wilkening). The time span required to complete each series is about thirty minutes. Most of the measurements are conducted at 3:00 PM. The four space series are shown in Figures (A.2) to (A.5), and data of these series are documented in Table (A.1). These data are the values registered on he pressure indicator. They are neither corrected for the hydrostatic pressure in the tensiometer nor adjusted according to calibration. It is clear from Figures (A.2) to (A.5) that the spatial variations of soil capillary pressure are significant. The variations of soil capillary pressure are also associated with strong trends as illustrated by the figure. The pressure readings at the first five hundred feet tend to be much higher than the rest of the pressure readings. Due to the presence of the trend, the series are separated into two sections for estimation of their statistical properties. The first section consists of data from the first fifty measurements.

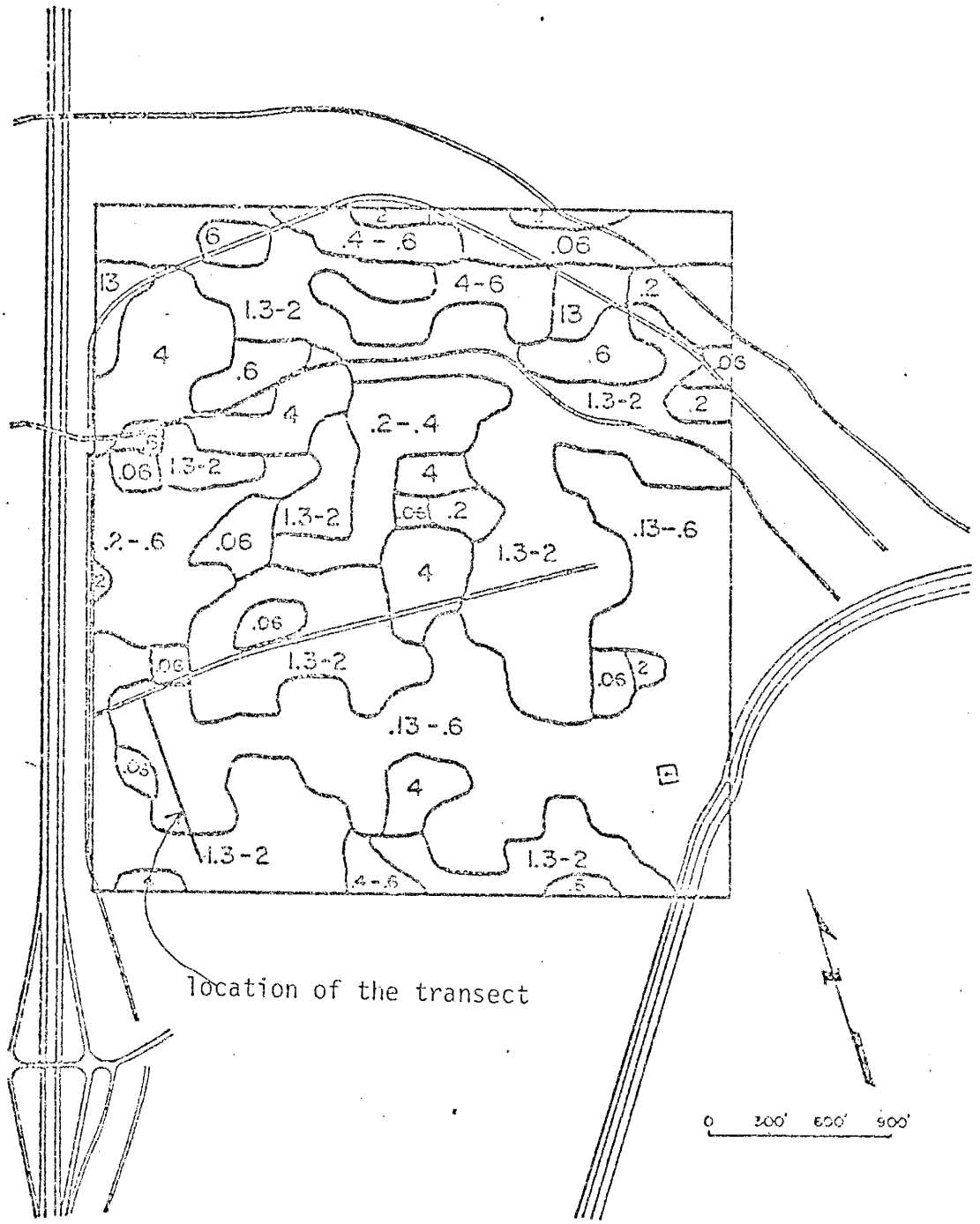

Figure A.1: Map showing the location of the transect and soil permeability distribution at the farm (after Wierenga et al., 1979)

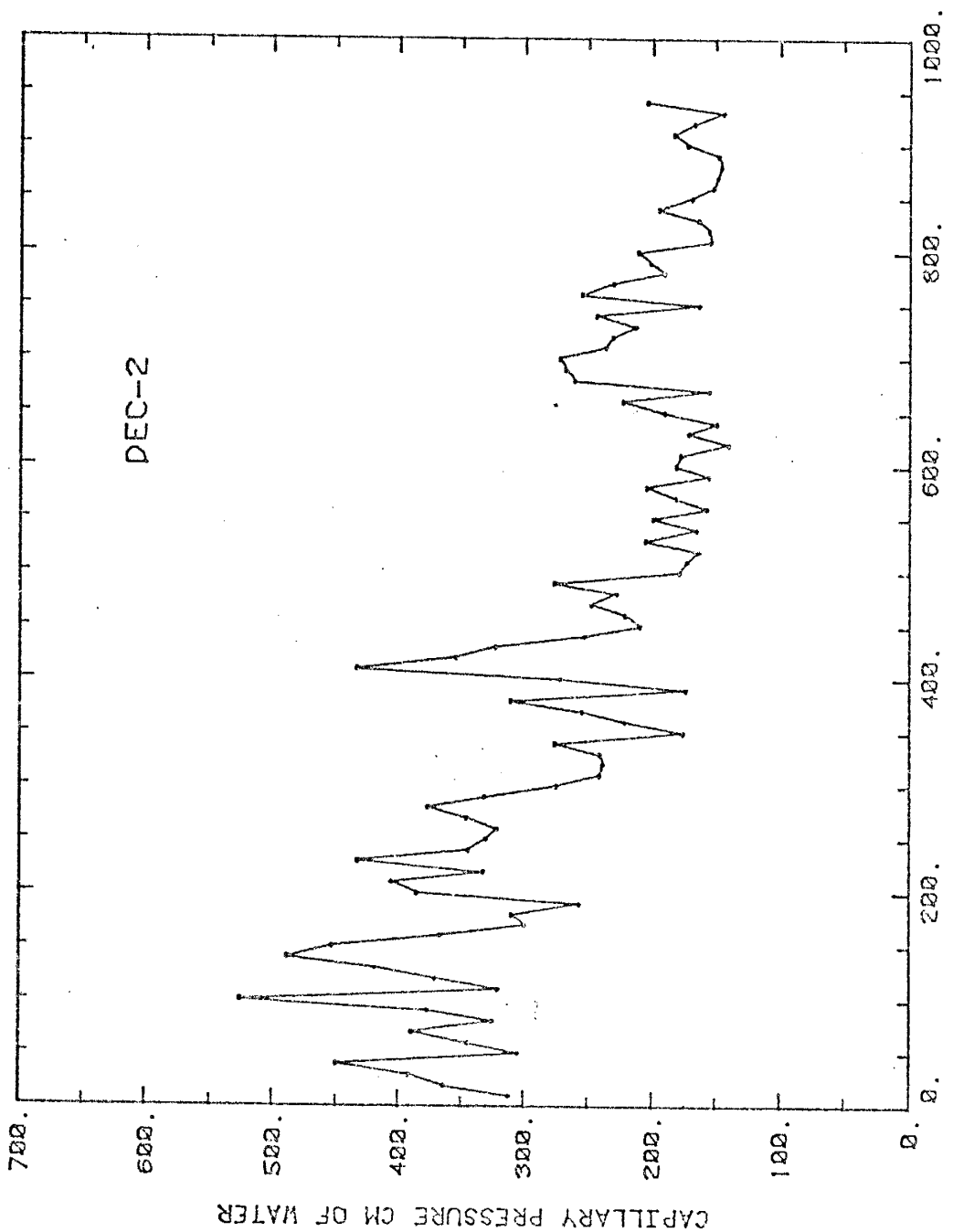

Figure A.2: Soil capillary pressure variation along the transect.
(December 2, 1981)

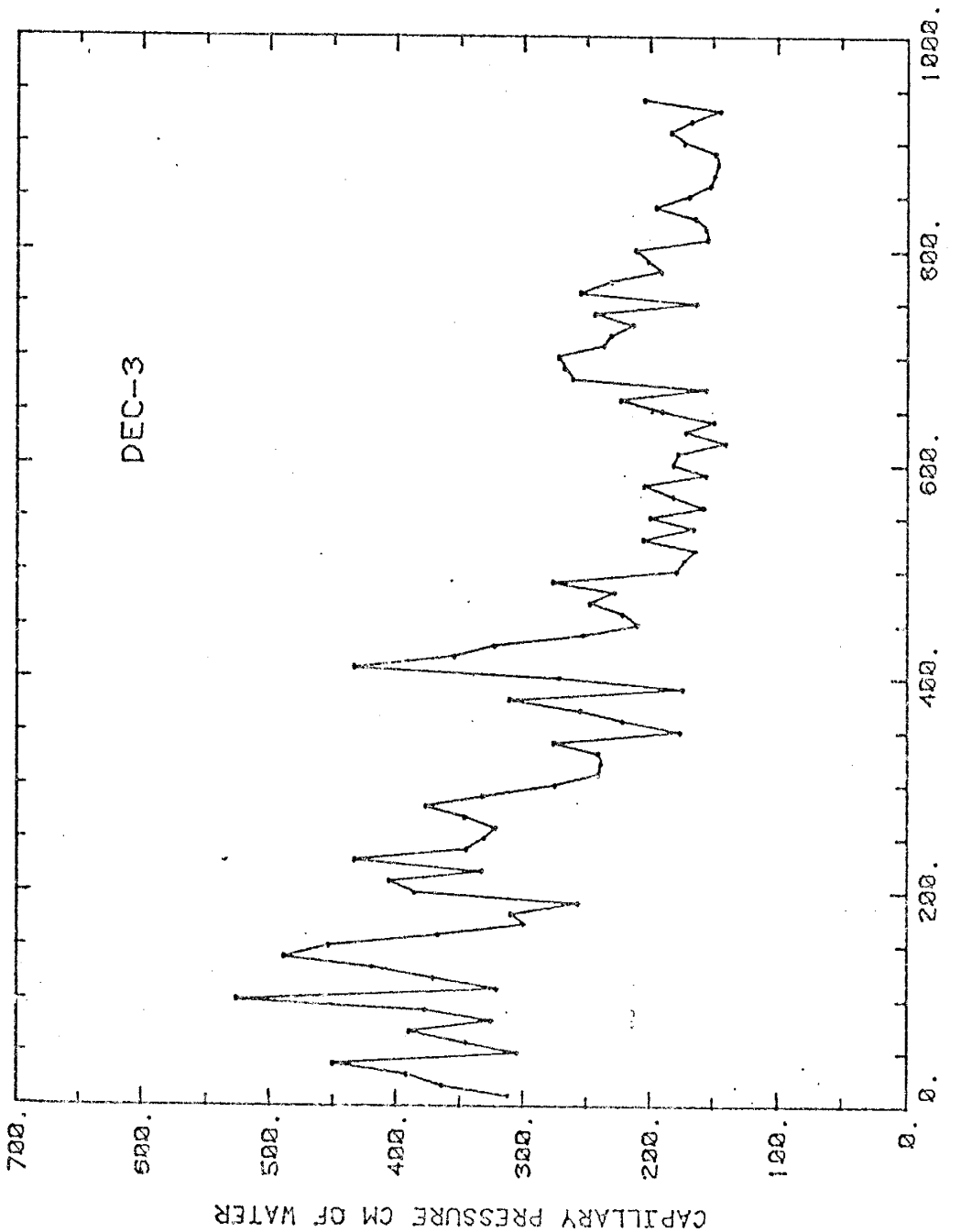

Figure A.3: Soil capillary pressure variation along the transect.
(December 3, 1981)

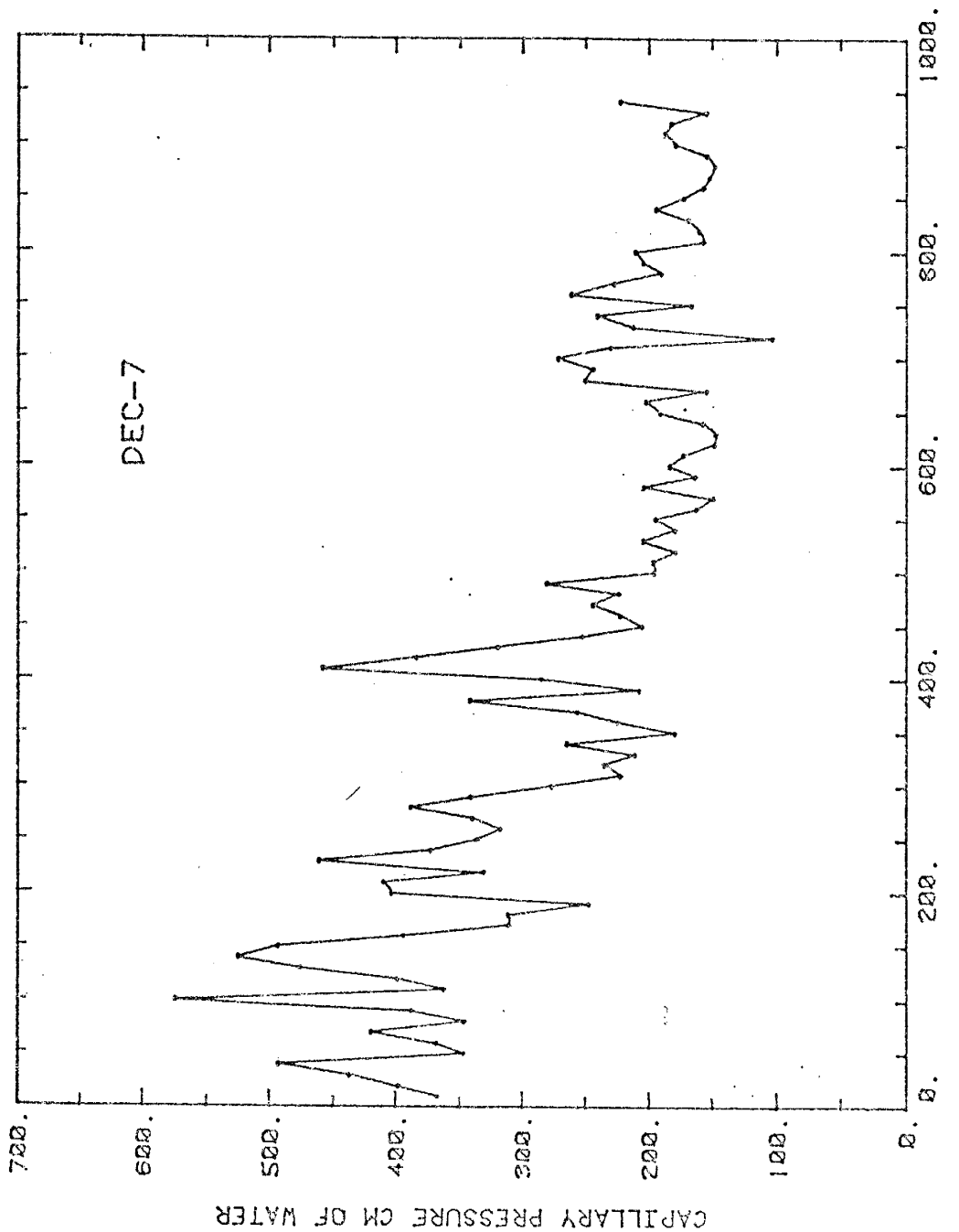

Figure A.4: Soil capillary pressure variation along the transect.
(December 7, 1981)

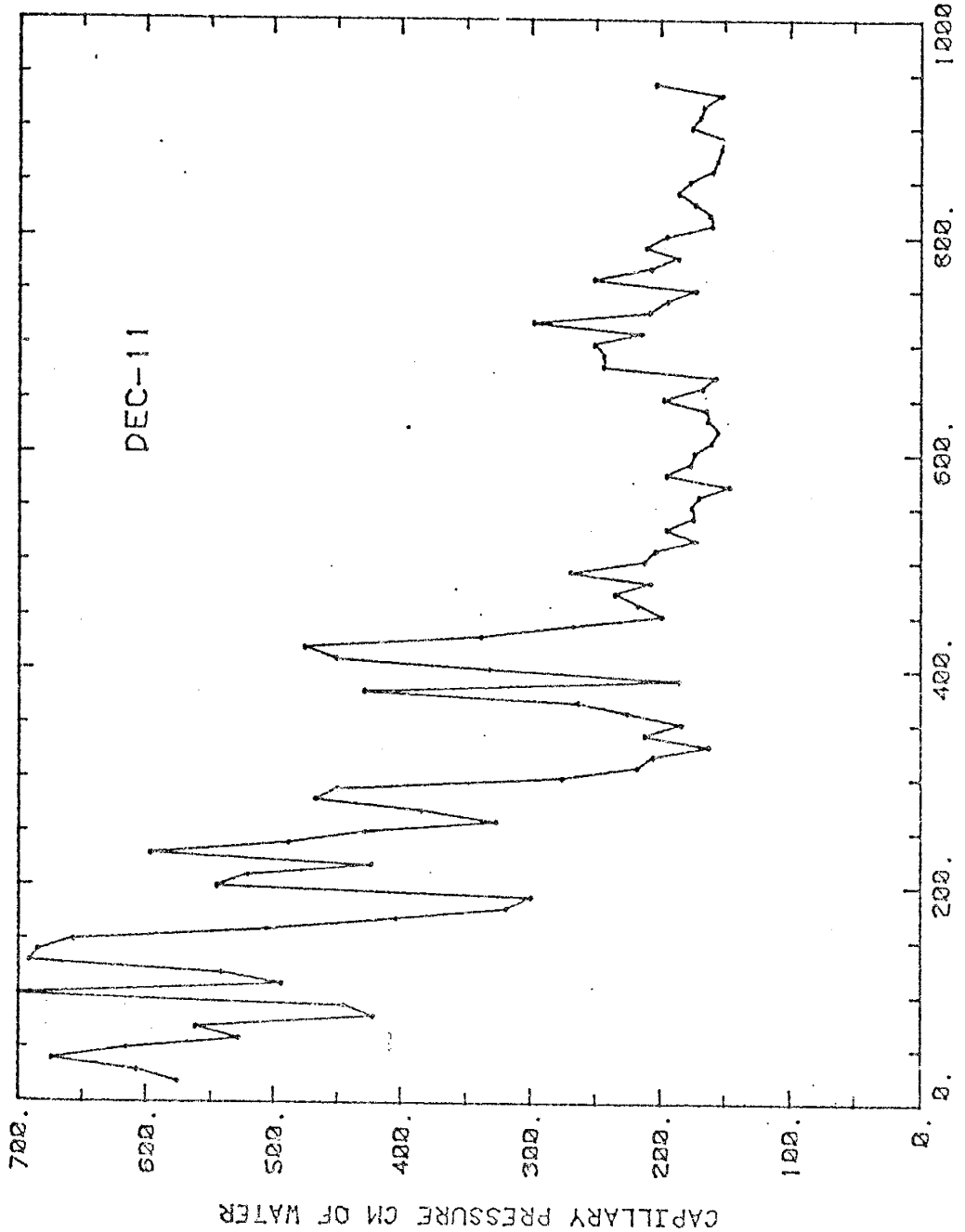

Figure A.5: Soil capillary pressure variation along the transect.
(December 11, 1981)

collected along the transect in an alfalfa field, San Acacia, New Mexico.

Distance	DEC-2	DEC-3	DEC-7	DEC-11
10.0	311.0	366.0	438.0	0.0
20.0	363.0	397.0	455.0	575.0
30.0	391.0	436.0	508.0	607.0
40.0	449.0	492.0	580.0	673.0
50.0	304.0	346.0	464.0	615.0
60.0	344.0	367.0	410.0	527.0
70.0	389.0	419.0	463.0	561.0
80.0	324.0	345.0	313.0	421.0
90.0	376.0	387.0	374.0	444.0
100.0	525.0	573.0	651.0	711.0
110.0	320.0	361.0	385.0	493.0
120.0	370.0	398.0	431.0	541.0
130.0	418.0	475.0	594.0	690.0
140.0	487.0	524.0	590.0	684.0
150.0	452.0	492.0	564.0	656.0
160.0	366.0	393.0	397.0	504.0
170.0	299.0	310.0	306.0	403.0
180.0	309.0	310.0	241.0	318.0
190.0	256.0	247.0	206.0	299.0
200.0	385.0	403.0	429.0	544.0
210.0	405.0	409.0	396.0	520.0
220.0	332.0	330.0	331.0	422.0
230.0	432.0	460.0	499.0	596.0
240.0	344.0	372.0	378.0	487.0
250.0	330.0	335.0	326.0	427.0
260.0	321.0	317.0	250.0	326.0
270.0	345.0	339.0	297.0	384.0
280.0	376.0	387.0	354.0	466.0
290.0	331.0	340.0	347.0	449.0
300.0	274.0	276.0	213.0	275.0
310.0	240.0	222.0	187.0	217.0
320.0	238.0	235.0	158.0	205.0
330.0	240.0	210.0	136.0	162.0
340.0	275.0	264.0	225.0	212.0
350.0	175.0	179.0	157.0	183.0
360.0	221.0	224.0	194.0	225.0
370.0	254.0	256.0	210.0	263.0
380.0	310.0	341.0	341.0	428.0
390.0	173.0	207.0	137.0	185.0
400.0	271.0	284.0	256.0	331.0
410.0	433.0	457.0	461.0	450.0
420.0	354.0	383.0	377.0	475.0
430.0	322.0	319.0	276.0	338.0
440.0	252.0	252.0	223.0	267.0
450.0	209.0	205.0	175.0	198.0
460.0	221.0	222.0	183.0	217.0
470.0	247.0	244.0	196.0	235.0
480.0	227.0	223.0	185.0	207.0
490.0	276.0	280.0	226.0	269.0
500.0	178.0	195.0	192.0	212.0
510.0	172.0	196.0	183.0	203.0
520.0	163.0	178.0	155.0	172.0
530.0	205.0	204.0	164.0	195.0

540.0	165.0	179.0	150.0	174.0
550.0	199.0	194.0	144.0	175.0
560.0	157.0	162.0	149.0	170.0
570.0	181.0	149.0	125.0	146.0
580.0	204.0	203.0	154.0	195.0
590.0	155.0	163.0	156.0	176.0
600.0	181.0	183.0	153.0	173.0
610.0	177.0	172.0	137.0	160.0
620.0	140.0	148.0	144.0	155.0
630.0	171.0	147.0	141.0	163.0
640.0	149.0	157.0	150.0	164.0
650.0	190.0	191.0	178.0	197.0
660.0	223.0	202.0	130.0	167.0
670.0	155.0	154.0	134.0	157.0
680.0	261.0	250.0	200.0	244.0
690.0	268.0	244.0	207.0	244.0
700.0	272.0	271.0	220.0	251.0
710.0	236.0	230.0	184.0	214.0
720.0	231.0	103.0	129.0	298.0
730.0	213.0	212.0	185.0	208.0
740.0	243.0	240.0	155.0	194.0
750.0	163.0	166.0	167.0	172.0
760.0	254.0	261.0	201.0	251.0
770.0	230.0	227.0	189.0	207.0
780.0	191.0	190.0	168.0	186.0
790.0	201.0	204.0	188.0	211.0
800.0	211.0	210.0	164.0	195.0
810.0	154.0	157.0	158.0	160.0
820.0	156.0	161.0	149.0	162.0
830.0	164.0	169.0	166.0	173.0
840.0	195.0	194.0	171.0	186.0
850.0	169.0	172.0	170.0	177.0
860.0	152.0	157.0	147.0	159.0
870.0	149.0	152.0	150.0	156.0
880.0	146.0	148.0	149.0	153.0
890.0	148.0	154.0	143.0	151.0
900.0	172.0	179.0	169.0	175.0
910.0	183.0	187.0	170.0	169.0
920.0	167.0	182.0	158.0	166.0
930.0	144.0	154.0	149.0	152.0
940.0	204.0	222.0	196.0	203.0

The second section contains the rest. Estimates of variance of these series are included in Table (A.2). Note that the variance of the capillary pressure head increases with its mean. In other words, the drier the soil is, the larger the variance of pressure head. This mean-dependent behavior demonstrates the non-stationary nature of the soil capillary pressure. Also recognize that the variability of the pressure is correlated in space, although the correlation scale is not as long as we expected. The estimated autocorrelation functions of the two sections of each space series are shown in Figures (A.6) through (A.9). Since the presence of the strong trends in the first section of each space serie, before carrying out the statistical analysis, the data were detrended with the assumption of the presence of a linear trend. Ten lags were used in the estimation of the autocorrelation functions for the first sections of the series. No trends were removed from the second sections of the data and eight lags were used.

A.7 Conclusion

Some conclusions drawn from the results of this experiment are as follows:

(1) The tensiometer-transducer system used here is a useful method for rapidly monitoring spatial variations of soil capillary pressure. It also can be used in other practical purposes. The response of the device is fast, and its

pressures collected along the transect.

DATE	SECTION	MEAN (cm)	STANDARD DEVIATION (cm)
Dec. 2	1	325	80
	2	187	36
Dec. 3	1	336	95
	2	186	35
Dec. 7	1	334	137
	2	162	22
Dec. 11	1	402	170
	2	185	33

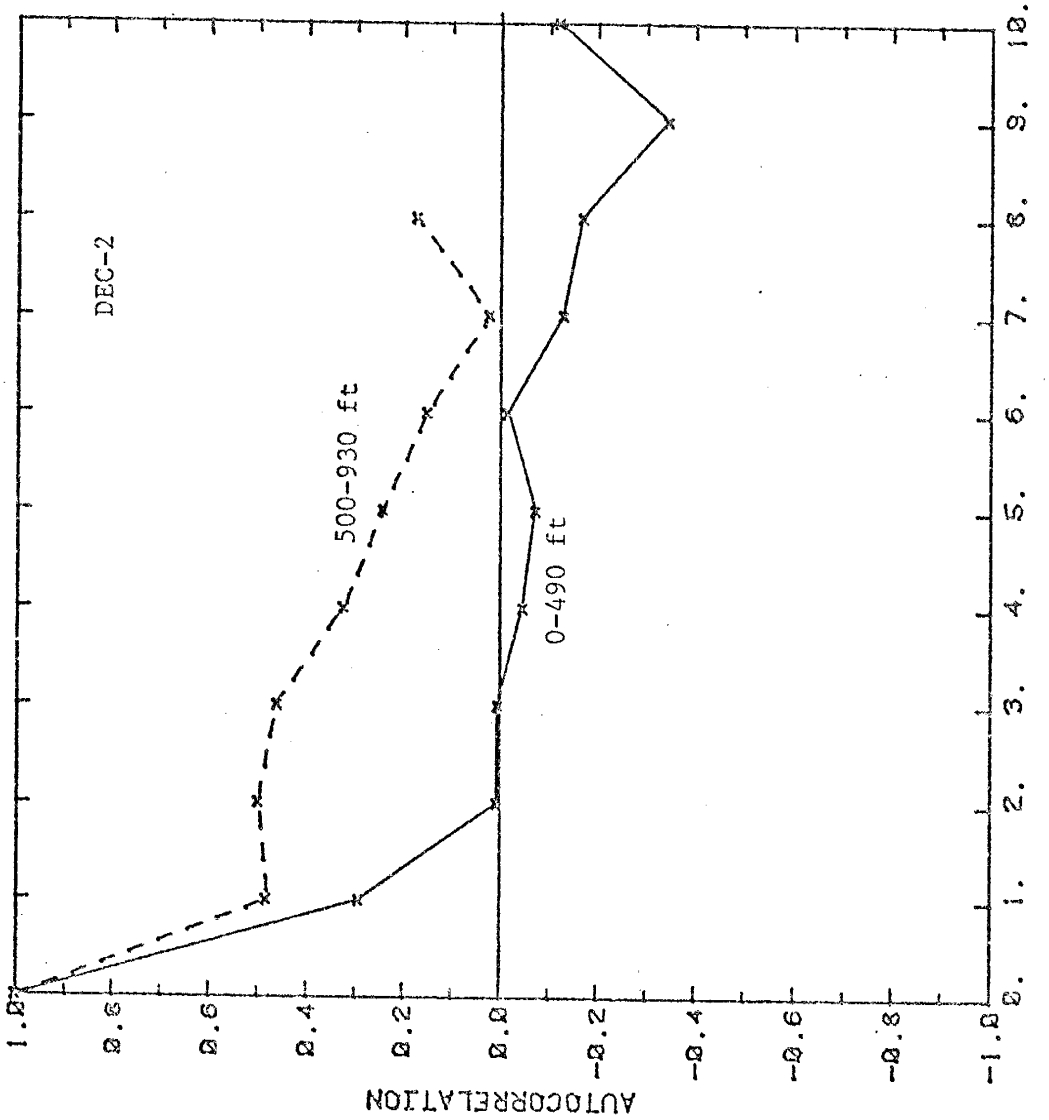

Figure A.6: Autocorrelation functions of the soil capillary pressures (December 2, 1981).

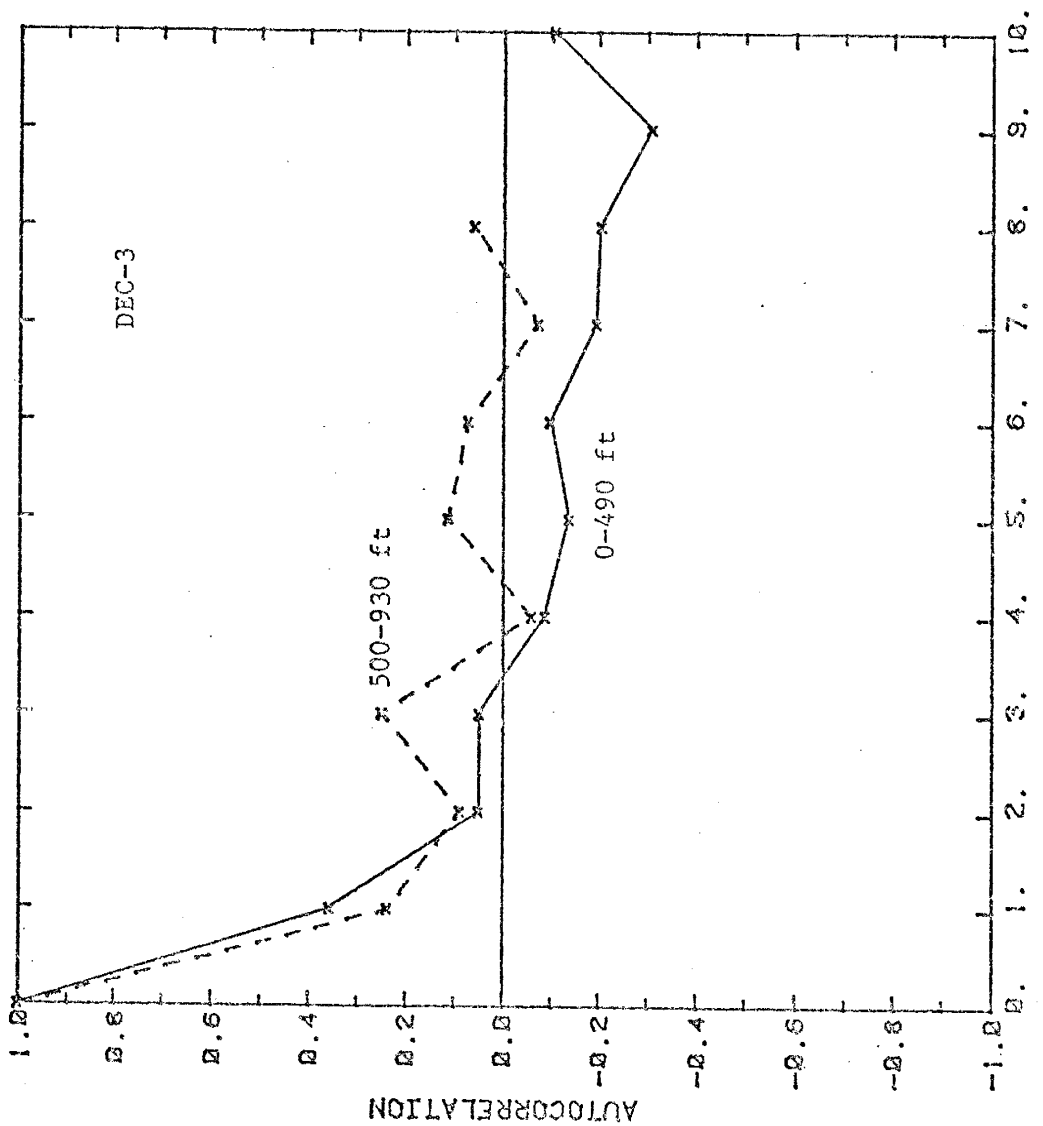

Figure A.7: Autocorrelation functions of the soil capillary pressures (December 3, 1981).

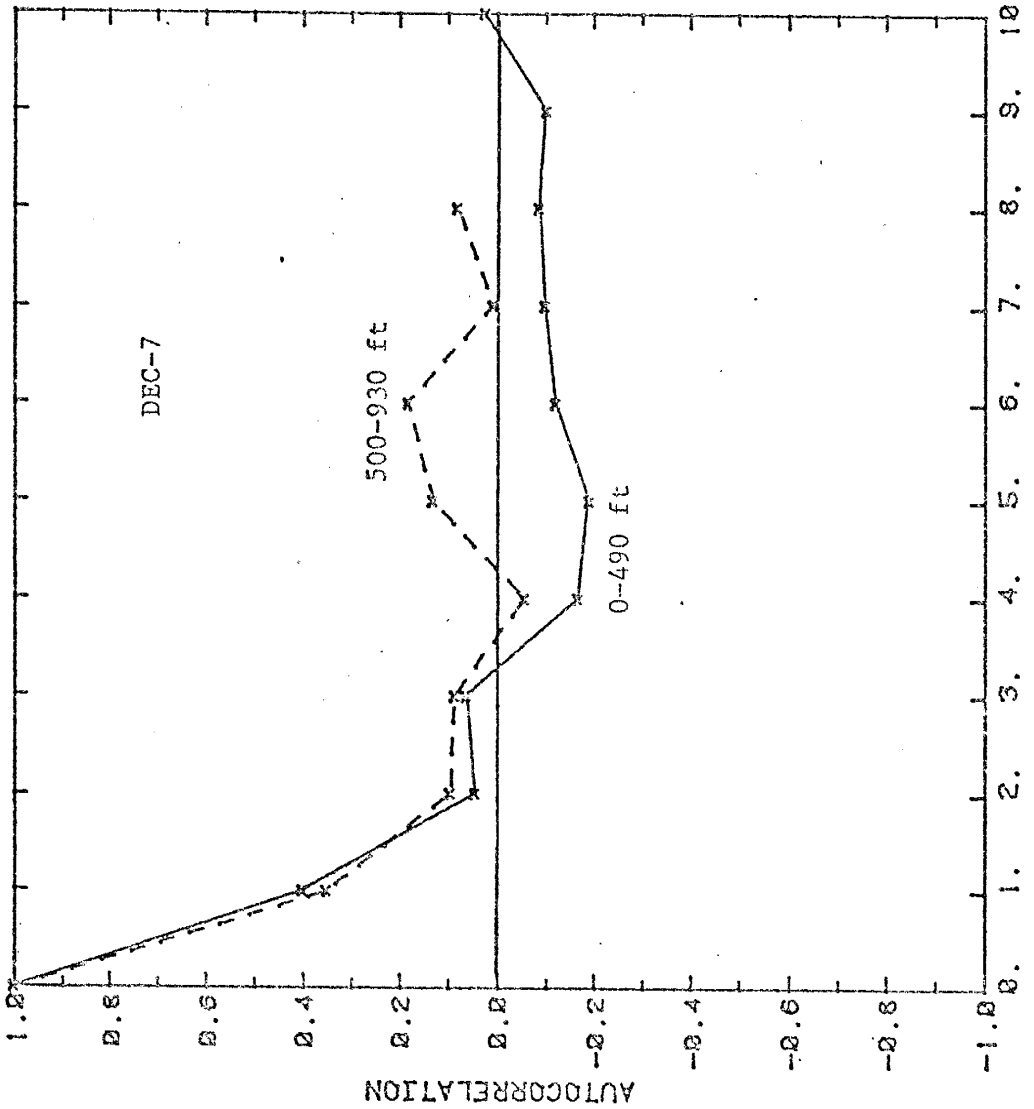

Figure A.8: Autocorrelation functions of the soil capillary pressures (December 7, 1981).

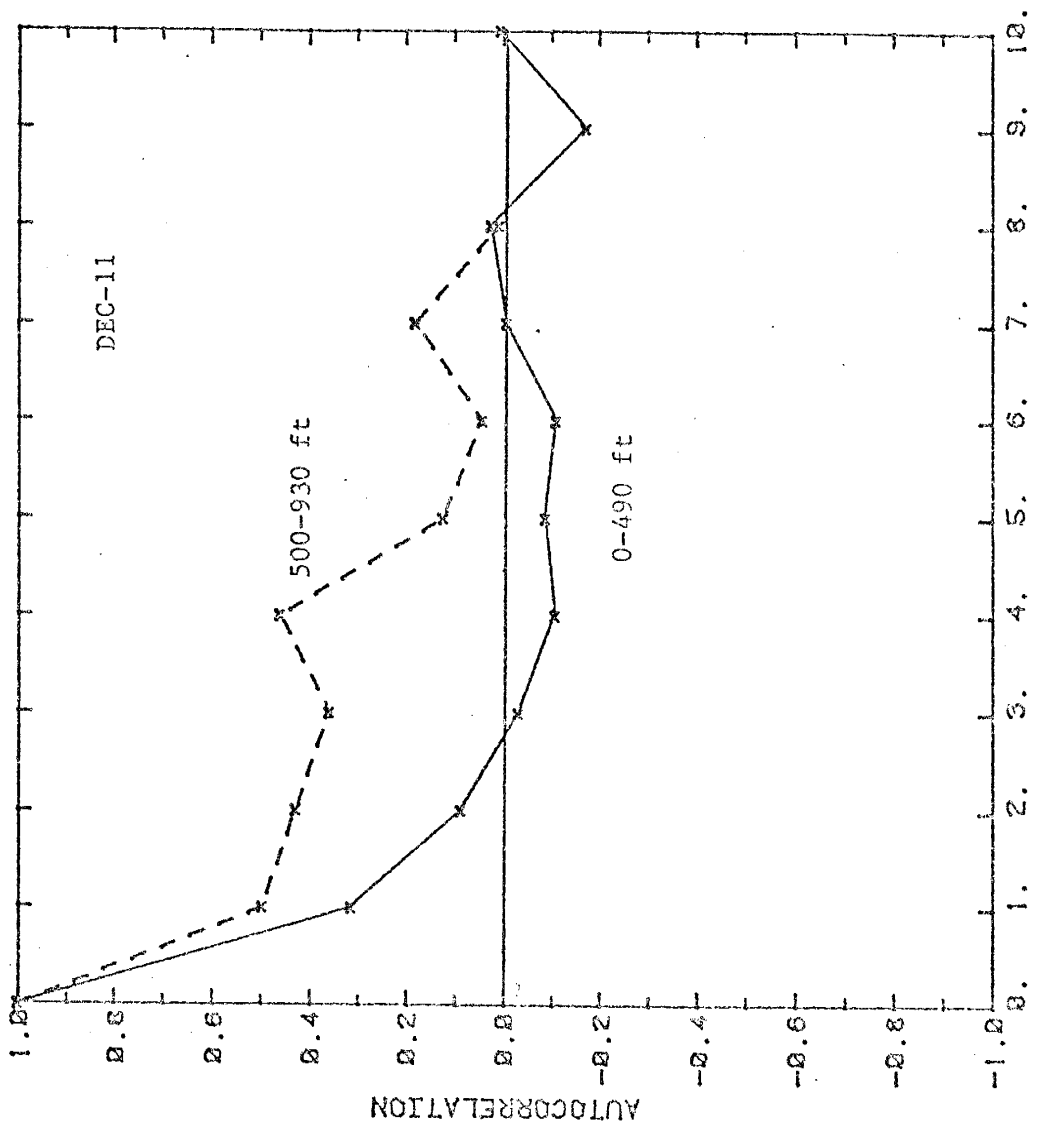

Figure A.9: Autocorrelation functions of the soil capillary pressures (December 11, 1981).

accuracy is as good as any other conventional devices.

(2) Results of this field experiment indicate that there is a large spatial variation in soil capillary pressure. This variation is spatially correlated and exhibits trends in both the mean and the variance at the tested site.

APPENDIX B

SOME INTEGRATION FORMULAS

A list of integration formulas used in the evaluation of variances from spectra are given in this section. These formulas can be verified by integration by the method of partial fractions.

$$\int_0^\infty \frac{U^2 dU}{(U^2+b^2)(U^2+a^2)^2} = \frac{\pi}{4a(a+b)^2} \tag{B1}$$

$$\int_0^\infty \frac{U^4 dU}{(U^2+b^2)(U^2+a^2)^2} = \frac{\pi(a+2b)}{4(a+b)^2} \tag{B2}$$

APPENDIX C

EVALUATION OF HEAD VARIANCE σ_h^2 IN (3.3.13)

This appendix describes the detailed integration procedures used in obtaining the head variance expression given in (3.3.13).

To obtain the head variance, one can integrate the spectrum of the head flucturation given in (3.3.12). This can be written as follows:

$$\sigma_h^2 = \frac{J^2\sigma_f^2}{\pi^2\lambda}\int_{-\infty}^{\infty}\int\int \frac{k_1^2 dk_1 dk_2 dk_3}{(k^4+\beta^2k_1^2)(k^2+1/\lambda^2)^2} \qquad (C.1)$$

Express k_i (i=1,2, and 3) by the following spherical coordinates:

$$k_1=k\cos\Phi,\ k_2=k\sin\Phi\sin\theta,\ \text{and}\ k_3=k\sin\Phi\cos\theta \qquad (C.2)$$

This spherical relationships are illustrated in Figure (C.1). After this spherical transformation, (C.1) becomes:

$$\frac{J^2\sigma_f^2}{\pi^2\lambda}\int_{\theta=0}^{2\pi}\int_{\Phi=0}^{\pi}\int_{k=0}^{\infty} \frac{k^2\cos^2\Phi\sin\Phi dk d\Phi d\theta}{(k^2+1/\lambda^2)^2(k^2+\beta^2\cos^2\Phi)} \qquad (C.3)$$

If we let $t = \cos\Phi$, and integrate (C.3) over θ, the resulting integrand is:

$$\frac{4J^2\sigma_f^2}{\pi\lambda}\int_0^1\int_0^\infty \frac{k^2t^2\,dk\,dt}{(k^2 + 1/\lambda^2)^2(k^2 + \beta^2t^2)} \qquad (C.4)$$

By letting $V = \beta t$, and integrating (C.4) over k with the formula provided in (B.1), (C.4) can be reduced to:

$$\frac{J^2\sigma_f^2\beta}{\beta^3}\int_0^1 \frac{V^2\,dV}{(1/\lambda + V)^2} \qquad (C.5)$$

Therefore, the head variance can be obtained by integrating (C.5) over V. The result is given as:

$$\sigma_h^2 = \frac{J^2\sigma_f^2\lambda^2}{\lambda^2\beta^2}\left[1 - \frac{2\ln|1 + \lambda\beta|}{\lambda\beta} + \frac{1}{1 + \lambda\beta}\right]$$

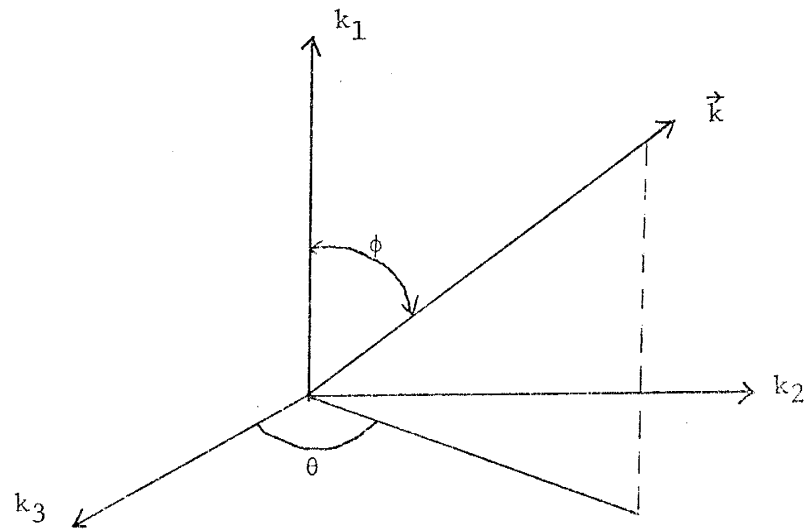

Figure C.1: Spherical coordinate system used in the integration.

APPENDIX D

EVALUATION OF THE THREE-DIMENSIONAL HEAD COVARIANCE FUNCTION IN SECTION 3.3

From (3.3.12) and (3.3.14), the three-dimensional head covariance function resulting from the exponential covariance function (3.3.9) is given by

$$R_{hh}(\xi,\chi) = \frac{J^2\sigma_f^2\lambda^3}{\pi^2}\iiint_{-\infty}^{\infty}\frac{e^{i\vec{k}\cdot\vec{\xi}}k_1^2 d\vec{k}}{(k^2\lambda^2+1)^2(k^4+\beta^2k_1^2)} \tag{D.1}$$

Taking advantage of (3.3.15), one can rewrite (D.1) as:

$$R_{hh}(\xi,\chi) = \frac{J^2\sigma_f^2}{\pi^2\lambda}\int_{k=0}^{\infty}\int_{\theta=0}^{2\pi}\int_{\Phi=0}^{\pi}\frac{e^{i\vec{k}\cdot\vec{\xi}}q^2k^2\sin\Phi dk d\Phi d\theta}{(k^2+1/\lambda^2)(k^2+\beta^2q^2)} \tag{D.2}$$

Furthermore, the expression within the integral of (D.2) can be expressed as partial fractions in the form:

$$R_{hh}(\xi,\chi) = \frac{J^2\sigma_f^2}{\pi^2\lambda}\int_{k=0}^{\infty}\int_{\theta=0}^{2\pi}\int_{\Phi=0}^{\pi}\frac{e^{i\vec{k}\cdot\vec{\xi}}}{(b^2-a^2)^2}\left[\frac{-b^2}{(k^2+b^2)}+\frac{b^2}{(k^2+a^2)}-\frac{a^2(b^2-a^2)}{(k^2+a^2)^2}\right]q^2\sin\Phi dk d\Phi d\theta \tag{D.3}$$

in which $a=1/\lambda$, and $b=\beta q$. Thus, the expression in (3.3.16) can be obtained by integrating (D.3) over k.

APPENDIX E

EVALUATION OF E[fj] TERM IN (3.5.10a)

Since the imaginary part of (3.5.10a) is odd on k_1, it will vanish after integration. Therefore, (3.5.10a) can be rewritten as:

$$E[f\ j] = \frac{-J\sigma_f^2\lambda^3}{\pi^2}\iiint_{-\infty}^{\infty}\frac{k_1^2k^2dk_1dk_2dk_3}{(k^4+k_1^2\beta^2)(k^2\lambda^2+1)} \qquad (E.1)$$

Transforming the above expression to the spherical coordiantes by using the relationships in (C.2), (E.1) can be expressed as:

$$\frac{-J\sigma_f^2\lambda^3}{\pi^2}\int_{k=0}^{\infty}\int_{\theta=0}^{2\pi}\int_{\Phi=0}^{\pi}\frac{k^4\cos^2\Phi\sin\Phi dkd\theta d\Phi}{(k^2+\beta^2\cos^2\Phi)(k^2\lambda^2+1)^2} \qquad (E.2)$$

Integrating over θ and substituting U for $\beta\cos\Phi$, one can reduce (E.2) to

$$\frac{-4\sigma_f^2J}{\pi\lambda\beta^3}\int_0^{\infty}\int_0^{\beta}\frac{k^4U^2dkdU}{(k^2+U^2)(k^2+1/\lambda^2)^2} \qquad (E.3)$$

By ultilizing the expression in (B.2), one can obtains the result of integration of (E.3) over k which is given as follows:

$$\frac{-J\sigma_f^2}{\lambda\beta^3}\left[\int_0^{\beta}\frac{U^2dU}{(U+1/\lambda)} + \int_0^{\beta}\frac{U^3dU}{(U+1/\lambda)^2}\right] \qquad (E.4)$$

This will yields, after integration, the final expression for the cross-covariance of f and j in (3.5.10b)

APPENDIX F

EVALUATION OF σ_j^2 and $\sigma^2_{q_1'}$ TERMS

To determine the variance of q_1', the term, $k_1^2 S_{hh}$, which is equal to S_{jj}, has to be integrated to obtain its variance. The cross-covariances of S_{fh}, and S_{fj} are evaluated previously, and given in (3.4.4) and (3.5.10).

$$\sigma_j^2 = \int_{-\infty}^{\infty} k_1^2 S_{hh} d\vec{k} = \frac{J^2\lambda^3\sigma_f^2}{\pi^2}\iiint_{-\infty}^{\infty} \frac{k_1^4 dk_1 dk_2 dk_3}{(k^4+\beta^2 k_1^2)(1+k^2\lambda^2)^2} \qquad (F.1)$$

Using the relationships in (C.2), the above equation can be writtern in term of the spherical coordiante system and takes the form:

$$\frac{J^2\sigma_f^2}{\pi^2\lambda}\int_{k=0}^{\infty}\int_{\theta=0}^{2\pi}\int_{\Phi=0}^{\pi} \frac{k^4\cos^4\Phi \sin\Phi dk d\Phi d\theta}{(k^2+\beta^2\cos^2\Phi)(k^2+1/\lambda^2)^2} \qquad (F.2)$$

After integrating over θ, and letting $t=\cos\Phi$, the above expression can be reduced to:

$$\frac{4J^2\sigma_f^2}{\pi\lambda}\int_0^{\infty}\int_0^{1} \frac{k^4 t^4 dk dt}{(k^2+\beta^2 t^2)(k^2+1/\lambda^2)^2} \qquad (F.3)$$

Integration of k is carried out by taking advantage of (B.2), it yields:

$$J^2\sigma_f^2\int_0^1 \frac{(1+2\lambda\beta t)t^4 dt}{(1+\lambda\beta t)^2} \qquad (F.4)$$

Thus, the variance of this term is determined by integrating over t. The resulting variance of j, σ_j^2, can be written as:

$$\sigma_j^2 = J^2\sigma_f^2\left[\frac{1}{2y} - \frac{1}{y^2} + \frac{2}{y^3} - \frac{5}{y^4} + \frac{6\ln|1+y|}{y^5} - \frac{1}{y^4(1+y)}\right] \qquad (F.5)$$

where $y = \lambda\beta$. The variance of q_1' is evaluated by summing up the contributions from all the terms in (3.6.3). This results in the expression given in (3.6.4)

APPENDIX G

EVALUATION OF $\sigma^2_{q'_2}$ TERM IN SECTION 3.6

From (3.6.6.b), the integrant for $\sigma^2_{q'_2}$ can be written as:

$$\sigma^2_{q'_2} = \frac{K_m^2 J^2 \sigma_f^2 \lambda^3}{\pi^2} \int_{-\infty}^{\infty}\int\int \frac{J^2 \sigma_f^2 k_1^2 k_2^2 dk_1 dk_2 dk_3}{(k^4+\beta^2 k_1^2)(1+\lambda^2 k^2)} \qquad (G.1)$$

As in the previous analysis, (G.1) can be transformed to the spherical coordiantes as defined in (C.2). After integrating over θ, (G.1) becomes:

$$\sigma^2_{q'_2} = \frac{2K_m^2 J^2 \sigma_f^2}{\pi\lambda} \int_0^{\infty}\int_1^0 \frac{k^4 t^2 (t^2-1) dk dt}{(k^2+1/\lambda^2)^2 (k^2+\beta^2 t^2)} \qquad (G.2)$$

where $t=\cos\Phi$. Let $t\beta=b$, and $1/\lambda=a$. Integration over k is conducted by employing the formula (B.2). This results in:

$$\sigma^2_{q'_2} = \frac{K_m^2 J^2 \sigma_f^2}{2\lambda\beta^5} \left[\int_{\beta}^{0} \frac{(a+2b) b^4 db}{(a+b)^2} - \beta^2 \int_{\beta}^{0} \frac{(a+2b) b^2 db}{(a+b)^2} \right] \qquad (G.3)$$

The first integral in (G.3), after integration, produces:

$$X = a^4 + 5a^3\beta - 2a^2\beta^2 + a\beta^3 - \frac{\beta^4}{2} - 6a^4 \ln\left|1+\frac{\beta}{a}\right| - \frac{a^5}{a+\beta} \qquad (G.4)$$

Similarly, the second integral in (G.3) yields:

$$Y = \beta^2(a^2 + 3a\beta - \beta^2 - 4a^2 \ln|1+\frac{\beta}{a}| - \frac{a^3}{a+\beta})$$

Therefore, the $\sigma^2_{q'_2}$ term is determined by

$$\sigma^2_{q'_2} = \frac{K_m^2 J^2 \sigma_f^2}{2\lambda\beta^5}(X - Y)$$

This yields the expression in (3.6.4)

APPENDIX H

EVALUATION OF σ_h^2 AND $E[fj_1]$ TERMS IN SECTION 4.2

A more detailed evaluation of the variance resulting from equation (4.2.10) is given in the following paragraphs.

The variance of the head perturbation can be obtained by integrating the head spectrum (4.2.10) over the wave numbers, that is,

$$\sigma_h^2 = \int_{-\infty}^{\infty} S_{hh} d\vec{k} = \frac{J^2\sigma_f^2\lambda_1\lambda_2\lambda_3}{\pi^2}\iiint_{-\infty}^{\infty}\frac{k_1^2 dk_1 dk_2 dk_3}{(k^4+\beta^2k_1^2)(1+u_i^2)^2} \qquad (H.1)$$

where i=1,2, and 3. We now let $u_i=\lambda_i k_i$ (no sum on i) and assume $\lambda_2=\lambda_3=\lambda$. Equation (H.1) can be written as:

$$\sigma_h^2 = \frac{J^2\sigma_f^2\lambda_1^2\rho^4}{\pi^2}\iiint_{-\infty}^{\infty}\frac{u_1^2 du_1 du_2 du_3}{[(\rho^2u_1^2+u_2^2+u_3^2)^2+\rho^4g^2u_1^2](1+u^2)^2} \qquad (H.2)$$

where $\rho=\lambda/\lambda_1$, and $g=\lambda_1\beta$. The remaining integral can be evaluated as follows: First, we can express equation (H.2) in spherical coordinates:

$$u_1=u\cos\Phi,\ u_2=u\sin\Phi\sin\theta,\ \text{and}\ u_3=u\sin\Phi\cos\theta$$

This results in a form:

$$\sigma_h^2 = \frac{J^2\sigma_f^2\lambda_1^2\rho^4}{\pi^2}\int_0^{\infty}\int_0^{\pi}\int_0^{2\pi} \frac{u^2\cos^2\Phi\sin\Phi d\Phi du d\theta}{[u^2(\sin^2\Phi+\rho^2\cos^2\Phi)^2+\rho^4 g^2\cos^2\Phi](1+u^2)^2} \qquad (H.3)$$

After integrating over θ, (H.3) becomes:

$$\frac{2J^2\sigma_f^2\lambda_1^2\rho^4}{\pi}\int_0^{\infty}\int_0^{\pi} \frac{u^2\cos^2\Phi\sin\Phi d\Phi du}{[u^2(\sin^2\Phi+\rho^2\cos^2\Phi)^2+\rho^4 g^2\cos^2\Phi](1+u^2)^2} \qquad (H.4)$$

Taking advantage of the integration formula devolped in Appendix B to integrate equation (H.4) over u, equation (H.4) yields:

$$\sigma_h^2 = \frac{J^2\sigma_f^2\lambda_1^2\rho^4}{2}\int_0^1 \frac{t^2 dt}{[(\rho^2-1)t^2+\rho^2 gt+1]^2} \qquad (H.5)$$

where $t = \cos\Phi$.

Finally, the integration of equation (H.5) over t can be obtained by ultilizing the formula provided by Dwight (160.22, p39). The head variance resulting from equation (H.5) is expressed by equations (4.2.11 a and b).

Evaluation of $E[fj_1]$ Term

The spectrum S_{fj_1} takes the form:

$$S_f j_1 = \frac{-J\sigma_f^2 \lambda_1 \lambda^2 k_1^2 k^2}{\pi^2 (k^4 + k_1^2 \beta^2)(1+\lambda_i^2 k_i^2)^2} \tag{H.6}$$

Similarly, we will define new variables as previous analysis, and use spherical coordinate transformation. Equation (H.6) thus becomes:

$$= \frac{-J\sigma_f^2 \rho^2}{\pi^2} \int_0^{2\infty} \int_0^{\pi} \int_0^{2\pi} \frac{u^4 (\rho^2 \cos^2\Phi + \sin^2\Phi)\cos^2\Phi \sin\Phi \, du \, d\Phi \, d\theta}{[(\rho^2\cos^2\Phi+\sin^2\Phi)^2 u^2 + \rho^4 g^2 \cos^2\Phi](1+u^2)^2} \tag{H.7}$$

Integrating over θ and substituting $t=\cos\Phi$ reduces equation (H.7) to the form:

$$\frac{4J\sigma_f^2\rho^2}{\pi} \int_1^0 \frac{t^2}{[(\rho^2-1)t^2+1]} \int_0^{\infty} \frac{u^4 \, du \, dt}{\left[u^2 + \frac{\rho^4 g^2 t^2}{[(\rho^2-1)t^2+1]^2}\right](u^2+1)^2} \tag{H.8}$$

Utilizing the formula (B.2), we write (H.8) as:

$$J\sigma_f^2 \rho^2 \int_1^0 \frac{t^2 (At^2+2Bt+1)\,dt}{(At^2+Bt+1)^2} \tag{H.9}$$

where $A = \rho^2 - 1$, and $B = \rho^2 g$. The above equation can be further reduce to (see Dwight 160.28, p39):

$$E[fj] = J\sigma_f^2\rho^2\left[\int_0^1 \frac{2t^2dt}{[(\rho^2-1)t^2+\rho^2gt+1]^2} - \frac{1}{\rho^2(g+1)}\right]$$

$$= J\sigma_f^2\rho^2\left[\frac{2\sigma_h^2}{J^2\sigma_f^2\lambda_1^2\rho^4} - \frac{1}{\rho^2(g+1)}\right] \qquad \text{(H.10)}$$

where the head variance σ_h^2 is given by equation (4.2.11a and 4.2.11b).

APPENDIX I

EVALUATION OF σ_h^2, AND F_{ij} IN SECTION 4.3

From equations (4.3.5 and 4.3.6), the head variance can be expressed as:

$$\sigma_h^2=\frac{J_1^2\sigma_f^2}{\pi^2}\iiint_{-\infty}^{\infty}\frac{(a_{11}^2k_1'^2+2a_{11}a_{21}k_1'k_2'+a_{21}^2k_2'^2)\lambda_1\lambda_2\lambda_3dk_1'dk_2'dk_3'}{[k'^4+\beta^2(a_{11}k_1'+a_{21}k_2')^2](1+\lambda_1^2k_1'^2+\lambda_2^2k_2'^2+\lambda_3^2k_3'^2)^2} \quad (I.1)$$

By letting $u_i' = \lambda_i k_i'$, $\lambda_2=\lambda_3=\lambda$ and $\rho=\lambda/\lambda_1$, equation (I.1) can be reduced to

$$\frac{J_1^2\sigma_f^2\lambda_1^2\rho^2}{\pi^2}\iiint_{-\infty}^{\infty}\frac{(a_{11}^2\rho^2u_1^2+2a_{11}a_{21}\rho u_1u_2+a_{21}^2u_2^2)du_1du_2du_3}{[(\rho^2u_1^2+u_2^2+u_3^2)^2+\rho^2g^2(a_{11}\rho u_1+a_{21}u_2)^2](1+u^2)^2} \quad (I.2)$$

Since the aspect ratio for the perfectly stratified medium is infinite, $\rho\to\infty$, equation (I.2) can be further simplified to:

$$\frac{J_1^2\sigma_f^2\lambda_1^2a_{11}^2}{\pi^2}\iiint_{-\infty}^{\infty}\frac{du_1du_2du_3}{(u_1^2+g^2a_{11}^2)(1+u^2)^2} \quad (I.3)$$

After transforming the variables to spherical coordinates, we may write (I.3) in the form:

$$\frac{J_1^2\sigma_f^2\lambda_1^2a_{11}^2}{\pi^2}\int_0^\infty\int_0^{2\pi}\int_0^{\pi}\frac{u^2\sin\Phi d\Phi du d\theta}{(u^2\cos^2\Phi+g^2a_{11}^2)(u^2+1)^2} \qquad (I.4)$$

The integration over θ and u in equation (I.4) leads to:

$$J_1^2\sigma_f^2\lambda_1^2a_{11}^2\int_0^1\frac{dt}{(t+ga_{11})^2} \qquad (I.5)$$

Thus, the head variance of this case can be obtained by evaluating (I.5) and is given as:

$$\sigma_h^2 = \frac{J_1^2\sigma_f^2\lambda_1^2a_{11}^2}{ga_{11}(1+ga_{11})} \qquad (I.6)$$

EVAULATION OF F_{ij} TERMS

In order to determine the effective hydraulic conductivity, the tensor F_{il} has to be evaluated. The results of F_{il} can be obtained by determining the invariant E_{mn} which is expressed in equation (4.3.8). For m=n=1, E_{11} is given by:

$$E_{11} = \frac{-1}{\pi^2}\int_{-\infty}^{\infty}\int\int\frac{k_1'^2[k'^2+i\beta(a_{11}k_1'+a_{21}k_2')]\lambda_1\lambda_2\lambda_3dk_1'dk_2'dk_3'}{[k'^4+\beta^2(a_{11}k_1'+a_{21}k_2')^2](1+\lambda_1^2k_1'^2+\lambda_2^2k_2'^2+\lambda_3^2k_3'^2)^2} \qquad (I.7)$$

By changing variables ($u_i=\lambda_ik_i'$), and assuming that $\lambda_2=\lambda_3=\lambda$

and $\rho \to \infty$, equation (I.7) is simplified to :

$$= \frac{-1}{\pi^2} \int_{-\infty}^{\infty} \int \frac{u_1^2 du_1 du_2 du_3}{(u_1^2 + g^2 a_{11}^2)(1+u^2)^2} \tag{I.8}$$

The integral can be evaluated by employing similar procedures to those used in previous analysis. The result is given by:

$$E_{11} = \frac{-1}{1+ga_{11}} \tag{I.9}$$

Since it is assumed that the aspect ratio is infinite, the contribution from E_{22} is always zero. Therefore,

$$F_{11}J_1 = \sigma_f^2 a_{11}^2 E_{11} J_1 = \frac{-J_1 \sigma_f^2 a_{11}^2}{1+ga_{11}} \tag{I.10}$$

Similarly,

$$F_{21}J_1 = \sigma_f^2 a_{11} a_{12} E_{11} J_1 = \frac{-J_1 \sigma_f^2 a_{11} a_{12}}{1+ga_{11}} \tag{I.11}$$

APPENDIX J

EVALUATION OF σ_h^2 AND E[fj] TERMS IN SECTION 4.4

The head variance (4.4.3) can be obtained by integrating the spectrum of the capillary pressure perturbations (4.4.2) over wave numbers. If we let $u_i=\lambda_i k_i'$, and assume that $\lambda_2=\lambda_3=\lambda$ and $\rho\to\infty$, the integral of the spectrum can be written as:

$$\sigma_h^2=\frac{\sigma_f^2\lambda_1^2(J_1a_{11}+J_2a_{12})^2}{\pi^2}\int_{-\infty}^{\infty}\int\frac{du_1du_2du_3}{(u_1^2+e^2)(1+u^2)^2} \qquad (J.1)$$

where $e=\alpha\lambda_1[(2J_1-1)a_{11}+2J_2a_{12}]$. Equation (J.1) is similar to equation (I.3). The same integration procedures can be applied to (J.1) to obtain the head variance which is given as:

$$\sigma_h^2=\frac{\sigma_f^2\lambda_1^2(J_1a_{11}+J_2a_{12})^2}{e(1+e)} \qquad (J.2)$$

The procedures to evaluate the covariance of fj_1 and fj_2 are the same as those employed in appendix D with the exception that the gradient component J_1a_{11} is replaced by $J_1a_{11}+J_2a_{12}$.

APPENDIX K

EVALUATION OF ONE-DIMENSIONAL HEAD COVARIANCE FUNCTION IN CHAPTER 5

This appendix describes the derivation of the head covariance function shown in (5.2.15). Using (5.2.12) and (3.2.18), the head covariance function of one-dimensional flow model is given by:

$$R(\xi) = \frac{2J^2\sigma_f^2\eta^3}{\pi}\int_{-\infty}^{\infty} e^{ik\xi}\left[\frac{(1-H\zeta)^2k^2}{(k^2+\beta^2)(1+k^2\eta^2)^2} + \frac{(J-1)^2\zeta^2}{(k^2+\beta^2)(1+k^2\eta^2)^2}\right]dk \qquad (K.1)$$

The result of the Fourier transform on the first term in (K.1) is similar to the head covariance function in (3.2.19) with the exception that σ_f^2 in (3.2.19) is replaced by $\sigma_f^2(1-H\zeta)^2$. The second term within (K.1) can be further expressed as partial fractions in the form:

$$\frac{(J-1)^2\zeta^2}{(\beta^2\eta^2-1)^2}\left[\frac{1}{(k^2+\beta^2)} - \frac{1}{(k^2+1/\eta^2)} - \frac{(1-\beta^2\eta^2)}{\eta^2(k^2+1/\eta^2)^2}\right] \qquad (K.2)$$

The Fourier transform of (K.2) leads to:

$$\frac{\pi\eta(J-1)^2\zeta^2}{2(\beta^2\eta^2-1)^2}\left\{\frac{2e^{-\beta|\xi|}}{\beta\eta} - \left[2 + (1-\beta^2\eta^2)\left(\frac{|\xi|}{\eta}+1\right)\right]e^{-|\xi|/\eta}\right\} \qquad (K.3)$$

Thus, the contribution from the second term in (K.1) can be derived by using the expression in (K.3). To obtain the expression (5.2.15) for one-dimensional head variance in the case where a and f are perfectly correlated, one can sum up the contributions from the results of the first and second terms in (K.1). The head covariance function for the case where a and f are uncorrelated can also be derived in a similar manners.

APPENDIX L

THE PROCEDURES AND THE COMPUTER CODE FOR THE EFFECTIVE HYDRAULIC CONDUCTIVITIES IN CHAPTER 6

This appendix describes the proceuder used to evaluate the anisotropy ratio of the hydraulic conductivity in Section 6.3. Since the aspect ratio in this case is finite, it is difficult to obtain the closed forms of the variance or covariance terms involved in the determination of the effective hydraulic conductivity. Therefore, numerical integration is employed to obtain these terms.

The head variance of the unsaturated flow in a formation with arbitrarily oriented stratification, under $J_1=1$, and $J_2,=J_3=0$ condition is given by (I.2). One can further express (I.2) in terms of the spherical coordinates (see Appendix H) as:

$$\int_0^{\pi}\int_0^{2\pi}\int_0^{\infty}\frac{J_1^2\sigma_f^2\lambda_1^2\rho^2(a_{11}\rho\cos\Phi+a_{21}\sin\Phi\sin\theta)^2u^2\sin\Phi d\Phi du d\theta}{\pi^2[u^2(\rho^2\cos^2\Phi+\sin^2\Phi)^2+\rho^2g^2(a_{11}\rho\cos\Phi+a_{21}\sin\Phi\sin\theta)^2](1+u^2)^2}$$

Taking the advantage of the integration formula (B.1), (L.1) can be simplified to

$$\int_0^{\pi}\int_0^{2\pi}\frac{J_1^2\sigma_f^2\lambda_1^2\rho^2(a_{11}\rho\cos\Phi+a_{21}\sin\Phi\sin\theta)^2\sin\Phi d\Phi d\theta}{\pi^2[(\rho^2\cos^2\Phi+\sin^2\Phi)+\rho g(a_{11}\rho\cos\Phi+a_{21}\sin\Phi\sin\theta)]^2}$$

Then (L.2) is evaluated numerically by using Simpson's rule.

From (I.7), after spherical transformation, the invariant E_{11} is given as:

$$\int_0^{\pi}\int_0^{2\pi}\int_0^{\infty} \frac{-J_1\sigma_f^2(\rho^2\cos^2\Phi+\sin^2\Phi)\rho^2\cos^3\Phi u^4\sin\Phi d\Phi du d\theta}{\pi^2[u^2(\rho^2\cos^2\Phi+\sin^2\Phi)^2+\rho^2g^2(a_{11}\rho\cos\Phi+a_{21}\sin\Phi\sin\theta)^2](1+u^2)}$$

Using the integration formula given in (B.2), one can integrate (L.3) over u to obtain

$$\int_0^{\pi}\int_0^{2\pi} \frac{-J_1\sigma_f^2\rho^2\cos^2\Phi\sin\Phi}{4\pi[(\rho^2\cos^2\Phi+\sin^2\Phi)+\rho g(a_{11}\rho\cos\Phi+a_{21}\sin\Phi\sin\theta)]^2} \cdot [(\rho^2\cos^2\Phi+\sin^2\Phi)+2\rho g(a_{11}\rho\cos\Phi+a_{21}\sin\Phi\sin\theta)]d\theta d\Phi$$

Similarly, the invariant, E_{22}, can be expressed as (L.4) with the exception that $\rho^2\cos^2\Phi$ is replaced by $\sin^2\Phi\sin^2\theta$. These equations are then numerically integrated over Φ and θ. The effective hydraulic conductivities are evaluated with these parameters and (5.3.8). The detailed procedures are given in the following computer code. Note that σ_f^2 is replaced by $(\sigma_f^2+\sigma_a^2H^2)$ to obtain the results for the case where α and $\ln K_s$ are considered stochastic processes and they are statistically independent.

```
C-----------------------------------------------------------------
C           PROGRAM  APNDL.FOR
C         *************************
C
C
C PROGRAM TO EVALUATE THE EFFECTIVE HYDRAULIC CONDUCTIVITY
C TENSON OF THE SOIL FORMATION WITH ARBITRARY STRATIFICATION
C ORIENTATION AND UNDER UNIDIRECTIONAL FLOW CONDITION.
C
C    THE POROUS MEDIUM CAN BE STATISTICALLY ISOTROPIC OR
C    ANISOTROPIC (I.E.  THE RATIO OF HORIZONTAL TO VERTICAL
C    CORRELATION LENGTHS IS OPTIONAL .)
C
C   PROGRAM ALSO DETERMINES THE ANISOTROPY RATIO OF HYDRAULIC
C   CONDUCTIVITY AS A FUNCTION OF SUCTION PRESSURE HEAD.
C   FOR J=1 ONLY.
C
C   CAPILLARY PRESSURE HEAD VARIANCE IS ALSO EVALUATED AS
C   A FUNCTION OF MEAN SUCTION HEAD( VALID FOR J=1.0)
C
C   ---------------------------------------------------------
C     ALPHA AND F ARE CONSIDERED AS STOCHASTIC VARIABLES.
C     THE SATURATED HYDRAULIC CONDUCTIVITY OF SOIL IS
C     CONSIDERED AS STATISTICALLY HOMOGENEOUS.  THE INTEGRAL
C     WAS REDUCED TO DOUBLE INTEGRAL FORMS AND THEN EVALUATED
C     BY THE NUMERICAL MOTHED BASED ON SIMPSION'S RULE
C-----------------------------------------------------------------
      IMPLICIT DOUBLE PRECISION(A-H,O-Z)
      REAL PHI,THETA,THETA1,GAMMA,J1,H(10),VAR(10),RATIO(10)
      DIMENSION HVAR(10),WCVAR(10)
     DATA H/0.0,20.0,40.0,60.0,80.0,100.0,120.0,140.0,160.0,
    1180.0/
C
C    HEAD VARIANCE FUNCTION TO BE INTEGRATED
C
      FN(A11,A21,C,D,E,F,G,CS,DS,FS,ES,J1)=
    1(J1*(A11*F*C+A21*D*E))**2.0/
    2(FS*CS+DS+F*G*(2.*J1-1.)*(A11*F*C+A21*D*E))**2.0
C
C     E11 INVARIANT TO BE EVALUATED
C
      E11(A11,A21,C,D,E,F,G,CS,DS,FS,ES,J1)=
```

```
     1FS*CS*(FS*CS+DS+2.0*F*G*(2.0*J1-1)*(A11*F*C+A21*D*E))/
    2(FS*CS+DS+F*G*(2.0*J1-1.)*(A11*F*C+A21*D*E))**2.0
C
C     E22 INVARIANT TO BE INTEGRATED
C
      E22(A11,A21,C,D,E,F,G,CS,DS,FS,ES,J1)=
     1DS*ES*(FS*CS+DS+2.0*F*G*(2.0*J1-1)*(A11*F*C+A21*D*E))/
     2(FS*CS+DS+F*G*(2.0*J1-1.)*(A11*F*C+A21*D*E))**2.0
C
C
C
C
      OPEN(UNIT=10,FILE='NPK11.DAT',ACCESS='SEQOUT',DEVICE='DSK')
      OPEN(UNIT=11,FILE='NPK22.DAT',ACCESS='SEQOUT',DEVICE='DSK')
      OPEN(UNIT=12,FILE='HRATIO.DAT',ACCESS='SEQOUT',DEVICE='DSK')
        WRITE(5,1)
1       FORMAT(' ',' OUTPUT ON THE TERMINAL--5, ON LPRT---3')
        READ(5,*)NPRNT
        WRITE(5,2)
2       FORMAT(' ',5X,' INPUT ROTATION ANGLE, J1, N1, N2')
        READ (5,*) GAMMA,J1,N1,N2
        WRITE(5,201)
201     FORMAT(' ',5X,' INPUT VARF, VARA, ALPHA, VSCAL, RO')
        READ(5,*)VARF1,VARA,ALPHA, SCAL1,RO
        WRITE(5,3)
3       FORMAT(' ','      INPUT  MOISTURE-PSI CONSTANT')
        READ(5,*)CNSTNT
        WRITE(NPRNT,4)
4       FORMAT(' ',//,'    OUTPUT FROM  MLTDR3.FOR',/30('*')//)
        WRITE(NPRNT,5)ALPHA,VARF1,VARA,SCAL1,CNSTNT
5       FORMAT(' ',/20X,'  ALPHA = ',F10.4/
     121X,' VARIANCE OF LNK = ',E13.5,/21X,' VARIANCE OF',
     2' ALPHA = ',E13.5,/21X,' VERTICAL SCALE  = ',F10.4,
     3/21X,' MOISTURE-PSI CONSTANT = ',E13.5//)
        WRITE(NPRNT,6)J1,RO
6       FORMAT(' ',//'  J1=',F5.2,
     1'  HORIZONTAL CORR. SCALE/VERTICAL CORR. SCALE=',F10.2)
        WRITE(NPRNT,7)GAMMA
7       FORMAT(' ',/'--------ROTATION ANGLE = ',F6.2,' ---------'//,
     &11X,'  H ',11X,'XK11',9X,'XK22',9X,'XK21',9X,'XK12',
     &9X,'PK11',9X,'PK22',9X,'G')
        DTHE=2.0*3.14159/FLOAT(N2)
```

```
                ALF=ALPHA*SCAL1
      DU=1.0/FLOAT(N1)
      FV=0.0
C
C   GAMMA IS THE ROTATION ANGLE OF THE STRATIFICATION
C
      A11=COSD(GAMMA)
      A12=SIND(GAMMA)
      A21=-SIND(GAMMA)
      A22=COSD(GAMMA)
      A=A11
      B=A21
      F=RO
      FS=F*F
      AS=A*A
      BS=B*B
      DUH=0.5*DU
C
C    G IS THE PRODUCT OF CORRELATION LENGTH IN VERTICAL DIRECTION
C    AND THE CAPILLARY FRINGE PARAMETER
C
C
      G=ALF
      SMFV=0.0
      SME11=0.0
      SME22=0.0
      THETA=0.0
C
C    THE NUMERICAL INTEGRATION STARTS HERE********
C
C
C  SUMMATION IN THE THETA DOMAIN
C
      DO 90 I=1,N2
      U=0.0
      E=SIN(THETA)
      ES=E*E
C
C  SUMMATION IN THE U DOMAIN
C
C
      SMDE11=0.0
```

```
                SMIE11=0.0
        SMDE22=0.0
        SMIE22=0.0
        SUMEND=0.0
        SUMID=0.0
        DO 100 K=1,N1
        U=FLOAT(K-1)*DU
        U1=U+DUH
        C=U
        D=DSQRT(1.0-U*U)
        CS=C*C
        DS=D*D
        C1=U1
        D1=DSQRT(1.0-U1*U1)
        CS1=C1*C1
        DS1=D1*D1
        FNE=FN(A11,A21,C,D,E,F,G,CS,DS,FS,ES,J1)
        FNO=FN(A11,A21,C1,D1,E,F,G,CS1,DS1,FS,ES,J1)
        SUMEND=SUMEND+FNE
        SUMID=SUMID+FNO
        SMDE11=SMDE11+E11(A11,A21,C,D,E,F,G,CS,DS,FS,ES,J1)
      SMIE11=SMIE11+E11(A11,A21,C1,D1,E,F,G,CS1,
     1DS1,FS,ES,J1 )
      SMDE22=SMDE22+E22(A11,A21,C,D,E,F,G,CS,DS,FS,ES,J1 )
      SMIE22=SMIE22+E22(A11,A21,C1,D1,E,F,G,CS1,DS1,FS,
     1ES,J1 )
100     CONTINUE
C
C    EVALUATION OF VARIANCE OF HEAD TERM
C
        FNA=FN(A11,A21,0.0,1.0,E,F,G,0.0,1.0,FS,ES,J1 )
        FNB=FN(A11,A21,1.0,0.0,E,F,G,1.0,0.0,FS,ES,J1 )
        FV=(2.0*SUMEND+4.0*SUMID-FNA+FNB)*DUH/3.0
C
C      EVALUATION OF THE INVARIANTS E11 AND E22 TERMS
C
C
      FNA11=E11(A11,A21,0.0,1.0,E,F,G,0.0,1.0,FS,ES,J1 )
      FNB11=E11(A11,A21,1.0,0.0,E,F,G,1.0,0.0,FS,ES,J1 )
        FE11=(2.0*SMDE11+4.0*SMIE11-FNA11+FNB11)*DUH/3.0
      FNA22=E22(A11,A21,0.0,1.0,E,F,G,0.0,1.0,FS,ES,J1 )
      FNB22=E22(A11,A21,1.0,0.0,E,F,G,1.0,0.0,FS,ES,J1 )
```

```
                FE22=(2.0*SMDE22+4.0*SMIE22-FNA22+FNB22)*DUH/3.0
      SMFV=FV*DTHE+SMFV
      SME11=FE11*DTHE+SME11
      SME22=FE22*DTHE+SME22
      THETA=THETA+DTHE
90    CONTINUE
      SMFV=FS*SMFV/(2.0*3.14159)
      SME11=-0.5*SME11/(3.14159)
      SME22=-0.5*SME22/(3.14159)
C
C     HYDRAULIC CONDUCTIVITY EVALUATION
C
C
      GS=G*G
C
C      VARF+VARA*H**2 LOOP  (J HAS TO BE 1)
C     THIS IS BASED ON THE UNCORRELATED MODEL.
C
      DO 500 I=1,10
      VARF=VARF1+VARA*H(I)*H(I)
      VAR(I)=VARF
      HVAR(I)=VARF*SCAL1*SCAL1*SMFV
      WCVAR(I)=CNSTNT*CNSTNT*HVAR(I)
      XK11=1.0+0.5*VARF*(1.0-GS*SMFV+2.0*SME11)
      XK12=VARF*(A11*A12*SME11+A22*A21*SME22)
      XK22=XK11-2.0*VARF*(SME11-SME22)*(A11*A11-A12*A12)
      XK21=XK12
C
C   DETERMINE THE PRINCIPAL HYDRAULIC CONDUCTIVITIES.
C
      AA=1.0
      BB=-(XK11+XK22)
      CC=(XK11*XK22-XK12*XK21)
      PK22=(-BB+SQRT(BB*BB-4.0*AA*CC))/2.0
      PK11=(-BB-SQRT(BB*BB-4.0*AA*CC))/2.0
            IF(XK11.LE.XK22) GO TO 1000
            TEMP11=PK22
            TEMP22=PK11
            PK11=TEMP11
            PK22=TEMP22
1000  TA=0.5*ATAN(2.0*XK21/(XK11-XK22))
      TA=TA*180.0/3.141596
```

```
      C
C   THE EXPONENTIAL GENERALIZATION OF
C   THE EFFECTIVE HYDRAULIC CONDUCTIVITIES
C
      PK11=EXP(PK11-1.0)
      PK22=EXP(PK22-1.0)
      WRITE(NPRNT,9)H(I),XK11,XK22,XK21,XK12,PK11,PK22,G
9     FORMAT(' ',8E13.5)
C
C    PRINT OUT THE NORMALIZED PRINCIPLE HYDRAULIC CONDUCTIVITY
C    PK11/KM AND PK22/KM
C
      WRITE(10,10)H(I),PK11
      WRITE(11,10)H(I),PK22
10    FORMAT(' ',2X,3(E13.5))
      RATIO(I)=PK22/PK11
500   CONTINUE
      WRITE(NPRNT,8)SMFV
8     FORMAT(' ',//6X,'NORMALIZED HEAD VARIANCE  = ',E13.5//)
      WRITE(NPRNT,11)
11    FORMAT(' ',/'  PSI',3X,'VARF+VARAH2',2X,
     1' PK22/PK11        VARH          VARWC'//)
      DO 600 I=1,10
      WRITE(12,12) H(I),RATIO(I)
      WRITE(NPRNT,12) H(I),VAR(I),RATIO(I),HVAR(I),WCVAR(I)
12    FORMAT(' ',F5.1,4E13.5)
600   CONTINUE
      STOP
      END
```